



NTNU – Trondheim
Norwegian University of
Science and Technology

Dynamic fault-detection in shipboard electric load sharing.

Ida Bohne Krogseth

Marine Technology

Submission date: June 2013

Supervisor: Roger Skjetne, IMT

Norwegian University of Science and Technology
Department of Marine Technology

PROJECT DESCRIPTION SHEET

- Name of the candidate:** Ida Bohne Krogseth
- Field of study:** Marine control engineering.
- Thesis title (Norwegian):** Dynamisk feildeteksjon i maritime elektriske lastdelingssystem.
- Thesis title (English):** Dynamic fault-detection in shipboard electric load sharing.

Background

During the last 20 years, maritime electric installations have increased in size and scope ranging from only few systems and installations to become an industry standard. Several research groups have addressed this topic from different perspectives both nationally and internationally. The Norwegian maritime industry has a leading role in the development of advanced technology improving safety and performance of advanced offshore vessels with electric propulsion.

Control of electric energy production, distribution, and consumption on marine vessels is done by high-level Power and Energy Management Systems (PMS/EMS) and lower-level feedback control loops. While PMS is primarily concerned with safe production of electric power, i.e. to avoid blackouts, the EMS is also concerned with its performance over time to ensure reduced emissions and fuel-efficient consumption. Low-level control of a diesel-generator (genset) is performed by the speed governor and the automatic voltage regulator (AVR). While the speed governor controls the speed of the engine and thereby the generated electric frequency within specified limits, the AVR controls the generated voltage amplitude within specified limits. In conventional systems, sharing of power between parallel-connected gensets is controlled in either droop or isochronous modes of operation.

Fault-detection and handling to avoid blackout in the power system of advanced marine vessels is the most important objective of the PMS. Commercially there are many methods for doing this, with varying success and with new products entering the market every year. In this project the aim is to use Fault-Tolerant Control (FTC) theory to develop dynamic fault-detection algorithms for a few highly relevant failure modes based on state observers for the load-sharing system.

Work description

1. Perform a literature review, providing relevant references, on:
 - Power management systems.
 - Typical failure modes in marine electric power systems. Of special interest are failures that cause frequency variations or voltage variations that may cause protection devices to trip due to under- or over-frequency or under- or over-voltage.
 - Commercial systems and functions for detecting and handling failures in advanced marine vessels.
2. Write a list with definitions and descriptions of terms, and explain particularly relevant concepts related to PMS safety functions (blackout prevention functions).
3. Define and explain 3-5 important failure modes in a shipboard electric load-sharing system with at least three gensets, to be included in your fault-detection system.
4. Develop the mathematical state-space model for a load-sharing system with at least three gensets. This model shall include the mechanical and electrical dynamics of the gensets, governor and AVR functions, the limiting effects of the turbocharger and air systems, and measurements of relevant electric and mechanical parameters.
5. Specify a set of particularly relevant normal and adverse simulation scenarios (tests), for instance related to load changes, generator trip, AVR faults, and governor faults. Perform simulations to verify the behavior of your load-sharing system model in response to each of these specified tests and present the results.

6. Study relevant theory within FTC and expand your model correspondingly to incorporate detection triggers of your proposed failure modes. Propose one or several fault-detection algorithms for your load-sharing system, simulate their performance, and report the results. At least one such fault-detection algorithm should be based on use of an observer. Provide a discussion on pros and cons for each design.

Guidelines

The scope of work may prove to be larger than initially anticipated. By the approval from the supervisor, described topics may be deleted or reduced in extent without consequences with regard to grading.

The candidate shall present his personal contribution to the resolution of problems within the scope of work. Theories and conclusions should be based on mathematical derivations and logic reasoning identifying the various steps in the deduction.

The report shall be organized in a rational manner to give a clear exposition of results, assessments, and conclusions. The text should be brief and to the point, with a clear language. The report shall be written in English (preferably US) and contain the following elements: Abstract, acknowledgements, table of contents, main body, conclusions with recommendations for further work, list of symbols and acronyms, references and (optional) appendices. All figures, tables, and equations shall be numerated. The original contribution of the candidate and material taken from other sources shall be clearly identified. Work from other sources shall be properly acknowledged using quotations and a Harvard citation style (e.g. *natbib* Latex package). The work is expected to be conducted in an honest and ethical manner, without any sort of plagiarism and misconduct. Such practice is taken very seriously by the university and will have consequences. NTNU can use the results freely in research and teaching by proper referencing, unless otherwise agreed upon.

The thesis shall be submitted in 3 printed copies, each signed by the candidate. The final revised version of this project description must be included. The report must appear in a bound volume or a binder according to the NTNU standard template. Computer code and a PDF version of the report should be included electronically.

A 15 min. presentation (conference style) on your status, intermediate results, and plan for completion may be asked for at a scheduled time midway into the project period.

Start date: January 2013 **Due date:** As specified by the administration.

Supervisor: Prof. Roger Skjetne
Co-advisor(s): PhD cand. Bo Zhao

Trondheim,

Roger Skjetne
Supervisor

Summary

The main contribution of this thesis is an investigation of different fault detection systems that can be used for marine diesel electric power plants.

The motivation of this thesis is to develop fault detection systems that are capable of detecting governor and AVR actuator faults for a marine diesel electric power plant. Faster detection of these types of faults reduces the risk of blackout, and might also enable more efficient operation of marine diesel electric power systems.

The studied system is a diesel electric power system consisting of three parallel connected gensets. The gensets share a common load sharing system and are run in droop mode. The gensets produce electric power, to supply the consumers on the vessel. A failure in the Governor or AVR, might cause all gensets to disconnect and hence cause a system blackout. Since diesel electric power systems are common for DP vessels, a blackout is a severe situation. If a failure occurs in one genset, this will influence the operation of the other connected gensets. The failure source might therefore be difficult to detect. Better fault detection systems, might therefore enable faster and more reliable protection of the power system.

In this thesis three fault detection systems are investigated. One of the fault detection systems is commonly used for marine power systems, and is based on the governor and AVR droop-curves. The two other fault detection systems are based on a simplified model of a marine diesel electric power system. The first is based on an analytical redundancy relation derived from the system model. The other fault detection system, is based on a nonlinear Luenberger-type observer.

To verify the performance of the fault detection systems, they are implemented in Matlab/Simulink. For this purpose, a more advanced power plant model is developed and implemented in Simulink. Simulations are run for several normal and faulty simulation modes. The fault detection systems perform well for all simulation modes, and are capable to detect the faults within reasonable time.

Sammendrag

Hovedbidraget fra denne masteroppgaven å undersøke ulike fail detekteringsmetoder som kan benyttes for marine diesel elektriske kraftsystemer.

Motivasjonen for denne avhandlingen er å utvikle et feildetekteringssystem som er i stand til å detektere aktuatorfeil i governor og AVR, i et marint diesel elektrisk kraftsystem. Raskere detektering av denne typen feil reduserer risikoen for blackout, og kan muliggjøre mer effektiv operasjon av marine diesel elektriske kraftsystemer.

Det studerte systemet er et diesel elektrisk kraftsystem, som består av tre parallellkoblede generatorsett. Generatorsettene har felles lastdelingssystem og er kjørt i droop. Generatorsettene produserer elektrisk kraft, for å forsyne forbrukerne på fartøyet. En fail i governor eller AVR, kan forårsake frakobling av alle generatorsettene, og dermed en full blackout. Diesel elektriske kraftsystemer er vanlige for fartøy med DP, derfor er en blackout en alvorlig situasjon. Hvis en fei oppstår i ett generatorsett, vill dette påvirke operasjonen av alle de andre tilkoblede generatorsettene. Kilden ti feilen kan derfor være vanskelig å detektere. Bedre feildeteksjonssystemer, kan derfor muliggjøre raskere og mer pålitelig beskyttelse av kraftssystemet.

I denne avhandlingen er tre feildeteksjonssystemer undersøkt. Et av faildeteksjonssystemene er vanlig i bruk for marine kraftsystemer, og er basert på droopkurvene til governoren og AVRen. De to andre feildeteksjonssystemene er basert på en forenklet modell av et diesel elektrisk kraftssystem. Den første er basert på en analytisk redundans relasjon, utledet fra modellen av systemet. Det andre feildeteksjonssystemet, er basert på en ulineær Luenbergertype estimator.

Verifisering av feildeteksjonssystemene er gjennomført ved å implementere dem i Matlab/Simulink. For dette formålet er det utviklet en mer avansert modell av en marin diesel elektrisk kraftssystem, som også er implementert i Simulink. Simuleringer er kjørt for flere normale situasjoner og feilmoder. Feildeteksjonssystemene var i stand til å oppdage alle failene innen rimelig tid.

Preface

This thesis is written as a part of my Master degree in Marine Technology at the Norwegian University of Science and Technology. The work was done between January and June 2013.

The work has been supervised by Professor Roger Skjetne, and with Ph.D. candidate Bo Zhao as co-advisor, both from the Department of Marine Technology at the Norwegian University of Science and Technology.

I would like to thank my supervisor Roger Skjetne for help and valuable feedback on the thesis. I would also give a special thanks to Ph.D. Torstein Ingebrigtsen Bø, Aleksander Veksler and Bo Zhao, for discussions and help.

I would like to thank my fellow students, and especially my office colleagues, for a good working environment.

Trondheim June 10., 2013

Ida Bohne Krogseth

Contents

1	Introduction	1
1.1	Background	1
1.2	Previous work	1
1.3	Motivation	1
1.4	Thesis outline	1
2	System description	3
2.1	Power management system	3
2.2	Equipment	4
2.3	Failure modes	5
2.3.1	Diesel engine and generator faults	6
2.3.2	Main generation and distribution switchboard faults	6
2.3.3	Load feeders faults	7
3	Commercial systems for detecting and handling failures	8
3.1	Protection relays	8
3.1.1	Generator protection relays	8
3.1.2	Bus bar protection relays	9
3.1.3	Feeder protection relays	10
3.2	Generator protection system	10
3.2.1	Generator protection by voting	10
3.2.2	Advanced Generator Protection	10
3.2.3	Kongsberg AGS	11
3.2.4	ABB DGMS	12
4	Implementation of failure modes	13
4.1	Fault handling	13
4.2	Speed control failure	13
4.3	Excitation failure	15
5	Power plant model	17
5.1	Engine and generator	17
5.1.1	Rotational dynamics	17
5.1.2	Steady state equations for the generator	19
5.2	Electrical system	20
5.3	Load sharing	22
5.3.1	Governor	22
5.3.2	AVR	24
5.4	Resulting simulation plant model	24
6	Simulation study	27
6.1	Normal operation modes	29
6.2	Active load increase	29
6.3	Reactive load increase	29
6.4	Disconnection of one genset	29

6.5	Governor faults	33
6.5.1	Governor to minimum	33
6.5.2	Governor to maximum	33
6.5.3	Governor frozen	33
6.6	AVR faults	38
6.6.1	AVR to minimum	38
6.6.2	AVR to maximum	38
6.6.3	AVR frozen	38
7	Control plant model and observer design	42
7.1	Nonlinear control plant model	42
7.2	Design of nonlinear Luenberger-type observer	43
7.2.1	State space model	43
7.2.2	Design of observer and fault detection algorithm	45
7.3	Observer verification	45
7.3.1	Normal operation	46
7.3.2	Failure modes	48
7.4	Observer performance	51
8	Advanced Generator Protection	56
8.1	Theoretical background	56
8.2	Simulation study	56
8.2.1	Fault detection without exceedance duration	56
8.2.2	Fault detection with exceedance duration	58
8.3	Resulting fault detection system	62
9	Analytical redundancy relation from nonlinear model	63
9.1	Model	63
9.2	Theoretical background for redundancy relations	63
9.3	Resulting redundancy relations	65
9.4	Redundancy relation testing and validation	67
9.5	Resulting fault detection system	73
9.6	Simulation results, simulation plant model	73
9.6.1	Fault detection without exceedance duration	76
9.6.2	Fault detection with exceedance duration	78
9.7	Resulting fault detection system	82
10	Observer based fault detection system	83
10.1	Theoretical background	83
10.2	Simulation study	83
10.2.1	Fault detection without exceedance duration	84
10.2.2	Fault detection with exceedance duration	86
10.3	Resulting fault detection system	90
11	Comparison of fault detection systems	91

12 Concluding remarks	93
12.1 Conclusion	93
12.2 Suggestions for further work	94
A Power plant systems	1
B Simulation study plots	3
B.1 Load change	3
C Simulation results for observer	7
C.1 Simulation against control plant model	7
C.1.1 Governor failure modes	9
C.1.2 AVR failure modes	12
C.2 Simulation against simulation plant model	14
C.2.1 Normal simulation modes	16
C.2.2 Governor failure modes	20
C.2.3 AVR failure modes	23
D Simulation results for analytical redundancy relation from nonlinear model	25
D.1 Simulation against control plant model	25
D.1.1 Sudden load change	26
D.1.2 Governor failure modes	28
D.1.3 AVR failure modes	30
D.2 Simulation against simulation plant model	32
D.2.1 Normal simulation modes	33
D.2.2 Governor failure modes	37
D.2.3 AVR failure modes	40

List of Tables

3.1	Common protective functions for generators. • normally or always available, × possibly or never available. Courtesy: IMCA (2010)	9
6.1	System parameters	27
6.2	Genset parameters	27
6.3	Governor and AVR controller gains and parameters	28
6.4	Failure mode parameters	28
8.1	Parameters for fault detection with exceedance duration.	58
8.2	Parameters for fault detection with exceedance duration.	62
9.1	First and second derivative redundancy relations' dependencies on faults. 1 means that there is a dependency.	66
9.2	Second derivative redundancy relations' dependencies on measurements.	66
9.3	Second derivative redundancy relations' dependencies on inputs.	67
9.4	Parameters for fault detection with exceedance duration.	79
9.5	Parameters for fault detection system based on redundancy relations.	82
10.1	Parameters for fault detection with exceedance duration.	87
10.2	Parameters for fault detection with exceedance duration.	90
11.1	Shortest possible fault detection times for the three fault detection systems.	91

List of Figures

2.1	Example of components and system layout for a semi-submersible rig. Courtesy: Ådnanes (2003)	4
2.2	Electric power plant. Courtesy: Marine Cybernetics (IPP Consulting, 2005)	5
3.1	Identification of faulty generator by AGP. Courtesy: Cargill (2007)	11
3.2	AGS signal flow. Courtesy: Kongsberg Maritime (Johannessen et al., 2009)	11
3.3	ABB DGMS interface. Courtesy: ABB (Hansen et al., 2009)	12
4.1	System with KM AGS, two generators connected, under-speed in one engine. Courtesy: Mathiesen (2012)	14
4.2	System with KM AGS, two generators connected, over-speed in one engine. Courtesy: Mathiesen (2012)	14
4.3	System with KM AGS, four generators connected, over-excitation in one generator. Courtesy: Mathiesen (2012)	16
5.1	Gensets connected in parallel, phase a, n gensets	20
5.2	Equivalent three phase power plant	20
5.3	Speed droop block diagram, with parameters in per-unit.	23
5.4	Two gensets sharing load by speed droop. Courtesy: IMCA (2010)	23
5.5	Voltage droop block diagram, with parameters in per-unit.	24
5.6	Simulation plant block diagram.	25
5.7	Resulting simulation plant model	26
6.1	Results from simulation with sudden active load increase occurring after 20 seconds.	30
6.2	Results from simulation with sudden reactive load increase occurring after 20 seconds.	31
6.3	Results from simulation with sudden disconnection of Genset 3 after 20 seconds.	32
6.4	Results from simulation with failure mode governor to minimum for Genset 1, occurring after 20 seconds.	35

6.5	Results from simulation with failure mode governor to maximum for Genset 1, occurring after 20 seconds.	36
6.6	Results from simulation with failure mode governor frozen for Genset 1, occurring after 20 seconds.	37
6.7	Results from simulation with failure mode AVR to minimum for Genset 1, occurring after 20 seconds.	39
6.8	Results from simulation with failure mode AVR to maximum for Genset 1, occurring after 20 seconds.	40
6.9	Results from simulation with failure mode AVR frozen for Genset 1, occurring after 20 seconds.	41
7.1	Measurement and state error, for observer run against control plant model, normal operation	47
7.2	Measurement and state errors, for observer run against control plant model, Governor to maximum occurring after 20 seconds	49
7.3	Measurement and state errors, for observer run against control plant model, AVR to maximum occurring after 20 seconds	50
7.4	Measurement and state errors, for observer run against control plant model, Sudden active load increase occurring after 20 seconds.	52
7.5	Measurement and state errors, for observer run against control plant model, Governor to maximum occurring after 20 seconds. Failure implemented in Genset 1.	53
7.6	Measurement and state errors, for observer run against control plant model, sudden reactive load increase occurring after 20 seconds.	54
7.7	Measurement and state errors, for observer run against control plant model, AVR to maximum occurring after 20 seconds. Failure implemented in Genset 1	55
8.1	Minimum and maximum difference between actual and expected frequency and voltage, for each simulation scenario, and for all durations of the values. Values from the first 10 seconds of the simulation, are not represented.	57
8.2	Difference between actual and expected frequency and voltage, for different simulation scenarios, with event occurring after 20 seconds. The dotted lines represent the maximum and minimum deviation values, presented in Table 8.1, the value closest to zero is used.	60
8.3	Minimum and maximum difference between actual and expected frequency and voltage, for each simulation scenario, and for error durations as defined in Table 8.1. Values from the first 10 seconds of the simulation, are not represented.	61
8.4	AGP block diagram	62
9.1	Nonlinear redundancy relations and state estimation error, run against nonlinear control plant model, with sudden active load increase occurring after 20 seconds	69
9.2	Nonlinear redundancy relations and state estimation error, run against nonlinear control plant model, with Governor to maximum occurring after 20 seconds	70
9.3	Nonlinear redundancy relations and state estimation error, run against nonlinear control plant model, with sudden reactive load increase occurring after 20 seconds	71
9.4	Nonlinear redundancy relations and state estimation error, run against nonlinear control plant model, with AVR faults occurring after 20 seconds	72
9.5	Nonlinear redundancy relations and state estimation error, run against control plant model, with sudden active load decrease occurring after 20 seconds.	75
9.6	77

9.7	Measurement estimation errors, for observer run against simulation plant model, events occurring after 20 seconds.	80
9.8	Minimum and maximum values of redundancy relations, for each simulation scenario, and with maximum duration of the values 0.001 second.	81
9.9	Block diagram for fault detection based on redundancy relations	82
10.1	85
10.2	Measurement estimation errors, for observer run against simulation plant model, events occurring after 20 seconds. The failure modes are implemented in Genset 1.	88
10.3	89
10.4	State-space implementation of nonlinear Luenberg-type observer based fault detection	90
B.1	Results from simulation with sudden active load decrease occurring after 20 seconds.	4
B.2	Results from simulation with sudden reactive load increase occurring after 20 seconds.	5
B.3	Results from simulation with sudden reactive load decrease occurring after 20 seconds.	6
C.1	Measurement and state errors, for observer run against control plant model, Governor to minimum occurring after 20 seconds	9
C.2	Measurement and state errors, for observer run against control plant model, Governor frozen occurring after 20 seconds	10
C.3	Measurement and state errors, for observer run against control plant model, AVR to min occurring after 20 seconds	12
C.4	Measurement and state errors, for observer run against control plant model, AVR frozen occurring after 20 seconds	13
C.5	Measurement and state errors, for observer run against control plant model, Sudden active load decrease occurring after 20 seconds.	16
C.6	Measurement and state errors, for observer run against control plant model, sudden reactive load decrease occurring after 20 seconds.	17
C.7	Measurement and state errors, for observer run against control plant model, suddendisconnection of Genset 3, occurring after 20 seconds.	18
C.8	Measurement and state errors, for observer run against simulation plant model, Governor to minimum occurring after 20 seconds. Failure implemented in Genset 1.	20
C.9	Measurement and state errors, for observer run against simulation plant model, Governor frozen occurring after 20 seconds. Failure implemented in Genset 1.	21
C.10	Measurement and state errors, for observer run against simulation plant model, AVR to minimum occurring after 20 seconds. Failure implemented in Genset 1.	23
C.11	Measurement and state errors, for observer run against simulation plant model, AVR frozen occurring after 20 seconds. Failure implemented in Genset 1.	24
D.1	Nonlinear redundancy relations and state estimation error, run against nonlinear control plant model, with sudden active load decrease occurring after 20 seconds	26
D.2	Nonlinear redundancy relations and state estimation error, run against nonlinear control plant model, with sudden reactive load decrease occurring after 20 seconds	27
D.3	Nonlinear redundancy relations and state estimation error, run against nonlinear control plant model, with Governor to minimum occurring after 20 seconds	28
D.4	Nonlinear redundancy relations and state estimation error, run against nonlinear control plant model, with Governor frozen occurring after 20 seconds	29
D.5	Nonlinear redundancy relations and state estimation error, run against nonlinear control plant model, with AVR to minimum occurring after 20 seconds	30

D.6	Nonlinear redundancy relations and state estimation error, run against nonlinear control plant model, with AVR frozen occurring after 20 seconds	31
D.7	Nonlinear redundancy relations and state estimation error, run against control plant model, with sudden active load increase occurring after 20 seconds.	33
D.8	Nonlinear redundancy relations and state estimation error, run against control plant model, with sudden reactive load increase occurring after 20 seconds.	34
D.9	Nonlinear redundancy relations and state estimation error, run against control plant model, with sudden reactive load decrease occurring after 20 seconds.	35
D.10	Nonlinear redundancy relations and state estimation error, run against control plant model, with sudden disconnection of Genset 3 occurring after 20 seconds.	36
D.11	Nonlinear redundancy relations and state estimation error, run against control plant model, with failure Governor to minimum occurring after 20 seconds.	37
D.12	Nonlinear redundancy relations and state estimation error, run against control plant model, with failure Governor to maximum occurring after 20 seconds.	38
D.13	Nonlinear redundancy relations and state estimation error, run against control plant model, with failure Governor frozen occurring after 20 seconds.	39
D.14	Nonlinear redundancy relations and state estimation error, run against control plant model, with failure AVR to minimum occurring after 20 seconds.	40
D.15	Nonlinear redundancy relations and state estimation error, run against control plant model, with failure AVR to maximum occurring after 20 seconds.	41
D.16	Nonlinear redundancy relations and state estimation error, run against control plant model, with failure AVR frozen occurring after 20 seconds.	42

List of Definitions

AVR Automatic Voltage Regulator, controls the reactive power and voltage produced by the generator.

Bus An electric component that distributes power.

Fuel rate The amount of fuel let into the engine.

Genset An engine connected to a generator, produce electric power to the bus.

Governor Controls the produced active power and frequency of a genset.

Protective relay An protective device which monitors the system. If a faulty condition is detected, it trips the circuit breaker surrounding the faulty part of the network

List of Acronyms

AGP Advanced Generator Protection

AVR Automatic Voltage Regulator

AGS Advanced Generator Supervisor

DGMS Diesel Generator Monitoring System

DP Dynamic Positioning

FLR Fast load reduction

IMCA International Marine Contractors Association

I/O Input/output

KM Kongsberg Maritime

PMS Power Management System

Nomenclature

Bases

- ω_b Electrical base frequency of the genset, is equal for the entire system [rad/s]
 $\omega_{m,b}$ Mechanical base velocity of the engine [rad/s]
 $S_{b,i}$ Base power for genset i , different values for bus and each genset [VA]
 V_b Base electric voltage, is equal for the entire system [V]
 $Z_{b,i}$ Base impedance for genset i , different values for bus and each genset $Z_{b,i} = V_b^2/S_{b,i}$ [Ω]

Variables

- δ Load angle [rad]
 η_c Non-dimensional combustion efficiency [-]
 θ_0 Electrical angle of the bus [rad]
 θ_e Electrical angle [rad]
 θ_m Mechanical angle [rad]
 ω Frequency/speed of genset [p.u.]
 ω_0 Bus frequency [p.u.]
 ω_e Electrical frequency of genset [rad/s]
 ω_m Mechanical angular velocity [rad/s]
 ω_t Rotational velocity of the turbocharger [rad/s]
(A/F) Air-to-fuel ratio [kg/kg]
 \tilde{E}_a Excitation voltage, phase a (complex phasor form) [V]
 \tilde{e}_a Excitation voltage, phase a [p.u.]
 \tilde{I}_{as} Current in stator winding a (complex phasor form) [A]
 I_{ds}^r Current in d-direction following rotor [A]
 I_{fd}^r Current in rotor field winding in substitute variables [A]
 P_e Active power produced by the generator [W]
 p_e Active power produced by the generator [p.u.]
 P_i Active power delivered by genset i [W]
 p_i Active power delivered from generator i [p.u.]

P_{load}	Active power consumed by the load [W]
p_{loss}	Electrical power loss, mainly from resistance in stator windings [p.u.]
Q_i	Reactive power delivered by genset i [var]
q_i	Reactive power delivered from the generator [p.u.]
Q_{load}	Reactive power consumed by the load [var]
s_i	Complex power for the generator i [p.u.]
T_D	Loss damping torque [Nm]
t_D	Loss damping torque [p.u.]
T_e	Electrical load torque from the generator [Nm]
t_e	Electrical load torque from the generator [p.u.]
T_m	Mechanical torque from the engine [Nm]
t_m	Mechanical torque from the engine [p.u.]
u	Fuel rack position [-]
\tilde{V}_{an}	Line-to-neutral voltage, phase a (complex phasor form), $\tilde{V}_{an} = \hat{V}_{an} \angle \theta$ [V]
\tilde{v}_{an}	Line-to-neutral voltage, phase a (complex phasor form), $\tilde{v}_{an} = \hat{v}_{an} \angle \theta$ [p.u.]
\hat{v}_{an}	Rms line-to-neutral voltage, phase a [p.u.]
\tilde{V}_{as}	Voltage in stator a (complex phasor form) [V]
V_f	Field voltage in the generator [V]
v_f	Field voltage in the generator [p.u.]
\hat{v}_{ll}	Rms line-to-line bus voltage, $\hat{v}_{ll} = \sqrt{3} \hat{v}_{an}$ [p.u.]
\tilde{V}_T	Thevenin equivalent voltage (complex phasor form) [V]
\tilde{v}_T	Thevenin equivalent voltage (complex phasor form) [p.u.]

Constants

$\tau_{e,i}$	Cylinder time constant for genset i , $\tau_e \approx \frac{0.9}{\omega_{m,b}}$ [s]
$\tau_{f,i}$	Field winding time constant for genset i , $\tau_f = \frac{L_f}{R_f}$ [s]
τ_t	Turbocharger time constant [s]
$(A/F)_{low}$	Lower air-to-fuel ratio for full combustion [kg/kg]
$(A/F)_n$	Nominal air-to-fuel ratio, at rated power and maximum turbocharger speed [kg/kg]

$(A/F)_{high}$	Higher air-to-fuel ratio for full combustion [kg/kg]
D_{fw}	Damping gain due to friction and windage [-]
H	Inertia constant [s]
J_m	Moment of inertia of the rotating masses in the genset [kgm^2]
L_f	Self-inductance of the magnetizing field winding [H]
$m_{a,0}$	Ratio between maximum airflow in the engine, with and without turbocharger [-]
N	Number of poles in the generator [-]
R_f	Resistance of the magnetizing field winding [ω]
r_f	Resistance of the magnetizing field winding [p.u.]
r_s	Stator resistance [p.u.]
x_s	Stator reactance [p.u.]
Z_i	Impedance for generator i , $Z = R_s + jX_s$ [Ω]
z_i	Impedance for generator i , $z = r_s + jx_s$ [p.u.]
Z_T	Thevenin impedance [Ω]

Notation

Per unit values. Upper case letters are with units, lower case letters are per unit, base values have subscript b .

Time derivatives are denoted with a dot diacritics, such as \dot{x} . The d 'th derivative is denoted with the superscript (d) . For example:

$$x^{(2)} = \ddot{x} \quad (0.1)$$

Bold letters, such as \mathbf{x} , are used to denote that the variable is a vector. Bold, capital letters, such as \mathbf{A} , are used for matrices.

The root mean square (rms) value of a variable, for example $x(t)$, is denoted with a hat diacritics, and is defined

$$\hat{x} = \lim_{T \rightarrow \infty} \sqrt{\frac{1}{T} \int_{t=0}^T x(t)^2 dt} \quad (0.2)$$

Complex phasor values are denoted with a tilde diacritics, and are defined

$$\tilde{x} = \hat{x}e^{j\theta} \quad (0.3)$$

1 Introduction

1.1 Background

Since marine diesel electric vessels, are dependent on reliable power supply, the power system is among the most important systems on a marine vessel. The safety systems protecting a marine power plant consist of several levels. The power plant safety hierarchy can be divided in (Mathiesen, 2012):

1. Primary protection system in breakers and switchboards.
2. Power management system and blackout prevention/consumer control system.
3. Load sharing monitoring system.

This thesis will mainly focus on level 3 in the hierarchy. The purpose of the load sharing monitoring system, is to prevent generator trip.

1.2 Previous work

Some research has been done on modeling of marine diesel electric power plants. Hansen (2000) made a model of a marine power system, with emphasis on the synchronous generators. Nord (2006) developed a model and investigated voltage stability issues in a dc power system. Pedersen (2009) used bond graphs to develop a marine power system model. A simulator model for an electric ship power system is also described by Ouroua et al. (2005) Models of diesel engines where the limitations in the turbocharger dynamics are included, is described by Guzzella et al. (2009) and Xiros (2002).

There are some research on observers for engines and generator. Batzel (2006) designed an observer capable of detecting faults in synchronous generator windings. Kyriakides et al. (2006) designed an observer for detection of internal machine faults, based on measurements at the terminals of the machine. And Dassanke et al. (2000) made an observer to detect and isolate faults in a turbofan engine model. There are also much work on observers made for control purposes, such as Laila et al. (2008) who designed a discrete-time partial state observer for a combustion engine test bench.

1.3 Motivation

According to the International Marine Contractors Association (IMCA), approximately 10-24% of DP incidents in the period between 2000 and 2009, was caused by power generation failures (Mathiesen, 2012). Even though DP2 and DP3 vessels have a high level of redundancy, if one single failure in one part of the system is not detected and properly handled, it may spread to the entire bus and may cause loss of the entire switchboard. Introduction of the new DNV DP class DYNPOS ER also opens up for DP2 and DP3 operation with closed bus tie. In such a system, proper fault detection and handling is fundamental.

1.4 Thesis outline

In the first part of the thesis an overview is given on typical failure modes in a marine diesel electric power plant. Then commercial fault detection and handling systems are described. Particularly

interesting failure modes are then defined. Then a power plant model and observation plant model is derived. A control plant model for the system is then developed, and this model is then used to develop a nonlinear observer design for the load sharing system. In the following three chapters, three fault detection systems are presented; the Advanced Generator Protection, a system based on an analytical redundancy relation, and lastly, a system based on the developed observer. All fault detection systems are verified by running them against the simulation plant model. Lastly, the results from the different methods are compared and commented.

2 System description

Marine diesel electric power systems are increasingly being utilized in the global maritime industry, and have become the industry standard for vessels with high need of electric power and large variations in power demand. In a marine diesel electric power system engines connected to synchronous generators are used to produce electric power. The power is then distributed to thrusters, drilling drives and other consumers. A fault in one part of the power production system, power distribution system, or one of the consumers, may effect the overall system, and in the worst case scenario it may cause total loss of power.

In this section the components, functionalities, and typical failure modes in marine electric power systems are described. First an overview of marine power management systems and their functionalities is given. Then, the subsystems where errors can occur are introduced. Lastly, typical failure modes for a marine power plant are described, together with a more detailed description of the failure modes that are typical for the different subsystems.

2.1 Power management system

The Power Management System (PMS) has the overall control of the power system, and ensures that there are sufficient available power for the consumers. The power system and PMS is therefore the interconnection point for all power equipment. The main functionalities of the PMS can be grouped in (Ådnanes, 2003):

- Power generation management: Control and monitoring of diesel engines and generators, with active and reactive load sharing. Load dependent start/stop of gensets, and coordination of control logic and interlocking functions.
- Load management: Monitoring and coordination of power limitation functions, load shedding, and start blocking of heavy consumers based on available power monitoring.
- Distribution management: Configuration and sequence control of reconfiguring the power distribution system.

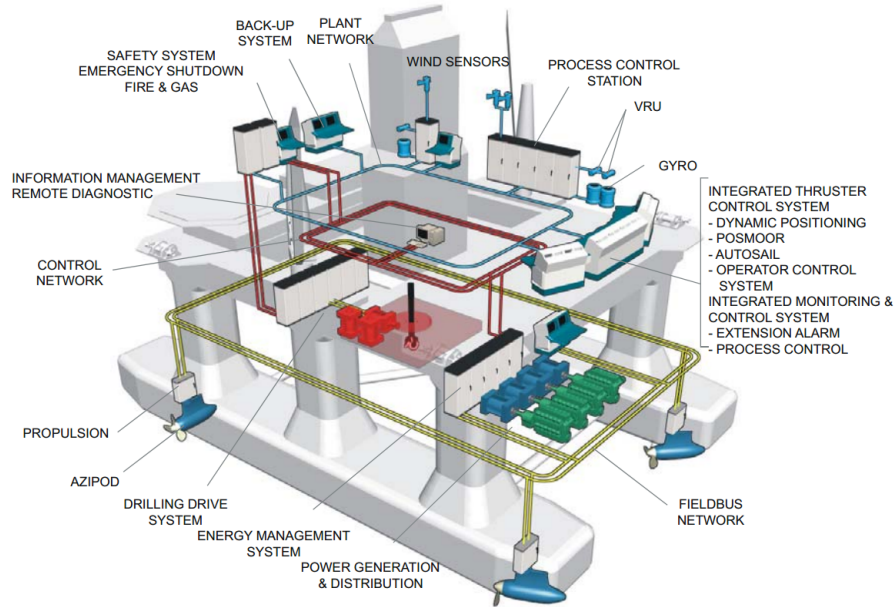


Figure 2.1: Example of components and system layout for a semi-submersible rig. Courtesy: Adnanes (2003)

2.2 Equipment

The main subsystems where faults can occur can be divided into (IPP Consulting, 2005):

- Diesel engines
- Generators
- Main switchboards (generation and distribution)
- Distribution transformers
- Motors
- Variable speed drives
- Fixed speed drives
- Interface to PMS system

A more detailed description of the subsystems is given in Appendix A.

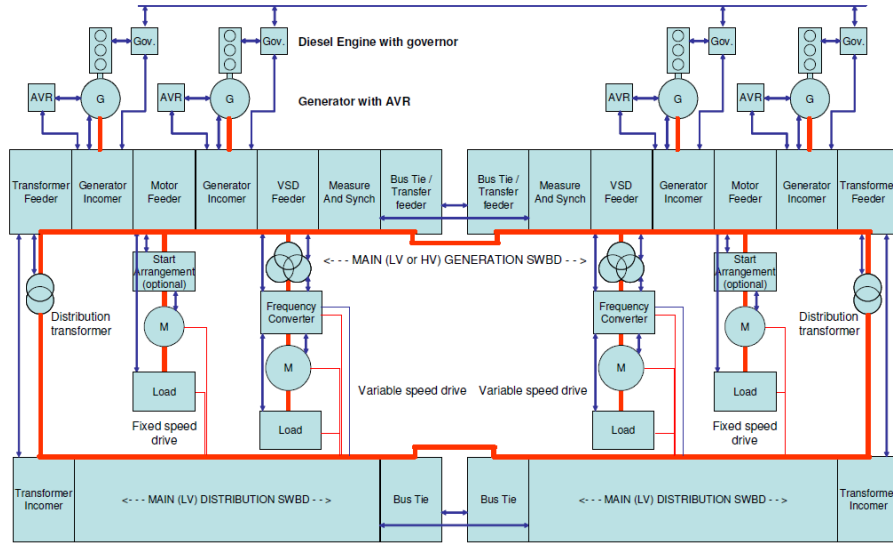


Figure 2.2: Electric power plant. Courtesy: Marine Cybernetics (IPP Consulting, 2005)

2.3 Failure modes

The following definitions are used for fault, failure, and failure mode: A fault is the actual defect in a component. A failure is defined as a components inability to perform its function. A failure mode is the effect of the failure, observed at the boundary of the component (Skjetne et al., 2006).

A power system can be said to be in a failure mode if a critical parameter has an unacceptable value for an unacceptable long period of time. The main critical parameters for a marine power system are voltage, current, frequency, harmonic distortion level, line current balance, and phase voltage balance. Based on this, the most important failure modes in a marine power system are (IMCA, 2010):

- Short circuit (for one or more phases).
- Open circuit (for one or more conductors).
- Earth fault.
- Over/under frequency.
- Over/under voltage.
- Over load (engine ratings exceeded).
- Over current (rating of alternator, bus, bar, cable, motor, transformer, or other consumer exceeded).
- Severe active power sharing imbalance.

- Severe reactive power sharing imbalance.
- Excessive regeneration of power.
- Severe waveform distortion.
- Loss of or incomplete synchronization.

In order to handle one of these failure modes, it is important to localize the source. This is often difficult, since several faults can cause the same failure mode. Also, a fault in one part of the system can cause abnormal operation of other initially healthy parts of the system. Safety systems designed to protect the power plant, such as protection relays, may also escalate the failure mode. To further describe these problems, the main systems and their most common faults and resulting failure modes are described.

2.3.1 Diesel engine and generator faults

Typical engine failure modes are sudden stop or tripping of one engine, unbalanced delivery of power; the faulty engine delivers too much or too little power, and for systems with isochronous load sharing; uneven load sharing due to failure in the load sharing line. For generators the main failure mode is uneven reactive load sharing; one generator produces too much or too little reactive power.

Several faults can cause an engine to be stopped, tripped, or produce less power than expected. Among these faults are mechanical problems in the engine, and fault in cooling system, sensor, governor or fuel supply system. When one faulty engine is tripped or delivers too little power, the other parallel connected engines will pick up the load. This will cause drop in voltage and frequency, until speed and voltage control is recovered. Further, this can cause too little available power for operation, and if the load increase is large enough, the healthy engines will be tripped because of overload.

In the opposite situation, a fault in governor or fuel supply system can cause the engine to run at full throttle. This situation will cause voltage and frequency variations and reduction of power for the other connected engines. Further, either the faulty engine will be tripped because of overload, or the healthy engines will be tripped due to reverse power.

If engines are run in isochronous mode, a failure in the load sharing line causes either uneven load sharing, all engines to zero, or all engines to full power. At least the two last situations may cause loss of all connected engines.

Failure in the excitation control loop can cause unbalanced reactive load sharing. The first consequence of this is voltage variations. If too much reactive power is produced by one generator, it can cause under-excitation trip of healthy generators. Further, the load current in the faulty generator may exceed limit values, which causes an over-current trip. If one generator decreases its production of reactive power, the opposite situation occurs. The faulty generator might trip because of under-excitation, while the healthy generators might trip due to overload.

2.3.2 Main generation and distribution switchboard faults

The most severe failure modes on a switchboard are earth faults, and short circuit. This might cause isolation of the switchboard and disconnection of all associated generators and loads. Further,

faults in sensors or protection relays can lead to undesired trip of equipment.

2.3.3 Load feeders faults

Severe faults will normally cause tripping of load. This might cause increase of other loads, for example thrusters in DP operation, with following frequency and voltage transients. A fault in the PMS might cause overloading of the power system, combined with reduction or shedding of other loads.

3 Commercial systems for detecting and handling failures

In commercial marine power plants there are two main systems for detecting and handling failures; protection relays and generator protection systems. While the main function of protection relays is to protect humans and equipment from damage caused by faults in the power system, the generator protection system is meant to insure continued operation. Design of a power system protection scheme is therefore a trade-off between safety of human life and equipment, and disconnection of as little equipment as possible. It is also important to keep in mind that one of these protection systems alone, does not ensure satisfactory protection of the power system. In the following, the main functionalities of protection relays and generator protection system are described.

3.1 Protection relays

The main function of protection relays is to protect electrical equipment and humans, from injury caused by faulty conditions in the electrical system. In modern power systems, digital protection relays are used to detect a wide range of failure modes, and to isolate the failure by tripping the appropriate circuit breakers. The protection relays can also be programmed to set alarms, shut down equipment, lock out equipment, and communicate with the PMS.

It is important that the protection functions are able to isolate a fault as close to the source as possible. For example, in case of an over-current when a power plant is operated with closed bus, the busbar breaker should be opened at a lower limit than the generator breakers. This way, the generators on the healthy switchboard can continue operating, while the generators on the faulty switchboard are disconnected.

In addition, the protection relays should not respond to normal operation transients, by tripping equipment. Therefore protection relays are programmed to react when a critical parameter exceeds its limit values, for an unacceptable duration of time. The limit values, exceedance duration, and disconnection sequence, is decided by equipment manufacturers, classification standards, and power system studies (IMCA, 2010).

The power system protection scheme can be divided into bus bar protection, feeder protection, and generator protection. In the following, the main properties of these protection systems are described.

3.1.1 Generator protection relays

The purpose of generator protection is both to protect the generator from power system faults, and to protect the power system from generator faults. Table 3.1 gives an overview of some typical protective functions and executive actions, that might be available in a generator multifunction relay. The functions presented here, are mainly those who might cause a sudden disconnection of a genset.

Function	Generator trip	Bustie (quick trip)	Excitation trip	Start all generators	Generator lockout	Alarm
Under-voltage	●	●	×	●	×	●
Reactive power	●	×	×	●	×	●
Over-voltage	●	●	●	×	×	●
Under-frequency	●	●	×	×	×	●
Loss of excitation	●	×	×	×	×	×
Reverse power	●	×	×	●	×	●
Phase over-current	●	×	×	×	×	×
Over frequency	●	●	●	×	×	●

Table 3.1: Common protective functions for generators. ● normally or always available, × possibly or never available. Courtesy: IMCA (2010)

The protection relay functions are (IMCA, 2010):

- Under-voltage: Too low voltage at the generator terminals. Typically activated by short circuit fault or direct online starting of a large motor. The function is often a class requirement.
- Reactive power: The generator produces too much reactive power. This is either caused by faults in excitation system, or due to high reactive power demand from a consumer.
- Over-voltage: Too high voltage at the generator terminals. Might be caused by AVR failure.
- Under-frequency: Caused by plant overload, or a common speed control fault in all engines. The function is often a class requirement.
- Loss of excitation: Shall prevent asynchronous running of the generator, and large drain of reactive power. Might be caused by an other generator that has failed to full excitation.
- Reverse power: Shall prevent a faulty generator from being motored by the healthy generators.
- Phase over-current: Shall protect the generator from thermal damage caused by over-current.
- Over frequency: Might be caused by engine governor failure, that causes an unacceptable increase in bus frequency.

3.1.2 Bus bar protection relays

The bus bar protection system is mainly designed to detect and isolate short circuit and earth fault. If one of these faults occur on a bus bar or on its connections, the appropriate breakers should be opened to isolate the fault. A fault on a bus bar is very severe, as all equipment connected to it also will be lost. However, bus bar fault is one of the most unlikely faults to occur in a marine power system (IMCA, 2010).

3.1.3 Feeder protection relays

The feeder protection system generally consist of over-current, and earth-fault protection. In addition, motors and transformers sometimes have special protection systems. Service transformers may have under voltage protection, and transformers and motors often have overload protection, to avoid overheating.

3.2 Generator protection system

Generator protection systems have as main function to obtain continuous operation of the generators. The goal is therefore to detect, locate, and isolate the source of a fault, before the failure mode escalates, and system parameters reach the limits of the protection relays. The generator protection systems are mainly concerned with failures in the speed and voltage control systems.

Four different generator protection systems are described; generator protection by voting, Advanced Generator Protection (AGP), Kongsberg Maritime's Advanced Generator Supervisor (AGS), and ABB Diesel Generator Monitoring System (DGMS).

3.2.1 Generator protection by voting

Protection systems based on voting, collect and compare information from all connected gensets. Normally, the active and reactive power produced by each genset, is compared. If one generator behaves different than the other generators, it is assumed to be faulty, and disconnected. The main weakness of voting is that it can not be used for less than three connected gensets, and it does not take into account that two gensets can have an simultaneous fault. In addition, the method can only be used for faults causing the generator to produce too much ,or too little power.

Voting protection systems can be improved by also including measurements of the bus frequency. A faulty generator producing to much power, will drive up the frequency. If however, the generator is taking on the load because the other generators are faulty and shed load, the frequency will not rise, but fall.

3.2.2 Advanced Generator Protection

Cargill (2007) introduced a method for generator protection called Advanced Generator Protection. The method is suitable for gensets operating in parallel, with droop load sharing. When the speed and voltage droop characteristics are known, the operating point of the healthy generators can be predicted. Figure 3.1 illustrates how the droop characteristics can be used to identify a faulty generator. A window is placed around the droop curve, to allow for the generators to have small deviations from the desired operation point. If however, one of the generators operates outside of the window for an unacceptable duration of time, the generator will be tripped.

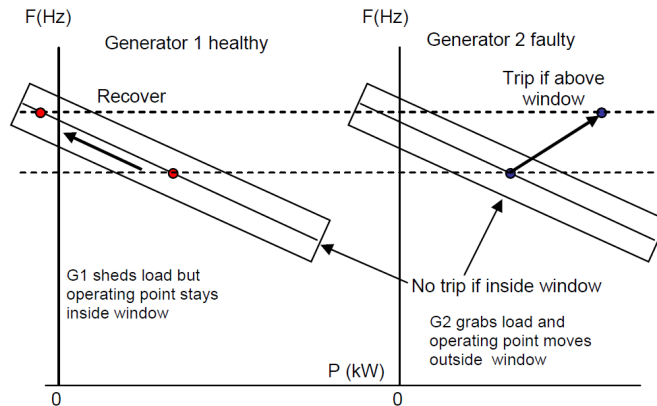


Figure 3.1: Identification of faulty generator by AGP. Courtesy: Cargill (2007)

3.2.3 Kongsberg AGS

Kongsberg Maritime's Advanced Generator Supervisor is an expansion of the Power Management System. The AGS contains a mathematical model of the system, which calculates expected system values. If a generator acts differently than expected, it is assumed that it has a faulty condition. Based on the operation mode from the PMS, Kongsberg AGS monitors the net voltage and frequency, generator active and reactive power, field current, and fuel rack position. If a faulty condition is detected, a standby generator is started and an alarm is set. If the deviation between the expected and the measured values continues, the faulty generator is disconnected and the bus-tie breaker is tripped (Johannessen et al., 2009). Further description of the functionalities in the AGS, is given in Section 4.1.

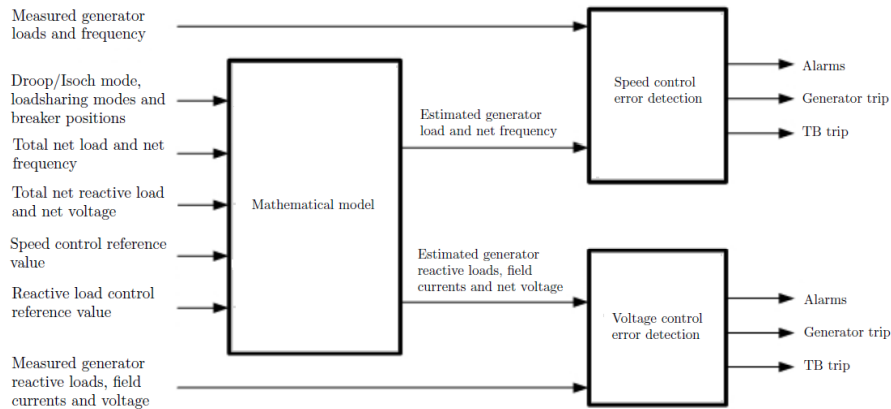


Figure 3.2: AGS signal flow. Courtesy: Kongsberg Maritime (Johannessen et al., 2009)

3.2.4 ABB DGMS

ABB Diesel Generator Monitoring System is designed to detect faults that are not directly detected by the protection relays. One DGMS cabinet is installed per generator to maintain redundancy. The DGMS communicates with the generator, engine, AVR, governor, and switchboard, as shown in Figure 3.3. If the system is operating in isochronous speed mode, the Ethernet ring is used for communication between the systems.

The ABB DGMS detects failures by comparing measured genset values with normal operating curves. The system monitors (Hansen et al., 2009):

- Speed, by comparing expected and measured system frequency and generator active power.
- Voltage, by comparing expected and measured system voltage and generator reactive power.

If a deviation is detected the following fault handling list is used:

1. Set alarm.
2. Start standby generator.

If the pre-set trip limit is crossed:

3. Disconnect faulty genset.

If faulty condition is still observed:

4. Open bus-tie-breaker (isolate switchboard section).

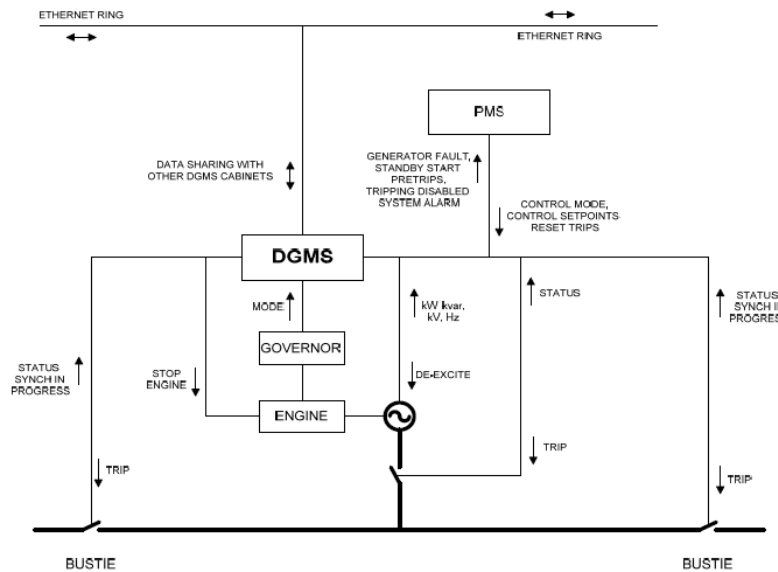


Figure 3.3: ABB DGMS interface. Courtesy: ABB (Hansen et al., 2009)

4 Implementation of failure modes

In this thesis it is desired to develop a simulator of a marine diesel electric power system, and to extend this simulator to incorporate some failure modes of interest. This will enable use of the simulator in testing and development of a suitable model-based fault detection scheme for the genset. The failure modes that will be further investigated are speed control failure and excitation failure. Since the purpose of incorporating faults into the model is to make it suitable for fault detection, both the faults of interest, and the system's actions when the fault is detected must be modeled.

4.1 Fault handling

Modern Power Management Systems (PMS) have routines for how faults are handled. If a failure is detected in one genset, either by a generator protection system or by the protection relays, the genset will be disconnected. This will cause the remaining gensets to pick up the load. To avoid overload of the healthy gensets, the Fast Load Reduction (FLR) reduces the load on the bus. Normally the reduction takes about 0.2 seconds, and often the load is reduced to the level at which the gensets produce the same power as before (Bø, 2012). After this, the load is slowly increased. To prepare for fault detection and handling in the simulator, these features must be implemented.

4.2 Speed control failure

Speed control failure is typically caused by a fault related to the governor, mechanical problems in the engine or associated systems, or in the fuel supply system. In all cases, the fault will affect the amount of fuel supplied to the engine cylinder. This will cause the faulty engine to have a different speed than desired, for example, frozen speed, under-speed, or over-speed. Further, this causes the faulty engine to produce too little or too much power. The load sharing system will then force the healthy engines to increase or decrease the load, accordingly with the faulty engine's decrease or increase in produced power. Both these scenarios will cause variations in voltage and frequency.

In Figure 4.1 and 4.2, the produced active power and net frequency are plotted for two gensets in droop mode, where one genset has a failure. In Figure 4.1 the faulty engine is forced to decrease the produced power, which causes the net frequency to decrease. In Figure 4.2 the faulty engine is forced to increase the produced power, which causes the net frequency to increase. It is seen that after some time, the AGS detects the situation and disconnects the faulty genset.

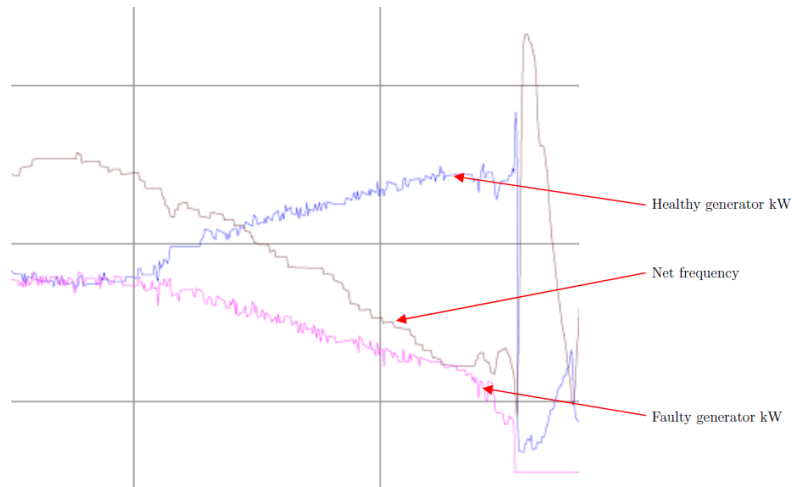


Figure 4.1: System with KM AGS, two generators connected, under-speed in one engine. Courtesy: Mathiesen (2012)

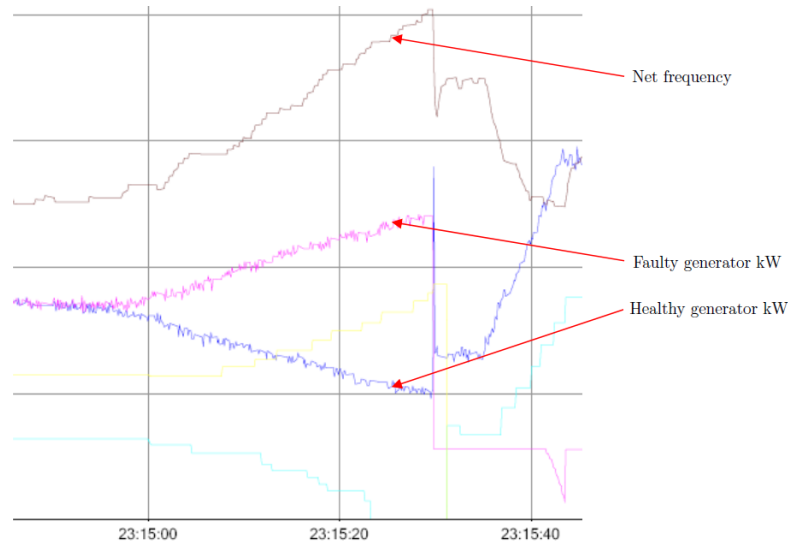


Figure 4.2: System with KM AGS, two generators connected, over-speed in one engine. Courtesy: Mathiesen (2012)

These failure modes can be implemented in the simulator as a forced set-point of the fuel index, or of the produced mechanical torque. In order to not exclude the turbocharger dynamics from the model of the faulty genset, the fuel index is considered to be the best choice. Speed control failures

are therefore modeled as additive, actuator faults. In order to implement this in the simulator, the fuel index from the governor (u), is replaced with a potentially faulty fuel index

$$u_{FM} = u + f_u \quad (4.1)$$

where f_u is the governor failure modes

$$f_u = \begin{cases} 0, & \text{Normal operation} \\ -u + u_{frozen}, & \text{Governor frozen} \\ -u + u_{max}, & \text{Governor to max} \\ -u + u_{min}, & \text{Governor to min,} \end{cases} \quad (4.2)$$

It is important to note that this is implemented as actuator faults. Hence, the governor is assumed to always work correctly, it is the execution of the signal in the engine that is faulty. This means that a fault detection system basing its operation on the governor output, will receive the correct, not the faulty fuel index. Due to this, this implementation does not represent faults in the actual governor, such as faults in sensors used by the governor. This also means that the notation "governor faults", as used in (4.2), is misleading. However, this notation will be used in the thesis to describe the type of faults presented here.

4.3 Excitation failure

A failure in the excitation control loop might cause the faulty generator to produce too little or too much reactive power. The load sharing system will then force the healthy generators to increase or decrease the produced reactive power. This will also cause voltage variations on the net.

Figure 4.3 shows four generators in droop mode, where one generator has a failure. The faulty generator is over-excited, and hence, forced to increase the field current and field voltage. This causes an increase in the reactive power produced by the faulty generator, and an increase in the net voltage. If the case had been under-excitation of one faulty generator, the opposite effect would have occurred. It is seen that after some time, the AGS detects the situation and disconnects the faulty genset.

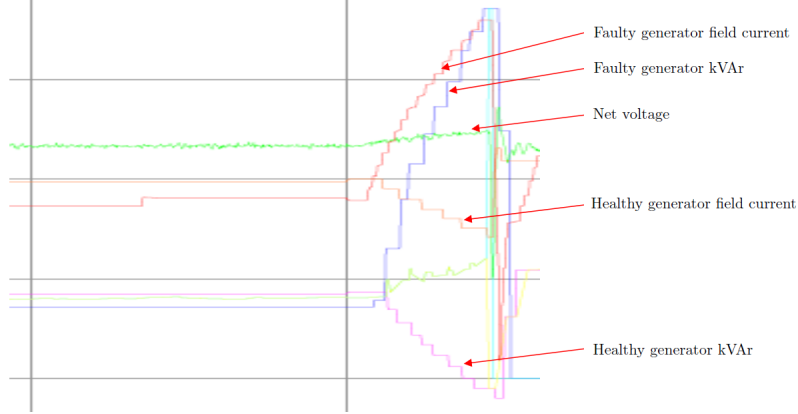


Figure 4.3: System with KM AGS, four generators connected, over-excitation in one generator. Courtesy: Mathiesen (2012)

Excitation errors can be implemented in the simulator as a forced set-point of the field voltage, or field current. In order to not exclude the field current dynamics from the simulation model, the excitation voltage is considered the best choice. Excitation failures are therefore modeled as additive, actuator faults. In order to implement this in the simulator, the field voltage from the AVR (v_f), is replaced with a potentially faulty field voltage

$$v_{f,FM} = v_f + f_{v_f}, \quad (4.3)$$

where f_{v_f} is the AVR failure modes

$$f_{v_f} = \begin{cases} 0, & \text{Normal operation} \\ -v_f + v_{f,frozen}, & \text{AVR frozen} \\ -v_f + v_{f,max}, & \text{AVR to max} \\ -v_f + v_{f,min}, & \text{AVR to min} \end{cases} \quad (4.4)$$

In the same way as with the speed control failures, or governor faults, the AVR failure modes are implemented as actuator faults. Hence, the actual AVR is assumed to work correctly, the error occurs during the execution of the desired field voltage. Despite of this, this type of faults will be called the somewhat misleading name, AVR faults, throughout this thesis.

5 Power plant model

In this section a model for a marine diesel-electric power plant is derived. The model is denoted a simulation plant model, as it is a detailed model, intended for simulating the system behavior. The engine model is a dynamic model, including the limiting effect of the turbocharger. The model for the generator, bus and load sharing system, is a steady-state model, and complex phasors are used for the electrical equations. The diacritics *tilde* ($\tilde{}$), and *hat* ($\hat{}$) are used to denote variables on complex phasor form, and root-mean-square (rms) values, respectively. As the system is a three phase system, the subscript $p = a, b, c$, means that the phasor is given for phase a, b, or c, respectively.

The variables can be expressed in per-unit, this means as the ratio to a base value. This is convenient because system values then easily can be changed, without changing the equations. Lower-case letters are used for per-unit variables, and the subscript b is used for the bases. In general, the per-unit value of a variable is defined as

$$\text{Per-unit value} = \frac{\text{Variable value}}{\text{Base value}}$$

It should be noted that the base voltage (V_b), and electrical base frequency (ω_b) are common for the whole system, while the base power ($S_{b,i}$), and hence also the base impedance ($Z_{b,i}$), are different for the bus and each generator.

5.1 Engine and generator

5.1.1 Rotational dynamics

Diesel engines and generators are rotating machines. Torque balance can therefore be expressed by Newton's second law for rotation

$$J_m \dot{\omega}_m = \sum T_j = T_m - T_e - T_D \quad (5.1)$$

where J_m is the moment of inertia of the rotating masses, ω_m is the engine angular velocity, T_m is the mechanical torque from the engine, T_e is the electrical load torque from the generator, and T_D is the loss or damping torque. The relationship between the mechanical and electrical angle, and mechanical and electrical velocity for a generator with N poles is

$$\theta_e = \frac{N}{2} \theta_m \quad (5.2)$$

$$\omega_e = \dot{\theta}_e = \frac{N}{2} \dot{\theta}_m = \frac{N}{2} \omega_m \quad (5.3)$$

From the definition of the per-unit value, it follows that per-unit angular velocity, and per-unit torque is

$$\omega = \frac{\omega_e}{\omega_b} = \frac{\omega_m}{\omega_{m,b}} \quad (5.4)$$

$$t_j = \frac{T_j}{T_b} \quad (5.5)$$

The inertia constant is defined as

$$H := \frac{J_m \omega_{m,b}}{2T_b} = \frac{\text{Stored kinetic energy at nominal speed}}{\text{Genset power rating}} \quad (5.6)$$

Inserting this into (5.1), gives the rotational dynamics in per-unit

$$2H\dot{\omega} = t_m - t_D - t_e \quad (5.7)$$

Mechanical torque is the torque generated by combustion of fuel in the diesel engine. An important limitation in the engine dynamics is the response time of the turbocharger. To enable the model to represent the effects of large and rapid load changes, some properties of the turbocharger should be included in the model. Veksler et al. (2012) suggests the following model for mechanical torque, that includes the limiting effect of the turbocharger

$$(A/F) = \frac{m_{a,0} + (1 - m_{a,0})\omega_t}{u} (A/F)_n \quad (5.8)$$

$$\eta_c = \begin{cases} 1 & (A/F) \geq (A/F)_{high} \\ \frac{(A/F) - (A/F)_{low}}{(A/F)_{high} - (A/F)_{low}} & (A/F)_{low} < (A/F) < (A/F)_{high} \\ 0 & (A/F) \leq (A/F)_{low} \end{cases} \quad (5.9)$$

$$\dot{\omega}_t = -\frac{1}{\tau_t}(\omega_t - t_m) \quad (5.10)$$

$$t_m = \frac{\eta_c u}{\omega} \quad (5.11)$$

where (A/F) , $(A/F)_n$, $(A/F)_{low}$, and $(A/F)_{high}$ is the air-to-fuel ratio, the nominal ratio (at rated power and maximum turbocharger speed), the lowest ratio, and the highest ratio for full combustion, respectively. Further, u is the fuel rack position, $m_{a,0}$ is the ratio between maximum airflow in the engine with and without turbocharger, ω_t is the rotational velocity of the turbocharger, η_c is the non-dimensional combustion efficiency, and τ_t is the turbocharger time constant.

Linear damping is used (Skjetne, 2012)

$$t_D = D_{fw}\omega \quad (5.12)$$

Electric load torque from the generator is

$$t_e = \frac{T_e}{T_b} = \frac{P_e/\omega_m}{S_b/\omega_{m,b}} = \frac{p_e}{\omega} \quad (5.13)$$

To account for the electrical losses it is assumed that $p_e = p + p_{loss}$, where p is the active power delivered from the generator and p_{loss} is the electrical power loss due to stator conductor loss. The electrical losses are mainly caused by resistance in the stator windings

$$p_{loss} = 3r_s \hat{i}_a^2 = 3r_s \frac{|s_a|^2}{\hat{v}_{an}^2} = r_s \frac{|s|^2}{\hat{v}_{ll}^2} = r_s \frac{p^2 + q^2}{\hat{v}_{ll}^2} \quad (5.14)$$

where r_s is the stator resistance, q is the delivered reactive power, and $\hat{v}_{ll} = \sqrt{3}\hat{v}_{an}$ is the rms line-to-line voltage.

5.1.2 Steady state equations for the generator

For the electrical system a steady-state model is used. This means that the electrical angular velocity of the rotor is constant and there are no change in flux linkages in the rotor windings. According to Krause et al. (2002) the following equations can be used for a generator in steady-state

$$\tilde{E}_a = \frac{1}{\sqrt{2}} [-\omega (X_d - X_q) I_{ds}^r + \omega X_{md} I_{fd}^r] e^{j\delta} \quad (5.15)$$

$$\tilde{V}_{as} = -(r_s + j\omega X_q) \tilde{I}_{as} + \tilde{E}_a \quad (5.16)$$

where \tilde{E}_a is the excitation voltage, \tilde{V}_{as} is the voltage out of the terminal, and \tilde{I}_{as} is the current in the stator winding. The load angle is defined as the difference between the electrical angle of the genset and the electrical angle of the bus

$$\delta = \theta_e - \theta_0 \quad (5.17)$$

Using (5.3), the load angle can be written as a function of the frequency and bus frequency, ω_0 ,

$$\dot{\delta} = \omega_b (\omega - \omega_0) \quad (5.18)$$

Because the generator rotor is circular, $X_d = X_q$, (5.15) becomes

$$\tilde{E}_a = \frac{1}{\sqrt{2}} \omega X_{md} I_{fd}^r e^{j\delta} \quad (5.19)$$

The rotor field current (I_{fd}^r) is altered by the AVR to control the excitation voltage. Combining this with the steady-state model presented by Skjetne (2012), we can set $R_f I_f = \frac{1}{\sqrt{2}} X_{md} I_{fd}^r$, where I_f is the field current. Further, the resistance and reactance in (5.16) can be replaced by the generator impedance, Z . The equations for field excitation voltage and terminal voltage then become

$$\tilde{E}_a = \omega R_f I_f e^{j\delta} \quad (5.20)$$

$$\tilde{V}_{as} = -Z \tilde{I}_{as} + \tilde{E}_a \quad (5.21)$$

By dividing with the base voltage V_b , the per-unit excitation voltage is

$$\tilde{e}_a = \omega r_f i_f e^{j\delta} \quad (5.22)$$

Skjetne (2012) suggests the following dynamical model for field current

$$\dot{i}_f = -\frac{1}{\tau_f} \left(i_f - \frac{1}{r_f} v_f \right) \quad (5.23)$$

where r_f is the magnetizing field windings resistance, $\tau_f = \frac{L_f}{R_f}$ is the field winding constant, and R_f and L_f are the magnetizing field windings resistance and self-inductance, respectively.

5.2 Electrical system

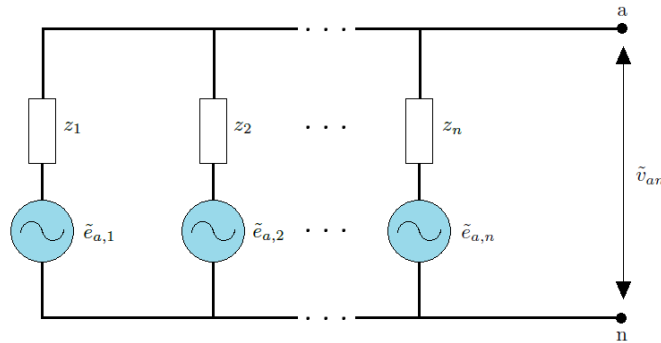


Figure 5.1: Gensets connected in parallel, phase a, n gensets

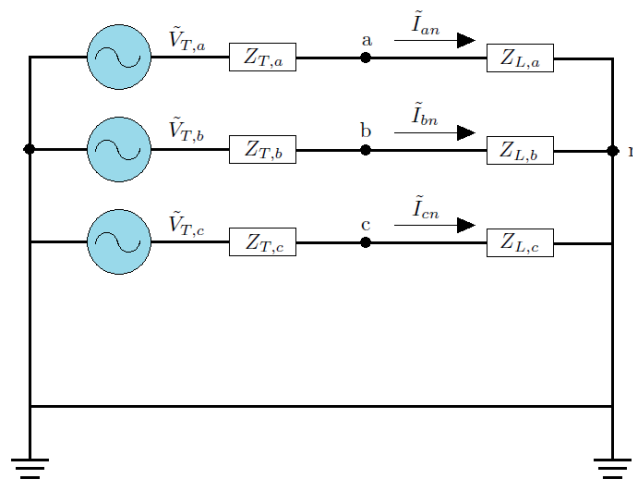


Figure 5.2: Equivalent three phase power plant

The per-phase circuit for n parallel connected gensets is shown in Figure 5.1, while Figure 5.2 shows the equivalent circuit for the power plant. As stated in the previous section, each generator will deliver the terminal voltage \tilde{V}_{as} . From Figure 5.1 it is then clear that when a generator is connected to the bus, the terminal voltage must be equal to the line-to-neutral voltage (\tilde{V}_{an}). Since the circuit is open, the sum of currents out of the gensets must be equal to zero. Hence, the

equivalent Thevenin circuit for a system with n gensets, can be described by (Rizzoni, 2007)

$$\tilde{E}_{a,i} - Z_i \tilde{I}_{as,i} = \tilde{V}_T \quad (5.24)$$

$$\tilde{I}_{as,1} + \tilde{I}_{as,2} + \dots + \tilde{I}_{as,n} = 0 \quad (5.25)$$

In per-unit

$$\tilde{e}_{a,i} - z_i \tilde{i}_{as,i} = \tilde{v}_T \quad (5.26)$$

$$\tilde{i}_{as,1} S_{b,1} + \tilde{i}_{as,2} S_{b,2} + \dots + \tilde{i}_{as,n} S_{b,n} = 0 \quad (5.27)$$

In matrix form this becomes

$$\begin{bmatrix} 0 & S_{b,1} & S_{b,2} & \dots & S_{b,n} \\ 1 & z_1 & 0 & \dots & 0 \\ 1 & 0 & z_2 & \dots & 0 \\ \vdots & \vdots & \vdots & \ddots & \vdots \\ 1 & 0 & 0 & \dots & z_n \end{bmatrix} \begin{bmatrix} \tilde{v}_T \\ \tilde{i}_{as,1} \\ \tilde{i}_{as,2} \\ \vdots \\ \tilde{i}_{as,n} \end{bmatrix} = \begin{bmatrix} 0 \\ \tilde{e}_{a,1} \\ \tilde{e}_{a,2} \\ \vdots \\ \tilde{e}_{a,n} \end{bmatrix} \quad (5.28)$$

Solving for the Thevenin voltage, yields

$$\tilde{v}_T = \frac{\frac{S_{b,1} \tilde{e}_{a,1}}{z_1} + \frac{S_{b,2} \tilde{e}_{a,2}}{z_2} + \dots + \frac{S_{b,n} \tilde{e}_{a,n}}{z_n}}{\frac{S_{b,1}}{z_1} + \frac{S_{b,2}}{z_2} + \dots + \frac{S_{b,n}}{z_n}} \quad (5.29)$$

The Thevenin equivalent impedance is calculated by removing the voltage sources in Figure 5.1, and calculating the resulting impedance as seen from the open-circuit

$$Z_T = \frac{1}{1/Z_1 + 1/Z_2 + \dots + 1/Z_n} \quad (5.30)$$

The active and reactive power consumed by the load is

$$P_{load} + jQ_{load} = 3\tilde{V}_{an} \tilde{I}_{an}^* \quad (5.31)$$

which leads to

$$\tilde{I}_{an} = \frac{P_{load} - jQ_{load}}{3\tilde{V}_{an}^*} \quad (5.32)$$

The equivalent load impedance of all loads connected to the bus is calculated by using Ohm's law

$$Z_L = \frac{\tilde{V}_{an}}{\tilde{I}_{an}} = \frac{3|\tilde{V}_{an}|^2}{P_{load} - jQ_{load}} \quad (5.33)$$

Ohm's law also gives the a-phase bus current and voltage

$$\tilde{I}_{an} = \frac{\tilde{V}_T}{Z_T + Z_L} \quad (5.34)$$

$$\tilde{V}_{an} = \tilde{I}_{an} Z_L = \frac{\tilde{V}_T Z_L}{Z_T + Z_L} \quad (5.35)$$

The per-unit equation for a-phase voltage can then be derived by dividing both sides of (5.35) by the base voltage (V_b)

$$\tilde{v}_{an} = \frac{\tilde{v}_T Z_L}{Z_T + Z_L} \quad (5.36)$$

The complex power for each generator is then found by inserting (5.24) into the general expression for complex power

$$S_i = 3\tilde{V}_{an}\tilde{I}_{an,i}^* = 3\tilde{V}_{an} \left(\frac{\tilde{E}_{a,i} - \tilde{V}_{an}}{Z_i} \right)^* \quad (5.37)$$

The per unit equation is easily found by dividing on both sides by $S_{b,i}$

$$s_i = 3\tilde{v}_{an} \left(\frac{\tilde{e}_{a,i} - \tilde{v}_{an}}{z_i} \right)^* \quad (5.38)$$

Now the active and reactive power are

$$P_i = Re(S_i) \quad (5.39)$$

$$Q_i = Im(S_i) \quad (5.40)$$

And in per unit

$$p_i = Re(s_i) \quad (5.41)$$

$$q_i = Im(s_i) \quad (5.42)$$

5.3 Load sharing

The distribution of active and reactive power between parallel-connected gensets must be controlled. Active power is controlled by the governor, and reactive power is controller by the AVR. There are two main types of load sharing; droop and isochronous. In the model presented in this paper, droop is used, and isochronous load sharing is not considered. Further reading on isochronous load sharing is available in Woodward (2004).

5.3.1 Governor

Droop is defined as "decrease in speed setting as the load increases" (Woodward, 2004). The equation for droop is (Woodward, 2004):

$$\%Droop = \frac{\text{No-load frequency} - \text{Full-load frequency}}{\text{Full-load frequency}} \times 100 \quad (5.43)$$

The engine reference frequency is then:

$$\omega_{error} = \omega_{ref} - \frac{\text{Delivered power}}{\text{Rated power}} \times \text{Droop} \quad (5.44)$$

The frequency error is then found by comparing the reference frequency with the actual frequency in per-unit:

$$e_\omega = \omega_{error} - \omega \quad (5.45)$$

This error is given to a PID-controller that calculates the fuel rate u , which is sent to the engine. Figure 5.3 shows the schematics of droop control of a genset.

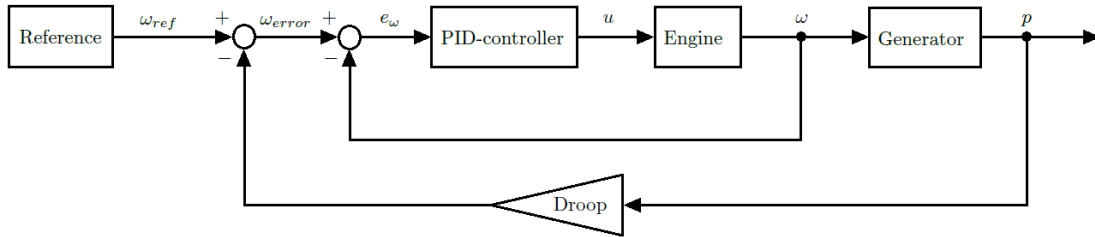


Figure 5.3: Speed droop block diagram, with parameters in per-unit.

When two or more parallel connected gensets share load by speed droop, the load is naturally shared at the balance point where the common network frequency intersects the droop lines. Figure 5.4 illustrates loadsharing between two equal gensets, with 3% droop, and total load equal to the rated power of one genset. The solid line represent equal load sharing, while the dashed line shows a scenario with unbalanced load sharing. As illustrated by the figure, the no-load frequency and droop decides the load sharing and network frequency.

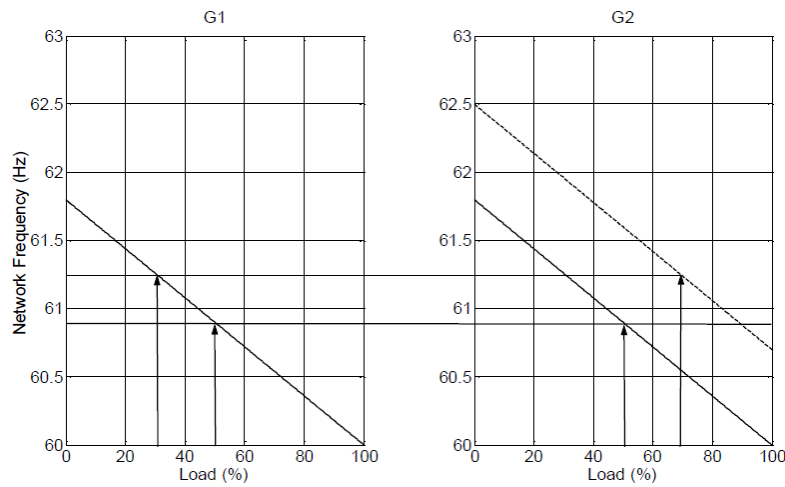


Figure 5.4: Two gensets sharing load by speed droop. Courtesy: IMCA (2010)

5.3.2 AVR

The Automatic Voltage Regulator (AVR) is used to control reactive power and bus voltage. The output of the AVR is the field excitation of the generator. Droop is commonly used for the AVR, and the field voltage is calculated from the reactive power. Figure 5.6 shows the schematics of droop control of a generator.

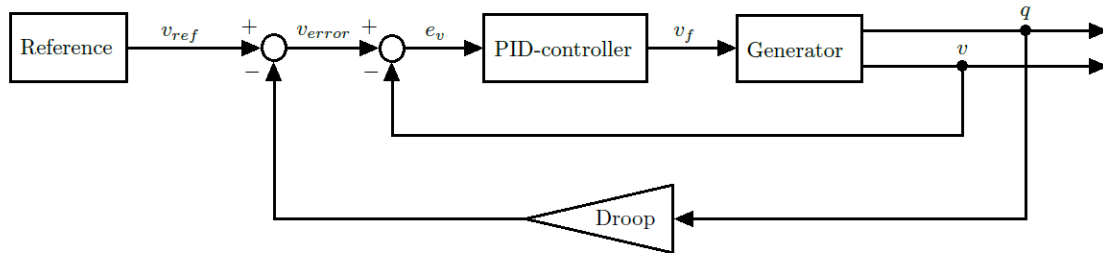


Figure 5.5: Voltage droop block diagram, with parameters in per-unit.

5.4 Resulting simulation plant model

The simulation plant model derived in this section, can now be summarized. Figure 5.6 shows the block diagram for the system, with one genset. The system equations are also displayed in Figure 5.7, for improved readability.

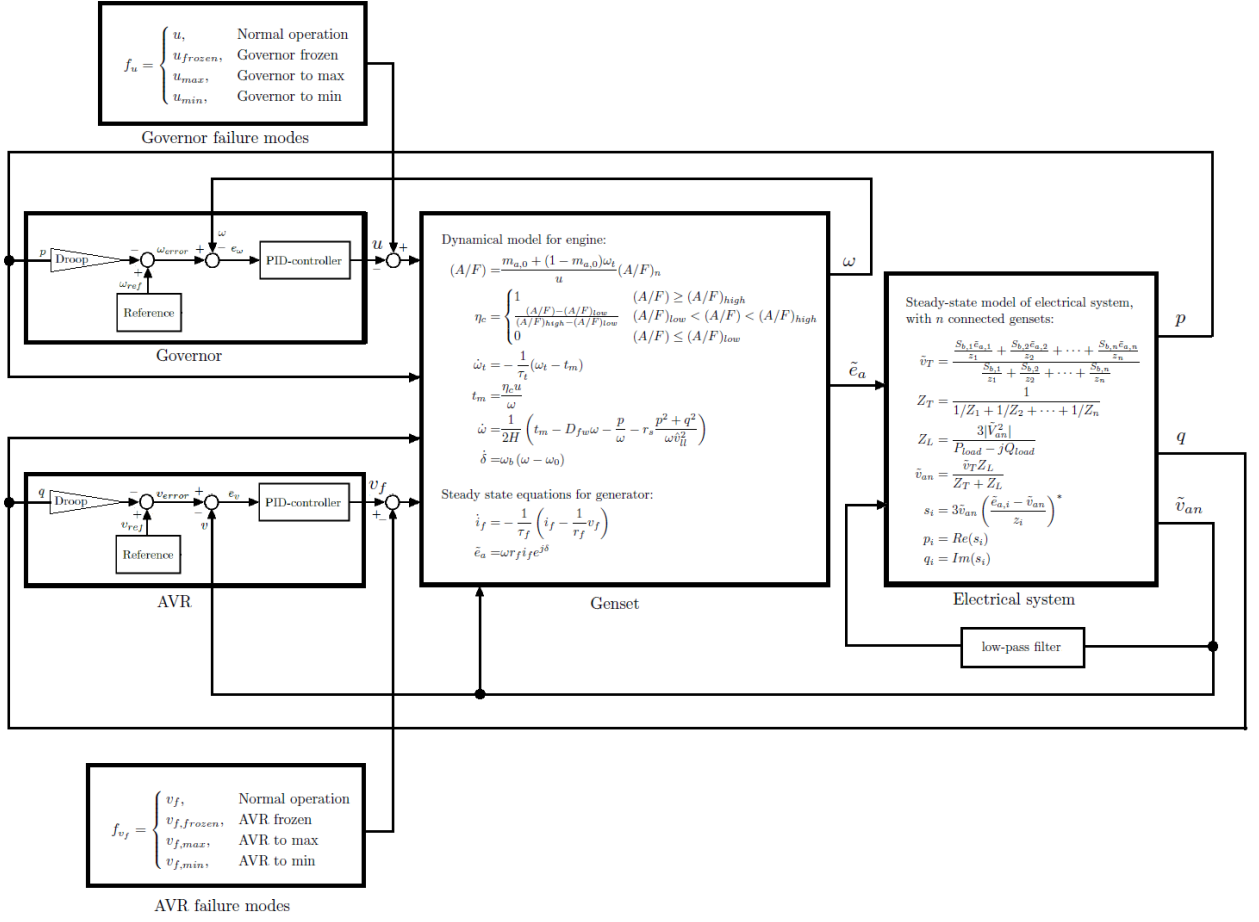


Figure 5.6: Simulation plant block diagram.

Dynamical model for engine:

$$(A/F) = \frac{m_{a,0} + (1 - m_{a,0})\omega_t}{u} (A/F)_n$$

$$\eta_c = \begin{cases} 1 & (A/F) \geq (A/F)_{high} \\ \frac{(A/F) - (A/F)_{low}}{(A/F)_{high} - (A/F)_{low}} & (A/F)_{low} < (A/F) < (A/F)_{high} \\ 0 & (A/F) \leq (A/F)_{low} \end{cases}$$

$$\dot{\omega}_t = -\frac{1}{\tau_t}(\omega_t - t_m)$$

$$t_m = \frac{\eta_c u}{\omega}$$

$$\dot{\omega} = \frac{1}{2H} \left(t_m - D_{fw}\omega - \frac{p}{\omega} - r_s \frac{p^2 + q^2}{\omega \hat{v}_{fl}^2} \right)$$

$$\dot{\delta} = \omega_b (\omega - \omega_0)$$

Steady state equations for generator:

$$i_f = -\frac{1}{\tau_f} \left(i_f - \frac{1}{r_f} v_f \right)$$

$$\tilde{e}_a = \omega r_f i_f e^{j\delta}$$

Steady-state model of electrical system, with n connected gensets:

$$\tilde{v}_T = \frac{\frac{S_{b,1}\tilde{e}_{a,1}}{z_1} + \frac{S_{b,2}\tilde{e}_{a,2}}{z_2} + \dots + \frac{S_{b,n}\tilde{e}_{a,n}}{z_n}}{\frac{S_{b,1}}{z_1} + \frac{S_{b,2}}{z_2} + \dots + \frac{S_{b,n}}{z_n}}$$

$$Z_T = \frac{1}{1/Z_1 + 1/Z_2 + \dots + 1/Z_n}$$

$$Z_L = \frac{3|\tilde{V}_{an}|^2}{P_{load} - jQ_{load}}$$

$$\tilde{v}_{an} = \frac{\tilde{v}_T Z_L}{Z_T + Z_L}$$

$$s_i = 3\tilde{v}_{an} \left(\frac{\tilde{e}_{a,i} - \tilde{v}_{an}}{z_i} \right)^*$$

$$p_i = Re(s_i)$$

$$q_i = Im(s_i)$$

The system contains an algebraic loop which contains Z_L and \tilde{v}_{an} . This is solved by using a low-pass filter.

Figure 5.7: Resulting simulation plant model

6 Simulation study

This section presents simulations done with the simulation plant model. In order to verify the behavior of the load-sharing system, different simulation scenarios are simulated. These scenarios are, normal operation, sudden load change, sudden disconnection of a genset, and all the defined failure modes.

All simulations are conducted with three gensets connected in parallel, and with the parameters displayed in Table 6.2 to ???. The generator parameters are found in (Krause et al., 2002), while the turbocharger parameters are found in (Xiros, 2002). However, some of the parameters are adjusted in order to make the simulator more stable.

The simulator requires careful tuning and initialization, in order to work in a desired way. The turbocharger imposes one challenge. The turbocharger model is made so that the fuel index must be within a small window of values, in order to enable maximum mechanical torque. Both too large and too small fuel index causes the mechanical torque to drop. This makes the tuning of the governor, and limitation of the fuel index, challenging. In addition, the algebraic loop necessary for calculating the bus voltage and load impedance, is unstable for too low excitation voltages. In order to ensure stability, the no-load frequency and no-load voltage are set quite high.

Parameter name	Symbol	Unit	Value
Base voltage	V_b	[kV]	45
Electric base frequency	ω_b	[rad/s]	377

Table 6.1: System parameters

Parameter name	Symbol	Unit	Genset 1	Genset 2	Genset 3
Number of poles	N	[-]	2	2	2
Rated power	$S_{b,i}$	[MVA]	835	835	835
Inertia constant	H	[s]	5.6	5.6	5.6
Damping gain	D_{fw}	[-]	0.03	0.03	0.03
Nominal air-to-fuel ratio	$(A/F)_n$	[kg/kg]	30	30	30
Lower air-to-fuel ratio	$(A/F)_{low}$	[kg/kg]	14	14	14
Higher air-to-fuel ratio	$(A/F)_{high}$	[kg/kg]	23	23	23
Airflow ratio	$m_{a,0}$	[-]	0.9	0.9	0.9
Turbocharger time constant	τ_t	[s]	5	5	5
Field winding time constant	τ_f	[s]	0.0024	0.0024	0.0024
Field winding resistance	r_f	[p.u.]	1	1	1
Stator resistance	r_s	[p.u.]	0.003	0.003	0.003
Stator reactance	x_s	[p.u.]	1.8	1.8	1.8

Table 6.2: Genset parameters

Parameter name	Unit	Genset 3	Genset 2	Genset 3
Droop in governor	[%]	5	5	5
No-load speed	[p.u.]	1.05	1.05	1.05
P-gain in governor	[-]	100	100	100
I-gain in governor	[-]	30	30	30
D-gain in governor	[-]	0	0	0
Fuel rate lower constraint	[-]	0.1	0.1	0.1
Fuel rate higher constraint	[-]	1.25	1.25	1.25
Droop in AVR	[%]	5	5	5
No-load voltage	[p.u.]	1.05	1.05	1.05
P-gain in AVR	[-]	10	10	10
I-gain in AVR	[-]	5	5	5
D-gain in AVR	[-]	0	0	0
Field voltage lower constraint	[p.u.]	0.5	0.5	0.5
Field voltage higher constraint	[p.u.]	2	2	2

Table 6.3: Governor and AVR controller gains and parameters

Parameter name	Unit	Value
Governor frozen	[-]	0.5
Governor to min	[-]	0
Governor to max	[-]	1.25
AVR frozen	[p.u.]	1.9
AVR to min	[p.u.]	1.799
AVR to max	[p.u.]	2

Table 6.4: Failure mode parameters

6.1 Normal operation modes

The normal operation modes, represent scenarios that should be handled by the fault detection system. These are also scenarios, suited for verifying the model behavior. The scenarios represented here are, sudden active load change, sudden reactive load change, and sudden disconnection of one genset. All simulations are run with three gensets connected in parallel, and all events occur after 20 seconds. The simulation results not displayed in this section are available in Appendix B.

6.2 Active load increase

Figure 6.1 shows the simulation results for the simulator with a sudden active load increase. The simulator is run with reactive load constant at 50 % of rated power. The active power increases from 1 % , to 100 % of total rated power.

It is seen that the simulator mostly behaves as expected. It is expected that the voltage would have some small variations. However, the expected voltage changes might not be simulated due to the steady state model of the genset, since the time delay of the stator flux linkage is not modeled. This is also confirmed by Bø (2011). Since the voltage change was expected to be short lasting, and then go back to the previous value, this disadvantage with the model is considered acceptable.

6.3 Reactive load increase

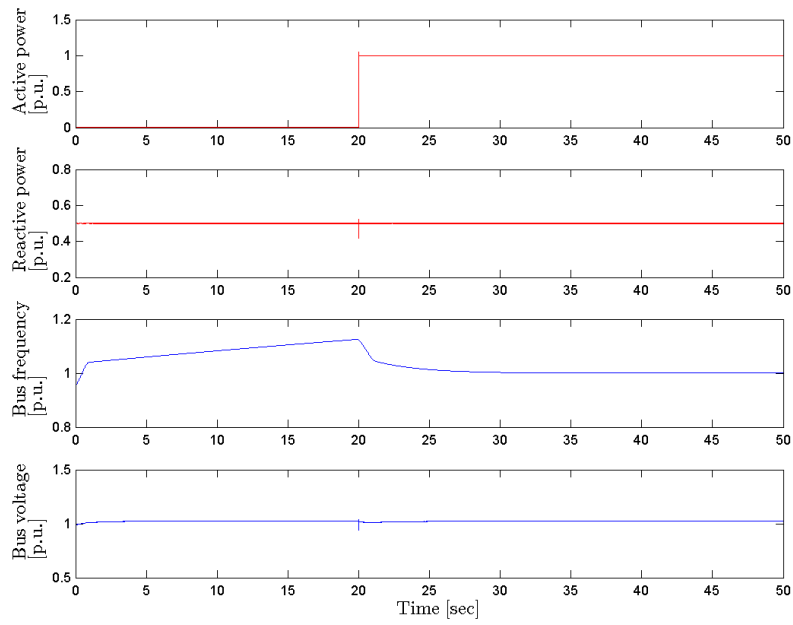
Figure 6.2 shows the simulation results for the simulator with a sudden reactive load increase. The simulator is run with active load constant at 100 % of rated power. The reactive power increases from 1% to 100 % of the total rated power.

It is seen that as the reactive power increase occurs, the bus voltage, reactive power and field current makes a step. This is as expected as these are the variables mostly dependent on the reactive power. It is also seen that the AVR quickly stabilizes the bus voltage on a new value.

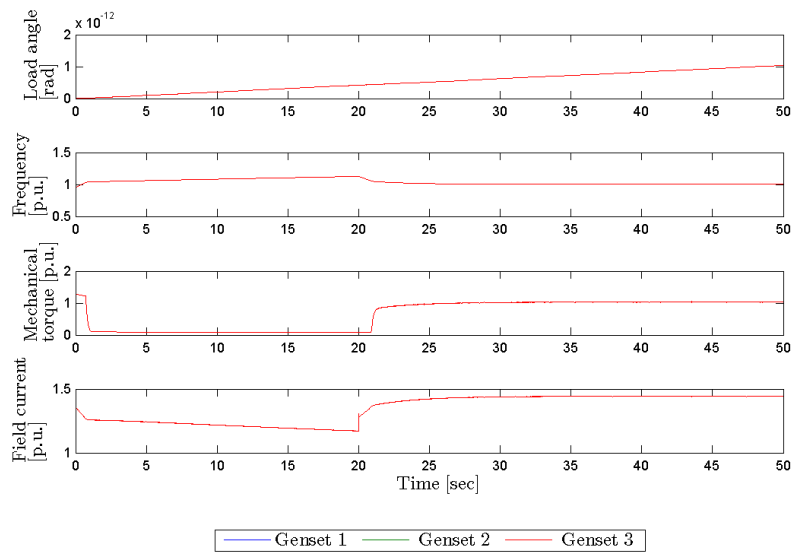
6.4 Disconnection of one genset

Figure 6.3 shows the simulation results for the simulator, when Genset 3 is disconnected after 20 seconds. The simulation is run with active load at 60 % of rated power, and reactive load % of rated power.

When the genset is disconnected, it is seen that the still connected gensets quickly picks up the active and reactive load. From the gensets states (Figure 6.3b) it is seen that the connected gensets quickly adjusts to the new situation, and increases the system variables accordingly. It is also seen that the bus frequency and bus voltage, have a quick deviation from the desired values, before they stabilize. The bus voltage and bus frequency both respond with a small drop, which is as expected since the disconnection causes the active and reactive power to increase.

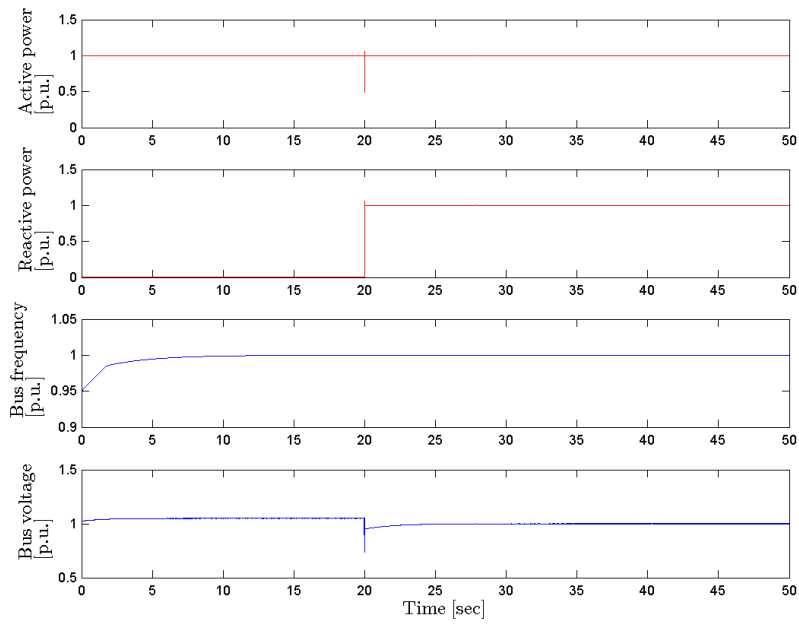


(a) Genset produced power and electrical parameters

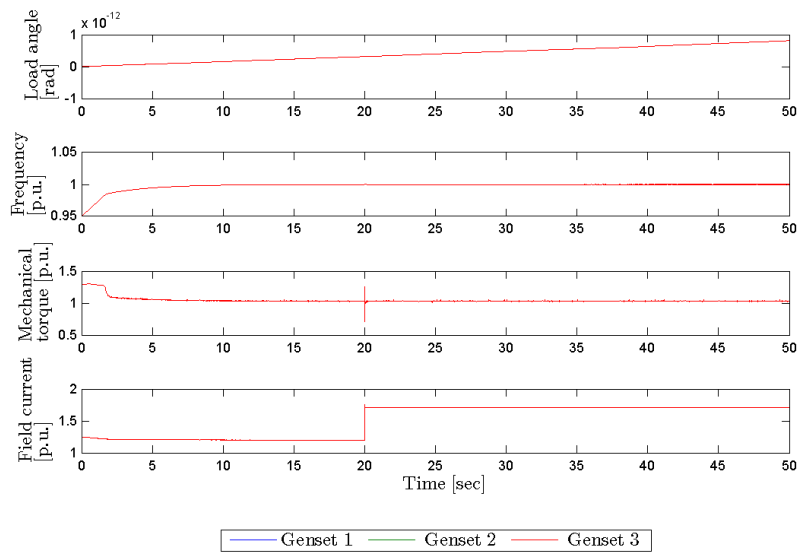


(b) Genset states

Figure 6.1: Results from simulation with sudden active load increase occurring after 20 seconds.

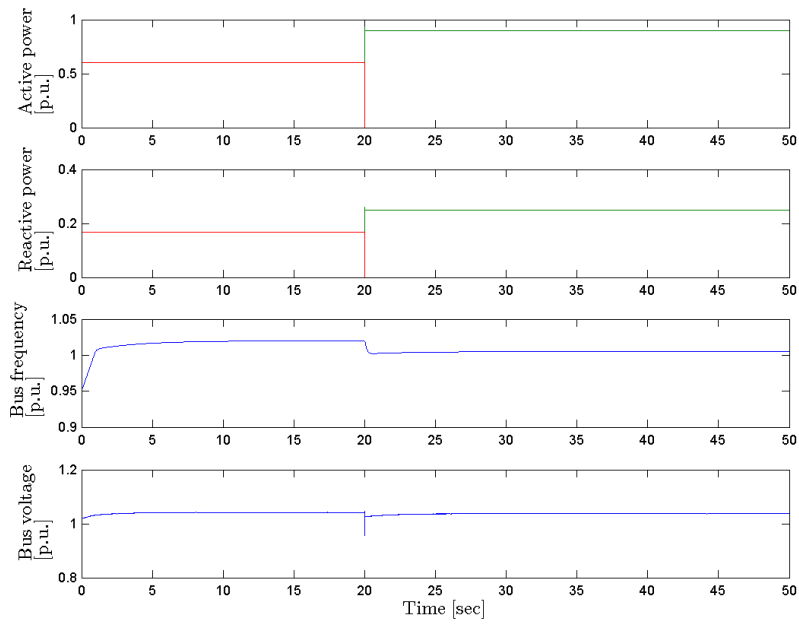


(a) Genset produced power and electrical parameters

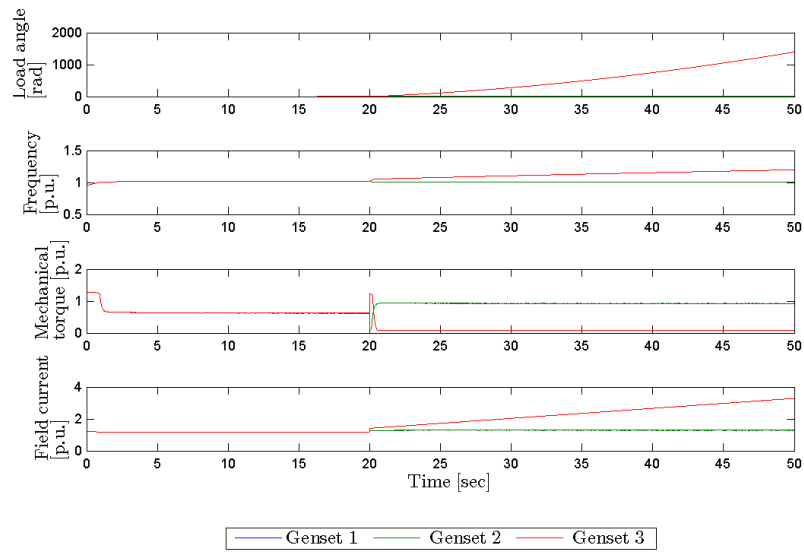


(b) Genset states

Figure 6.2: Results from simulation with sudden reactive load increase occurring after 20 seconds.



(a) Genset produced power and electrical parameters



(b) Genset states

Figure 6.3: Results from simulation with sudden disconnection of Genset 3 after 20 seconds.

6.5 Governor faults

The governor faults are implemented in accordance with (4.2), and with the values in Table 6.4. Further, all simulations are run with three parallel connected gensets, and with bus active load power equal to 60 % of total rated power, and bus reactive load power equal to 50% of the rated power. For all simulations the failure modes are implemented in Genset 1, and occurring after 20 seconds. The simulator has no fault detection and/or handling system, the long term reaction on the occurrence of a failure might therefore not be representative for a real system. For example, a real system would have protection relays installed, that would disconnect gensets and equipment when the system behaves abnormal.

6.5.1 Governor to minimum

Figure C.8 shows the simulation results, when the failure mode governor to minimum is implemented. As expected, the active power produced by the faulty genset decreases, while the active power produced by the healthy gensets increases accordingly. It is obvious that the healthy gensets are picking up the load discharged by faulty genset. Further, the bus frequency decreases. This is also as expected, the faulty genset frequency decreases since less fuel is supplied, while the healthy gensets frequency decreases, as the load increases. The reactive power, and bus voltage, are little affected by the fault. However, some voltage changes would be expected, if the simulator was not based on a steady-state model.

The simulated states for the three gensets are also as expected. The load angle increases or decreases according to the active power produced by the genset. As with the bus frequency, the genset frequencies are also decreasing. The faulty genset mechanical torque drops to zero, as too little fuel is injected, while the healthy gensets have a small increase, due to the increased load. To ensure prevent a voltage change, it is also seen that the field current is slowly increased.

6.5.2 Governor to maximum

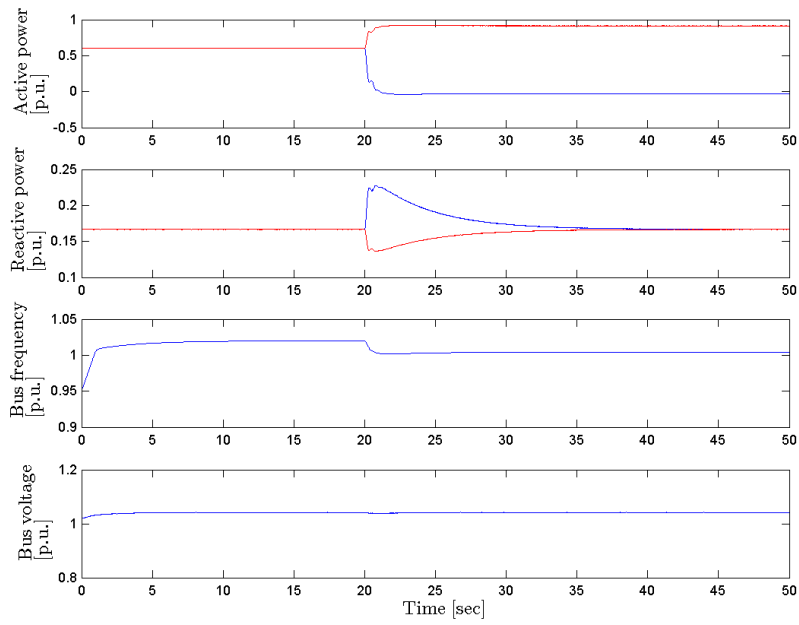
Figure 7.5 shows the simulation results, when failure mode governor to maximum is implemented. As expected, the faulty genset produces more active power, while the healthy gensets decreases the active power production accordingly. In addition, the bus frequency is increased, as would be expected. In the same way, the produced active power, and bus voltage, only have minor changes. In the same way as with the previous simulations, the lack of voltage changes, are due to the steady state genset model.

The states also behaves as expected. The load angle increases and/or decreases in accordance with the increased or decreased active power. As with the bus frequency, the genset frequencies have a small increase. The faulty genset mechanical torque, has a sudden jump to a high value where it stabilizes, as a reaction to the continuous high amount of injected fuel. While, the healthy gensets adjusts to a lower mechanical torque value, as a response to the lowered power requirement.

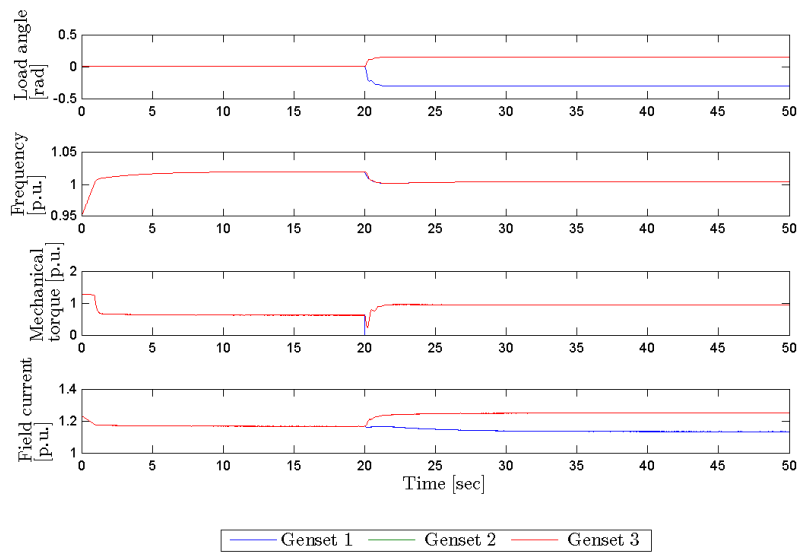
6.5.3 Governor frozen

Figure C.9 shows the simulation results, when the failure mode governor frozen is implemented. It is obvious that this failure mode, with the chosen fuel index, causes the faulty genset to produce

less active power than expected. Although the reaction to the fault is on a smaller scale, the same conclusions as with governor to minimum can be drawn.

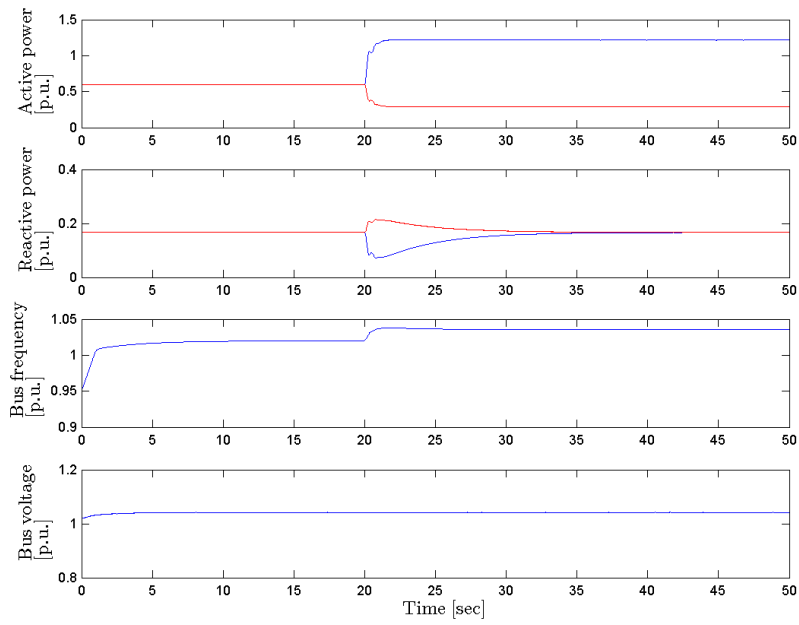


(a) Genset produced power and electrical parameters

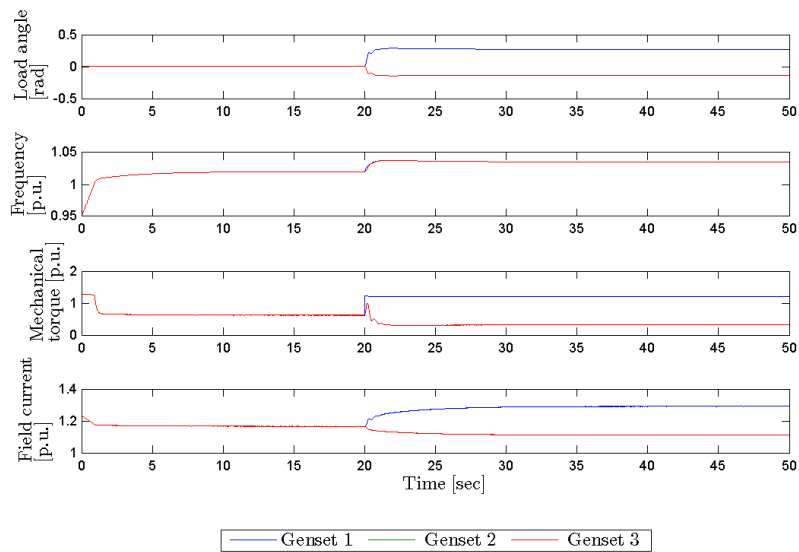


(b) Genset states

Figure 6.4: Results from simulation with failure mode governor to minimum for Genset 1, occurring after 20 seconds.

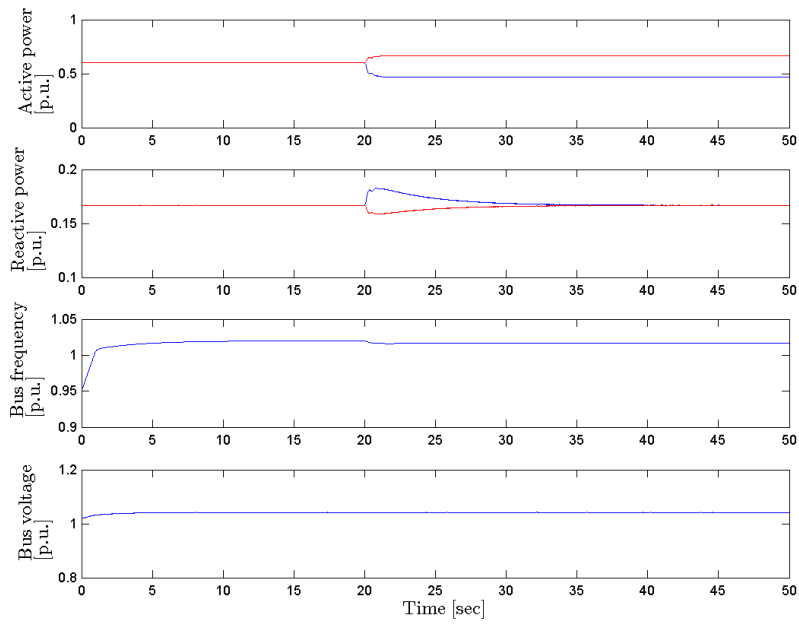


(a) Genset produced power and electrical parameters

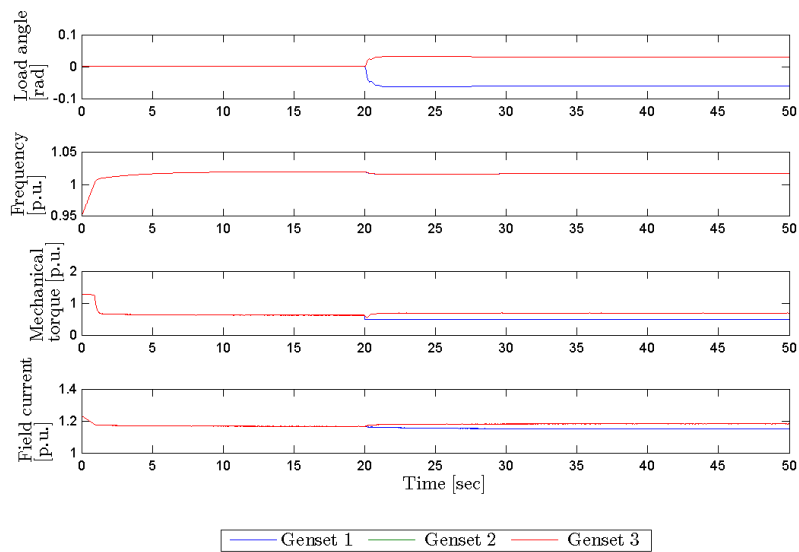


(b) Genset states

Figure 6.5: Results from simulation with failure mode governor to maximum for Genset 1, occurring after 20 seconds.



(a) Genset produced power and electrical parameters



(b) Genset states

Figure 6.6: Results from simulation with failure mode governor frozen for Genset 1, occurring after 20 seconds.

6.6 AVR faults

The governor faults are implemented in accordance with (4.4), and with the values in Table 6.4. As with the governor faults, all simulations are run with three parallel connected gensets, and with bus active load power equal to 60 % of total rated power, and bus reactive load power equal to 50% of the rated power. For all simulations the failure modes are implemented in Genset 1, and occurring after 20 seconds. The simulator has no fault detection and/or handling system, the long term reaction on the occurrence of a failure might therefore not be representative for a real system.

6.6.1 AVR to minimum

Figure C.10 shows the simulation results for failure mode AVR to minimum. As expected, it can be seen that the reactive power produced by the faulty genset drops to zero. As a response to this, the healthy gensets increase the produced reactive power accordingly. The bus voltage, however, does not decrease as expected. This might be caused by the steady state model for the genset and electrical system. Further, the fault only causes small variations in the active power, and bus frequency. This is also as expected, since the active power is controlled by the governor, and the bus frequency is mainly dependent on the genset frequencies

The states also behaves as expected. Both the change in load angle and frequency, are very small. The mechanical torque, need some time to adjust, but afterwards there is no change. The field current, however, is decreased.

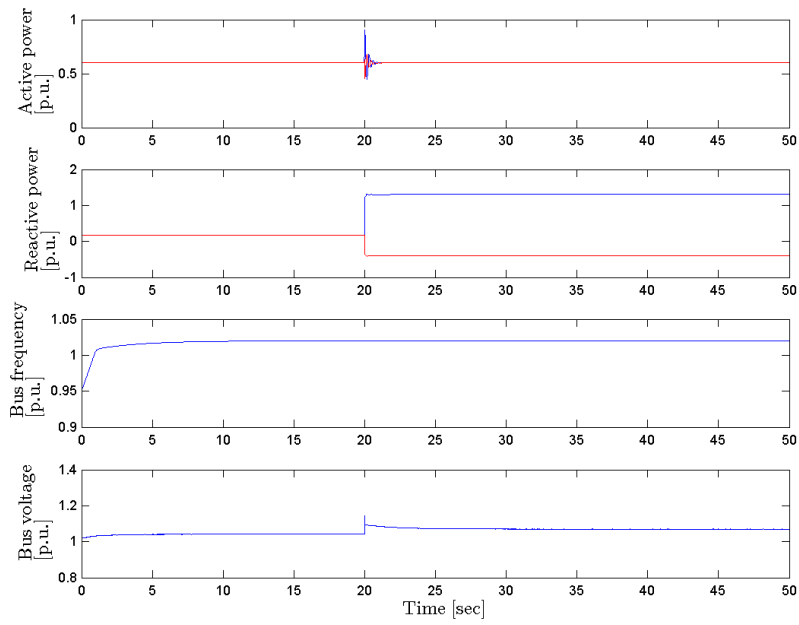
6.6.2 AVR to maximum

Figure 7.7 shows the simulation results for failure mode AVR to maximum. It can be seen that the reactive power produced by the faulty genset has a sudden increase. This causes the reactive power produced by the healthy gensets, to drop accordingly. As expected, the active power and bus frequency, are just slightly effected.

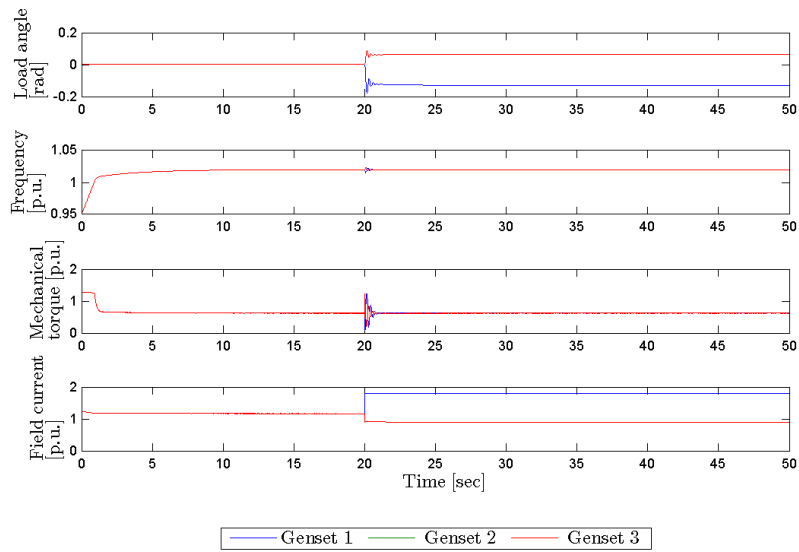
For the states, the field current is increasing for the faulty genset, while it is decreasing for the healthy gensets. This is as expected, since increased field voltage causes increased field current. Further, the mechanical torque, is unaffected after it have had some time to adjust, while the frequency has no reaction. The load angle, has a larger response than expected. However, it is still small enough to be considered acceptable.

6.6.3 AVR frozen

Figure C.11 shows the simulation results, when the failure mode AVR frozen is implemented. It is obvious that this failure mode, with the chosen field voltage, causes the faulty genset to produce more reactive power than expected. Although the reaction to the fault is on a smaller scale, the same conclusions as with AVR to maximum can be drawn.

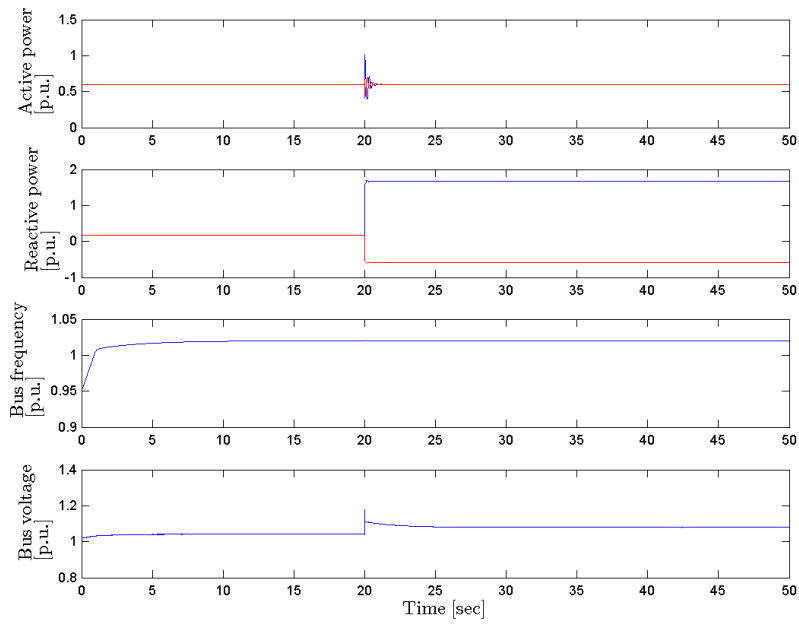


(a) Genset produced power and electrical parameters

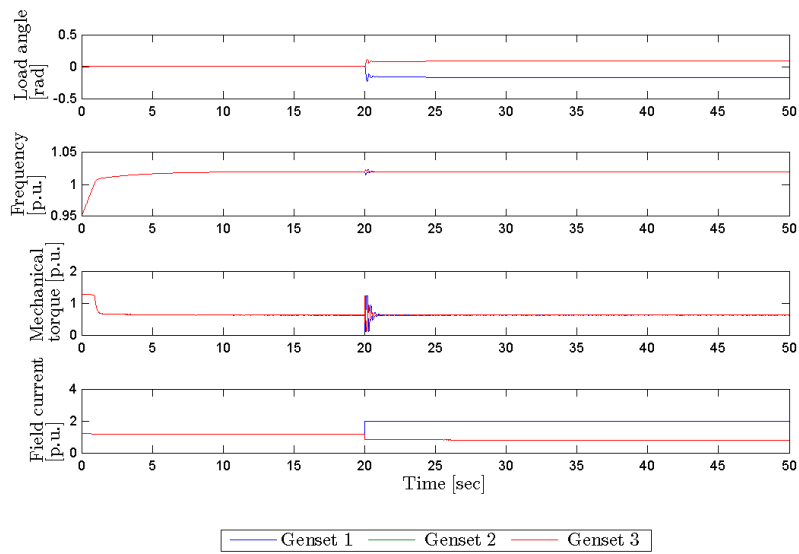


(b) Genset states

Figure 6.7: Results from simulation with failure mode AVR to minimum for Genset 1, occurring after 20 seconds.

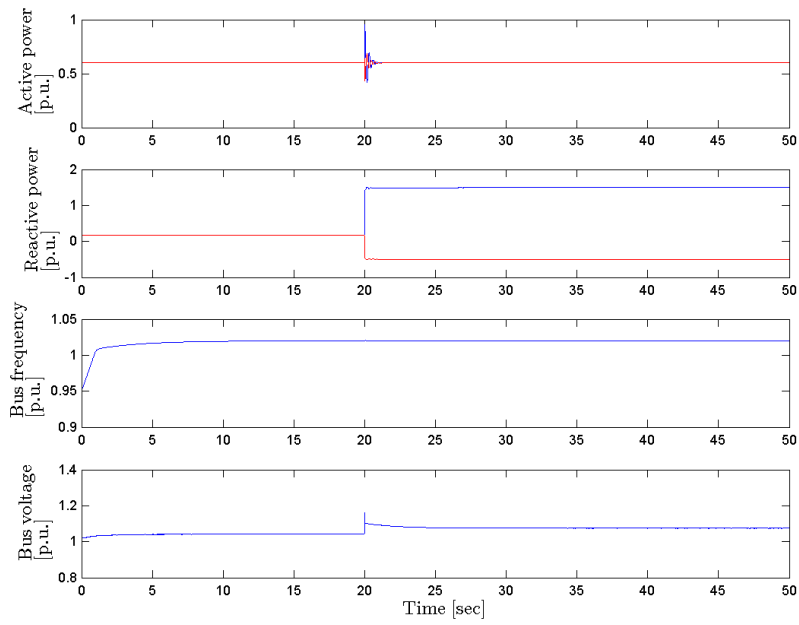


(a) Genset produced power and electrical parameters

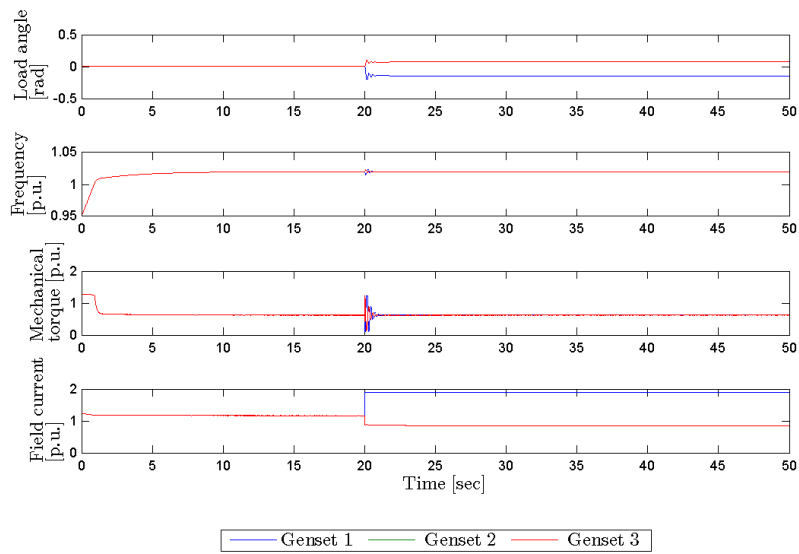


(b) Genset states

Figure 6.8: Results from simulation with failure mode AVR to maximum for Genset 1, occurring after 20 seconds.



(a) Genset produced power and electrical parameters



(b) Genset states

Figure 6.9: Results from simulation with failure mode AVR frozen for Genset 1, occurring after 20 seconds.

7 Control plant model and observer design

In this section the models used for development of the fault detection algorithms are derived. Two different model based fault detection algorithms are developed in this thesis; observer based fault detection, and analytical redundancy relations.

A control plant model is used to mirror the real system, and should be able to reflect the main characteristics of the system, while at the same time be quick enough to ensure real-time calculations. In addition, the model must be suitable as a basis for the observer or redundancy relation. The latter requirement often decides the complexity of the model, as a too advanced model both will be unsuited as a basis for design, and complicate the stability analysis of the fault detection algorithm.

In this section a control plant model for the load sharing system is derived. Then an observer based on the control plant model is developed. The control plant model estimates the real system behavior, based on inputs from the governor and AVR, and system measurements. In the control plant model the bus frequency (ω_0) and bus line-to-line voltage ($\hat{v}_{ll} = \sqrt{3}\hat{v}_{an}$), are taken as inputs. This is however, not correct as these clearly are not controller outputs, but must be measured in the real system. Since both the bus frequency and voltage are "relative variables", they are defined relative to a chosen reference frame, they can be considered as input reference values to the control plant model. For convenience however, in the following the bus frequency and voltage will be treated as regular system inputs.

7.1 Nonlinear control plant model

The nonlinear control plant model is a simplified version of the simulation plant model. The rotational dynamics is mainly the same as for the simulation plant model. The main difference is that the limiting effect of the turbocharger is not included, instead a steady state model of the mechanical torque is used. Skjetne (2012) suggests the following dynamic model for the states in a diesel-electric power plant

$$\dot{\delta} = \omega_b (\omega - \omega_0) \quad (7.1)$$

$$\dot{\omega} = \frac{1}{2H} \left(t_m - D_{fw}\omega - \frac{p}{\omega} - r_s \frac{p^2 + q^2}{\omega \hat{v}_{ll}^2} \right) \quad (7.2)$$

$$\dot{t}_m = -\frac{1}{\tau_e} t_m + \frac{D_{fw} + 1}{\tau_e} u \quad (7.3)$$

$$\dot{i}_f = -\frac{1}{\tau_f} i_f + \frac{1}{\tau_f r_f} v_f \quad (7.4)$$

Where $\tau_e \approx \frac{0.9}{\omega_{b,m}}$ is the time constant of the cylinder, and the other parameters are as defined in Section 5.

For the outputs the model suggested by Skjetne (2012) is used. The active and reactive power produced by the generator is initially quite similar to (5.41) and (5.42), used in the simulation plant model. However, the stator resistance is assumed to be negligible and the equations are

linearized around $\delta = 0$, $\omega = 1$, and $\hat{e}_a = \hat{v}_{an} = 1$. The resulting equations for the outputs are

$$\omega = \omega \quad (7.5)$$

$$p = \frac{1}{x_s} \delta \quad (7.6)$$

$$q = \frac{1}{x_s} (\hat{e}_a - \hat{v}_U) \quad (7.7)$$

where

$$\hat{e}_a = r_f \omega i_f \quad (7.8)$$

The faults of interest can be modeled in the control plant model, in the same way as described in Section 5. Further, inserting (7.6) and (7.7) in (7.2), and (7.8) in (7.7), then gives the nonlinear control plant model states

$$\dot{\delta}_i = \omega_b (\omega - \omega_0) \quad (7.9)$$

$$\dot{\omega} = \frac{1}{2H} \left(t_m - D_{fw} \omega - \frac{1}{x_s} \frac{\delta}{\omega} - \frac{r_s}{x_s^2} \frac{\delta^2}{\omega \hat{v}_U^2} - \frac{r_s}{x_s^2} \frac{(r_f \omega i_f - \hat{v}_U)^2}{\omega \hat{v}_U^2} \right) \quad (7.10)$$

$$\dot{t}_m = -\frac{1}{\tau_e} t_m + \frac{D_{fw} + 1}{\tau_e} u + \frac{D_{fw} + 1}{\tau_e} f_u \quad (7.11)$$

$$\dot{i}_f = -\frac{1}{\tau_f} i_f + \frac{1}{\tau_f r_f} v_f + \frac{1}{\tau_f r_f} f_{v_f} \quad (7.12)$$

and measurements

$$\omega = \omega \quad (7.13)$$

$$p = \frac{1}{x_s} \delta \quad (7.14)$$

$$q = \frac{1}{x_s} (r_f \omega i_f - \hat{v}_U) \quad (7.15)$$

7.2 Design of nonlinear Luenberger-type observer

In this section a nonlinear Luenberger-type observer is derived. First, based on the control plant model, the state space model used as basis for the design is derived, and the model observability is analyzed. Then, the nonlinear Luenberger-type observer is derived, and its stability properties are analyzed. To verify the observer design, tests are performed against a simulator based on the used control plant model. Finally, the actual performance of the observer is demonstrated, by simulation tests with the simulation plant model derived in Section 5.

7.2.1 State space model

The nonlinear Luenberger-type observer, is based on a control plant model where the state equations consist of a linear function of the states and the inputs, and a nonlinear function of the inputs and measurements. The measurements must be linear. This is achieved by using the nonlinear model for the states in (7.1) to (7.4). First order Taylor's expansion is then used to linearize (7.15),

about the points ω_p and $i_{f,p}$.

The derived system can then be written on the desired matrix form

$$\dot{\mathbf{x}} = \mathbf{A}\mathbf{x} + \mathbf{B}\mathbf{u} + \mathbf{f}(\mathbf{u},\mathbf{y}) \quad (7.16)$$

$$\mathbf{y} = \mathbf{C}\mathbf{x} + \mathbf{D}\mathbf{u} \quad (7.17)$$

where

$$\mathbf{x} = [\delta \quad \omega \quad t_m \quad i_f]^T \quad (7.18)$$

$$\mathbf{u} = [\omega_0 \quad \hat{v}_{ll} \quad u \quad v_f]^T \quad (7.19)$$

$$\mathbf{y} = [\omega \quad p \quad q]^T \quad (7.20)$$

$$\mathbf{A} = \begin{bmatrix} 0 & \omega_b & 0 & 0 \\ 0 & -\frac{1}{2H}D_{fw} & \frac{1}{2H} & 0 \\ 0 & 0 & -\frac{1}{\tau_e} & 0 \\ 0 & 0 & 0 & -\frac{1}{\tau_f} \end{bmatrix} \quad (7.21)$$

$$\mathbf{B} = \begin{bmatrix} -\omega_b & 0 & 0 & 0 \\ 0 & 0 & 0 & 0 \\ 0 & 0 & \frac{D_{fw}+1}{\tau_e} & 0 \\ 0 & 0 & 0 & \frac{1}{\tau_f r_f} \end{bmatrix} \quad (7.22)$$

$$\mathbf{f}(\mathbf{u},\mathbf{y}) = \begin{bmatrix} 0 \\ \frac{1}{2H} \left(-\frac{p}{\omega} - r_s \frac{p^2+q^2}{\omega \hat{v}_{ll}^2} \right) \\ 0 \\ 0 \end{bmatrix} \quad (7.23)$$

$$\mathbf{C} = \begin{bmatrix} 0 & 1 & 0 & 0 \\ \frac{1}{x_s} & 0 & 0 & 0 \\ 0 & \frac{1}{x_s} r_f i_{f,p} & 0 & \frac{1}{x_s} r_f \omega_p \end{bmatrix} \quad (7.24)$$

$$\mathbf{D} = \begin{bmatrix} 0 & 0 & 0 & 0 \\ 0 & 0 & 0 & 0 \\ 0 & -\frac{1}{x_s} & 0 & 0 \end{bmatrix} \quad (7.25)$$

Observability

The system is proved to be observable by calculating the observability matrix

$$\mathbf{O} = \left[\mathbf{C}^T \quad (\mathbf{C}\mathbf{A})^T \quad \dots \quad (\mathbf{C}\mathbf{A}^{n-1})^T \right]^T \quad (7.26)$$

where n is the number of states. For the above system n is equal to 4. Since \mathbf{O} has rank equal to n , the system is observable (Chen, 2009). Calculation of the observability matrix and the rank, is performed in Matlab.

7.2.2 Design of observer and fault detection algorithm

Observer design

Arcak et al. (2001) suggests that for a system on the same form as (7.16), a nonlinear Luenberg-type observer can be used. Hence, the observer is designed by duplicating the original system and adding a correcting term, $\mathbf{L}\tilde{\mathbf{y}}$

$$\begin{aligned}\dot{\hat{\mathbf{x}}} &= \mathbf{A}\hat{\mathbf{x}} + \mathbf{B}\mathbf{u} + \mathbf{f}(\mathbf{u}, \mathbf{y}) + \mathbf{L}\tilde{\mathbf{y}} \\ \hat{\mathbf{y}} &= \mathbf{C}\hat{\mathbf{x}} + \mathbf{D}\mathbf{u}\end{aligned}\tag{7.27}$$

where

$$\tilde{\mathbf{y}} = \mathbf{y} - \hat{\mathbf{y}}\tag{7.28}$$

The state estimation error is

$$\tilde{\mathbf{x}} = \mathbf{x} - \hat{\mathbf{x}}\tag{7.29}$$

Then the dynamics of the state estimation error is

$$\dot{\tilde{\mathbf{x}}} = (\mathbf{A} - \mathbf{L}\mathbf{C})\tilde{\mathbf{x}}\tag{7.30}$$

$$\tilde{\mathbf{y}} = \mathbf{C}\tilde{\mathbf{x}}\tag{7.31}$$

Observer stability

Equation (7.30) is linear and on the form $\dot{x} = Ax$. A system on this form is stable if A is Hurwitz. Therefore the observer is stable if the real part of all eigenvalues of $(\mathbf{A} - \mathbf{L}\mathbf{C})$ are negative (Khalil, 1996). Since the pair (\mathbf{A}, \mathbf{C}) is observable, all eigenvalues of $(\mathbf{A} - \mathbf{L}\mathbf{C})$ can be assigned arbitrarily by selecting a real constant vector \mathbf{L} (Chen, 2009). Hence, the observer can be tuned to be globally exponentially stable. This means that the error between the estimated state and the actual state will go towards zero.

7.3 Observer verification

To verify the performance of the observer, it is run against the control plant model used as basis for the design. The simulations are performed for both normal operation and the different failure modes.

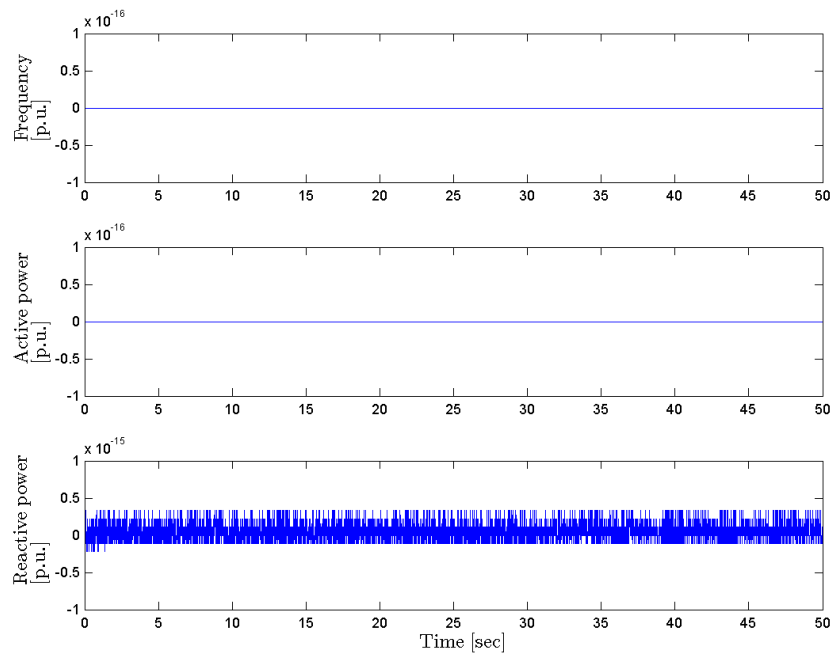
For this purpose, the control plant model in (7.16) and (7.17) is used to develop a simulator of the system in the Matlab/Simulink. In the simulator, the same governor, AVR, and faults, as in the simulation plant model are used. Further, the observer is implemented in the simulator and connected to the control plant model simulator. The governor and AVR signals used as observer input, do not include the modeled faults. The correcting term (\mathbf{L}) is set equal to zero, as the observer should give a perfect estimation of the states and measurements.

The main challenge when making the simulator, is the calculation of the input reference values, namely the bus line-to-line voltage (\hat{v}_{ll}), and bus frequency (ω_0). The calculation of these values introduces two algebraic loops to the system. Since the purpose of the simulator is to verify the observer, it is not acceptable that the calculations in the simulator and the observer are performed based on different inputs. Care must therefore be taken when choosing a method to solve the algebraic loops. For the bus frequency, this is solved by using the derivative of the load angle ($\dot{\delta}$)

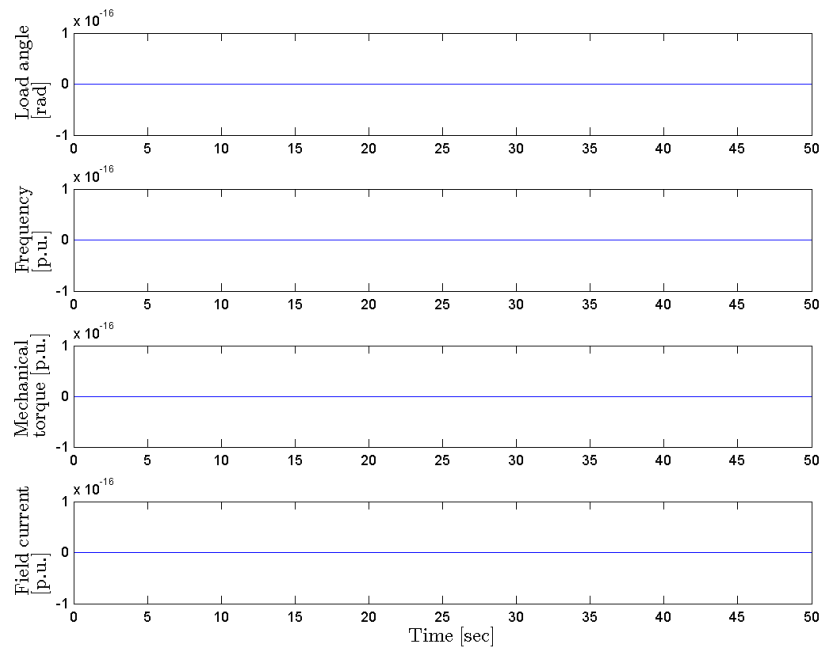
from the last time step, and the current frequency (ω), to solve (7.16) for the bus frequency. This should not have any effect on the observer verification, as the same bus frequency is used as input to both the simulator and the observer. For the bus line-to-line voltage, the reactive load power, frequency, and field current, is used to solve (7.17) for the bus voltage. This solution is somewhat unstable, and introduces a small instability in the order of 10^{-16} . This is however, considered small enough to be negligible.

7.3.1 Normal operation

Figure 7.1 shows the measurement and state estimation error for the observer run against the control plant model. It is seen that both states and measurements are perfectly estimated by the observer, there are zero error. The small reactive power estimation error in Figure 7.1a, is probably caused by the instability error introduced from calculating the bus voltage. The error is in the order of 10^{-16} , and is therefore so small that it can be considered negligible. Based on this, it can be concluded that the observer works as expected.



(a) Measurement estimation error



(b) State estimation error

Figure 7.1: Measurement and state error, for observer run against control plant model, normal operation

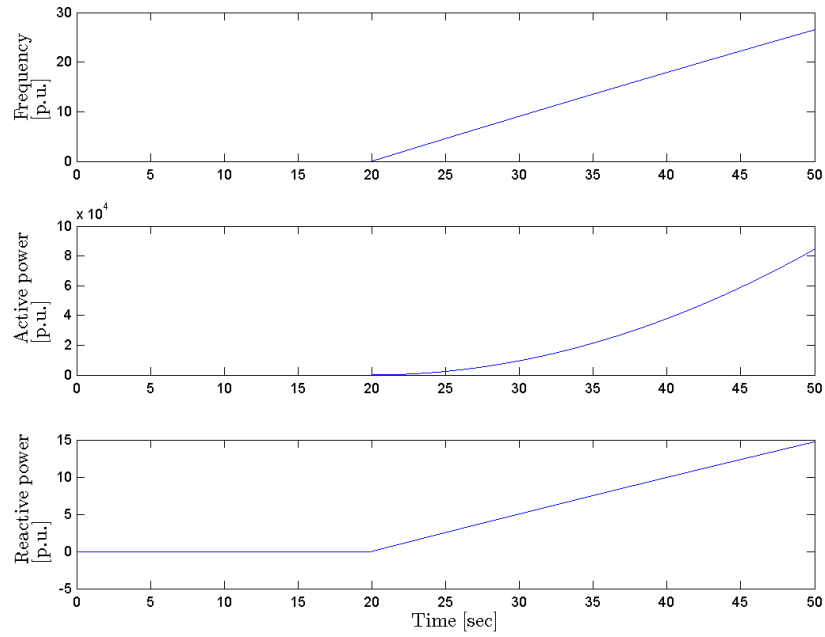
7.3.2 Failure modes

Figure 7.5 shows the behavior of the state and measurement error, when the fault governor to maximum is applied to the simulated control plant model after 20 seconds. The simulation results, for the other governor failure modes, can be found in Appendix C.1.1.

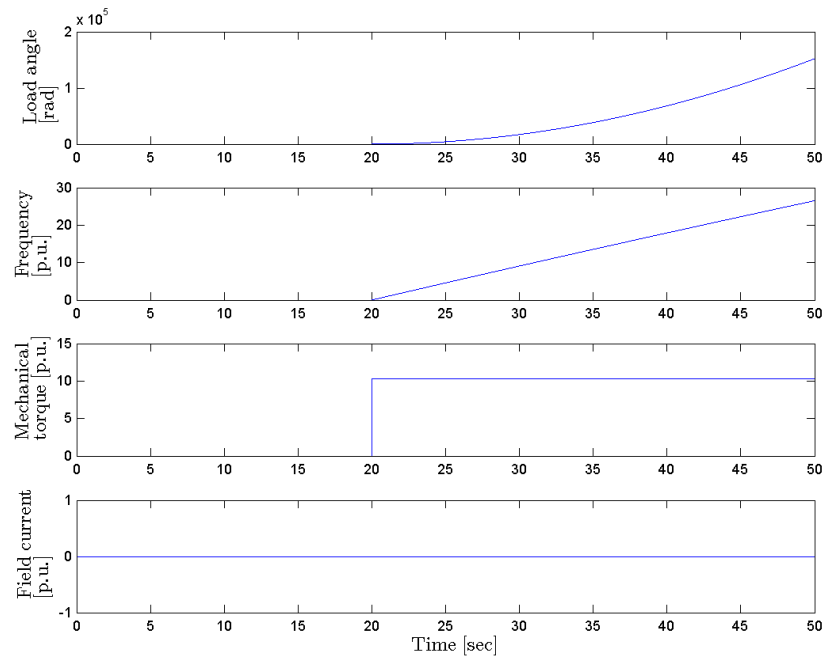
It can be seen that the governor fault has a sudden effect on the estimated mechanical torque error, before this stays on a steady error value. This is the only equation that has the fuel rack position as direct input, so this behavior is as expected. Further, the estimated load angle error, and the estimated frequency error, increases. Since both these states have the fuel rack position as indirect inputs, this is as expected. In the same way, the undisturbed value of the estimated field current error, is expected since it is independent of the fuel rack position.

Figure 7.7 shows the behavior of the state and measurement estimation error, when the fault AVR to maximum, is applied to the simulated control plant model after 20 seconds. The simulation results, for the other AVR failure modes, can be found in Appendix C.1.2. The AVR fault has sudden effect on the estimated field current error, before this stays on a steady state value. The other states are not effected by the fault. Since the field current is the only state that has the field voltage as input, this behavior is as expected.

The quite large effect the faults have on the measurement estimation error, especially on the estimated active power error, can be considered to be both an advantage and a disadvantage if the observer is to be used for fault detection. A large error when a fault occurs, is crucial to detect the fault. On the other hand, modeling differences between the "real plant" (here the simulation plant model) and the control plant model, might as well introduce large errors. The correcting term (\mathbf{L}), can be used to correct these errors, and large errors might therefore cause very aggressive correcting. However, too aggressive correcting might remove the error caused by faults as well as those caused by modeling differences. The tuning of \mathbf{L} should therefore not focus on minimizing the estimation error, but on making the failure modes as visible as possible. This problem is similar to the problem experienced when observers are used for estimating a noisy signal. The choice of correcting term is a trade-off between fast estimation and noise-rejection properties.

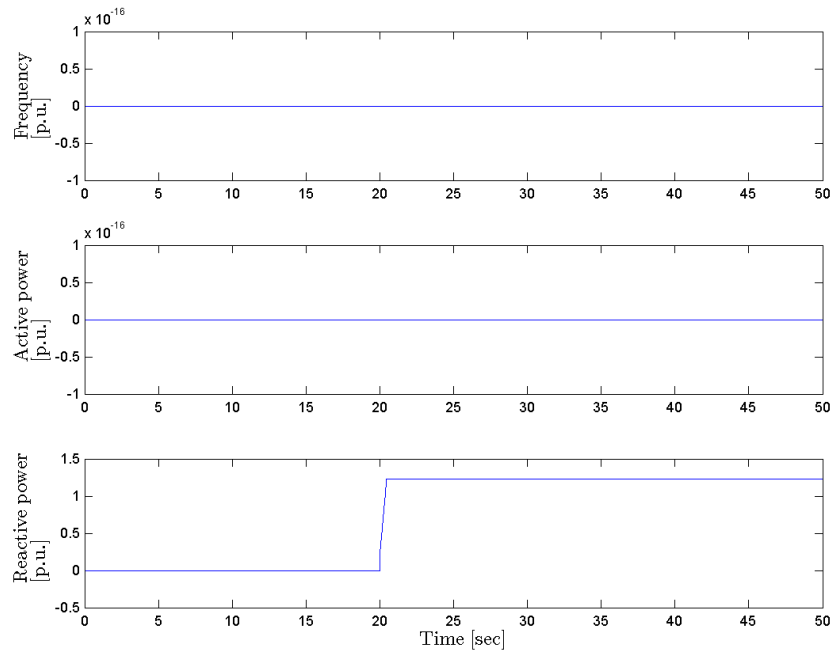


(a) Measurement estimation error.

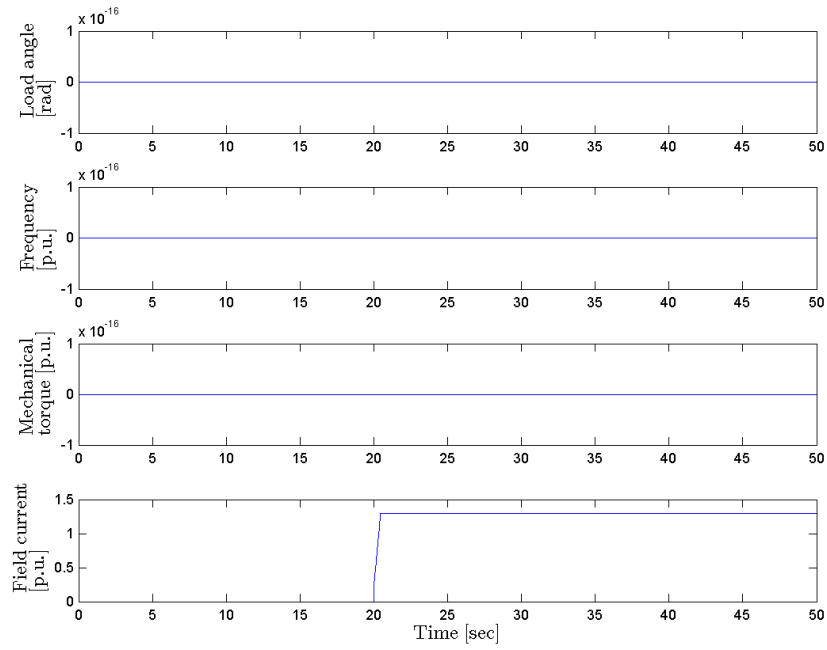


(b) State estimation error.

Figure 7.2: Measurement and state errors, for observer run against control plant model, Governor to maximum occurring after 20 seconds



(a) Measurement estimation error, AVR to maximum



(b) State estimation error, AVR to maximum

Figure 7.3: Measurement and state errors, for observer run against control plant model, AVR to maximum occurring after 20 seconds

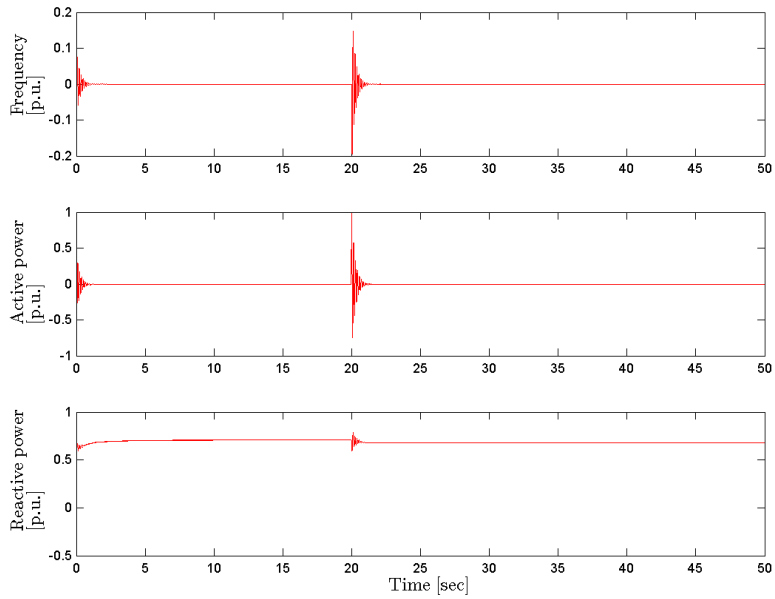
7.4 Observer performance

Figure 7.4 to 7.7 shows the state and measurement estimation error, for the nonlinear Luenberger-type observer, run against the simulation plant model. All simulation parameters are the same as in Section 6. Since the purpose of the observer is fault detection, the tuning of the correcting term has mainly had focus on maximizing the detection triggers, and not to make the estimation errors as small as possible. This is further discussed in Section 10.2. Results for all simulation modes are presented in Section C.2.

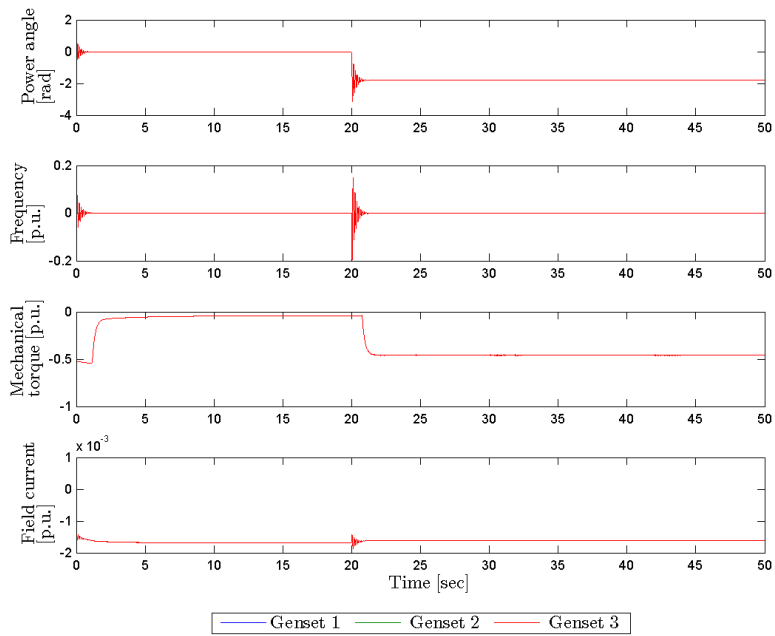
From Figure 7.4 it is seen that all states have values close to zero before the load change occurs. However, after the load change, the power angle and mechanical torque react with a step in value. From Figure B.3, it is seen that that this is also the case with the field current. The plots of the measurements in Figure 7.4, shows that this behavior is not continued by the measurements, frequency and active power. In Figure B.3, it is seen that the step also occurs for the measurement reactive power. This behavior might be an issue when the observer is used for fault detection.

Figure 7.5 shows that the estimation error for frequency and active power, responds with a sudden step in the value for the faulty genset. The same behavior is seen for the reactive power in Figure 7.7, but here the healthy gensets also have this behavior. It can also be seen that the frequency and active power, clearly have the largest reactions to the active load change and the governor fault. The reactive power has the largest reaction to the reactive power change and AVR faults.

Based on the above discussion, it can be concluded that the observer is suitable for use in fault detection. It is possible to detect governor faults from the frequency and active power estimation error, and to separate these from the normal operation modes. AVR faults can probably be detected by the reactive power estimation error, but this needs further analysis.

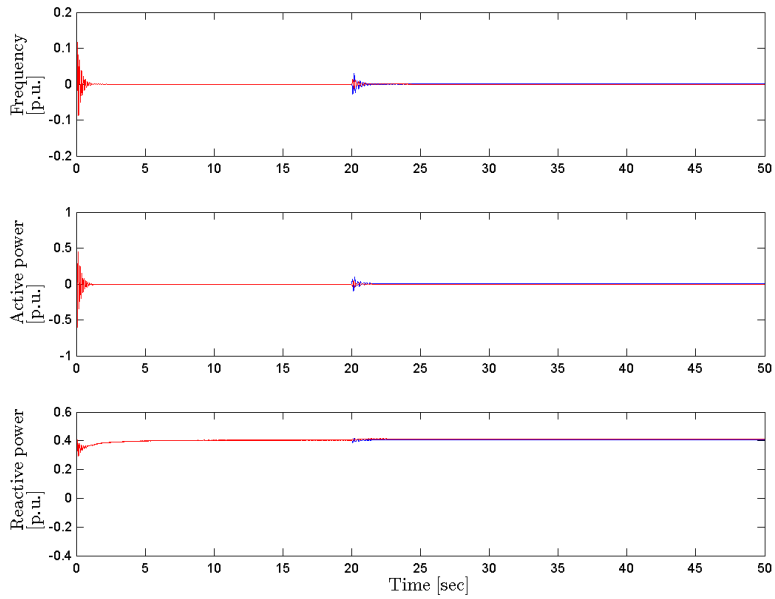


(a) Measurement estimation error.

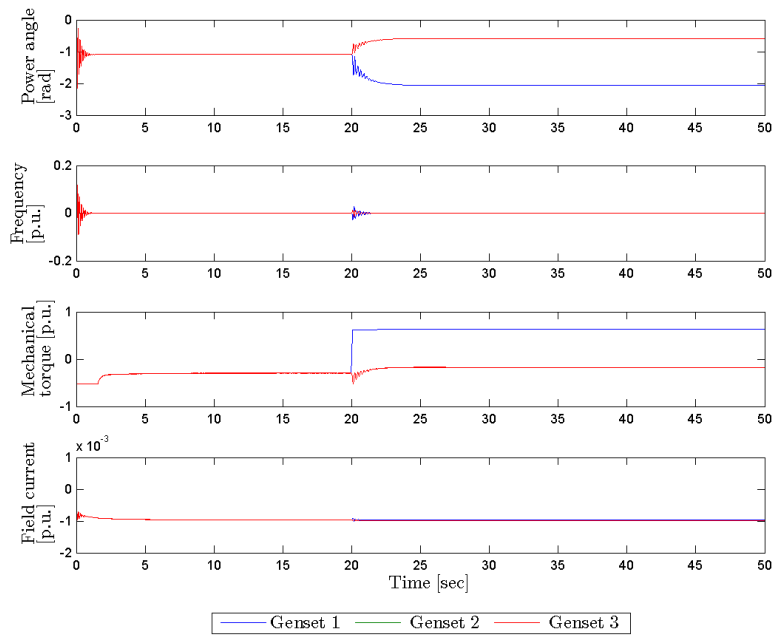


(b) State estimation error.

Figure 7.4: Measurement and state errors, for observer run against control plant model, Sudden active load increase occurring after 20 seconds.

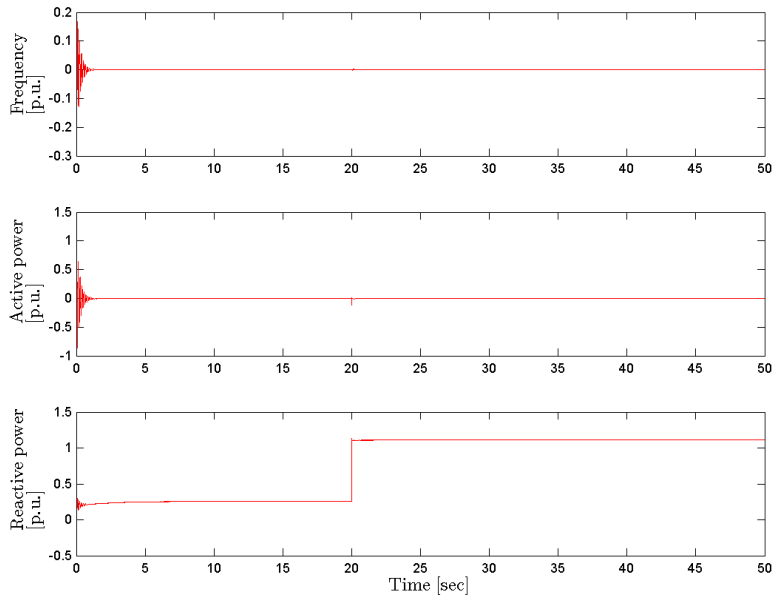


(a) Measurement estimation error.

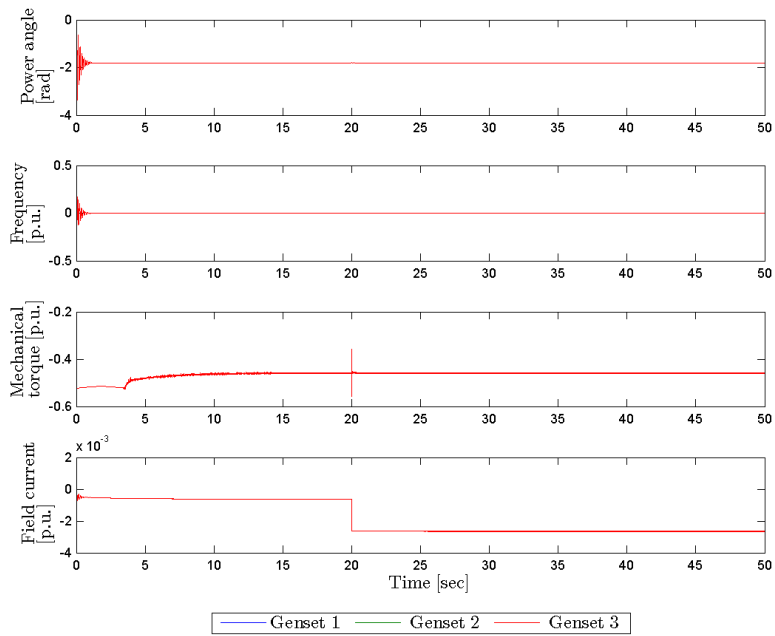


(b) State estimation error.

Figure 7.5: Measurement and state errors, for observer run against control plant model, Governor to maximum occurring after 20 seconds. Failure implemented in Genset 1.

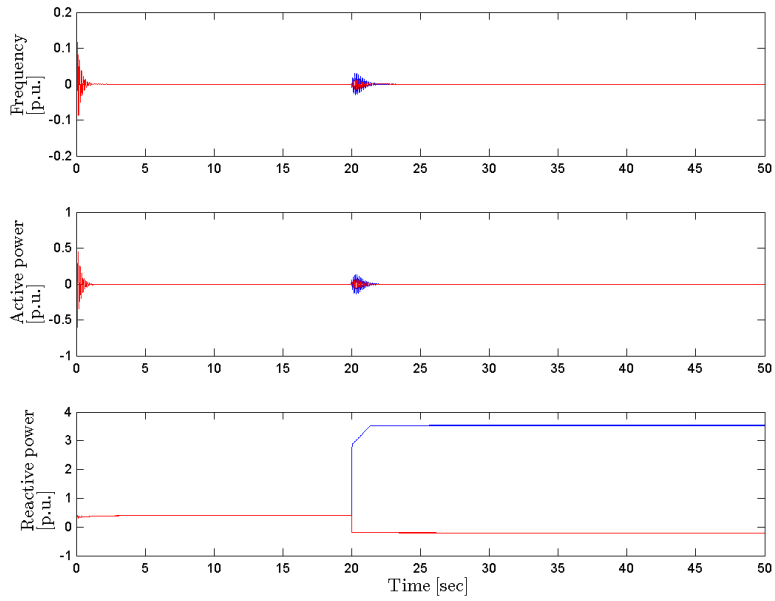


(a) Measurement estimation error.

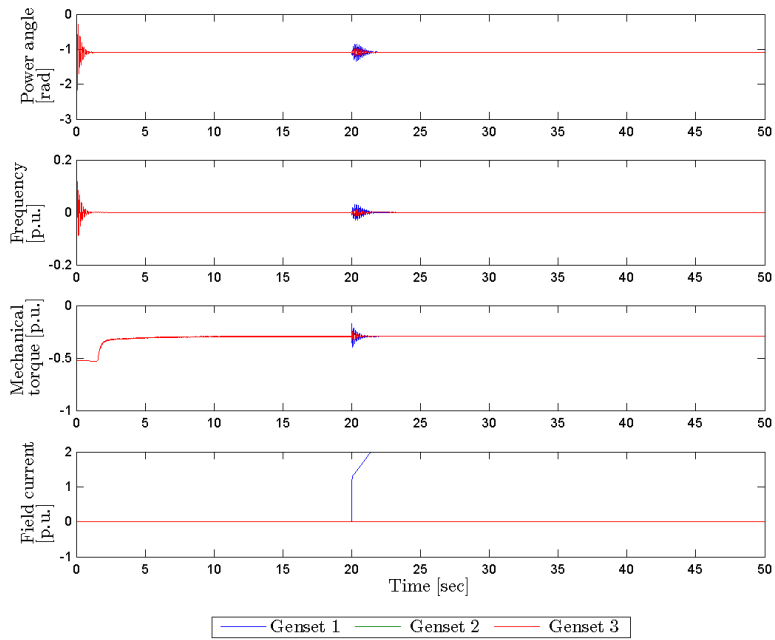


(b) State estimation error.

Figure 7.6: Measurement and state errors, for observer run against control plant model, sudden reactive load increase occurring after 20 seconds.



(a) Measurement estimation error.



(b) State estimation error.

Figure 7.7: Measurement and state errors, for observer run against control plant model, AVR to maximum occurring after 20 seconds. Failure implemented in Genset 1

8 Advanced Generator Protection

8.1 Theoretical background

The main principles behind the Advanced Generator Protection, are described in Section 3. A mathematical formulation of the expected frequency and voltage is

$$\omega_{exp} = \omega_{No-load} - p \times \text{Droop}_{\text{speed}} \quad (8.1)$$

$$v_{exp} = v_{No-load} - q \times \text{Droop}_{\text{voltage}} \quad (8.2)$$

where $\omega_{No-load}$ and $v_{No-load}$ is the frequency and voltage, when the genset has no active load (p) and no reactive load (q), respectively. The error between actual and expected frequency and voltage, is then

$$r_{\omega} = \omega - \omega_{exp} \quad (8.3)$$

$$r_v = \hat{v}_{an} - v_{exp} \quad (8.4)$$

The window around the droop curves can then be defined by the parameters $\Delta r_{\omega,max}$, $\Delta r_{\omega,min}$, $\Delta r_{v,max}$, and $\Delta r_{v,min}$. Then the resulting fault detection system can be formulated

$$\begin{array}{ll} \Delta r_{\omega,min} \leq r_{\omega} \leq \Delta r_{\omega,max} & \text{No fault detected} \\ r_{\omega} \geq \Delta r_{\omega,max} & \text{Governor fault detected} \\ r_{\omega} \leq \Delta r_{\omega,min} & \text{Governor fault detected} \end{array} \quad (8.5)$$

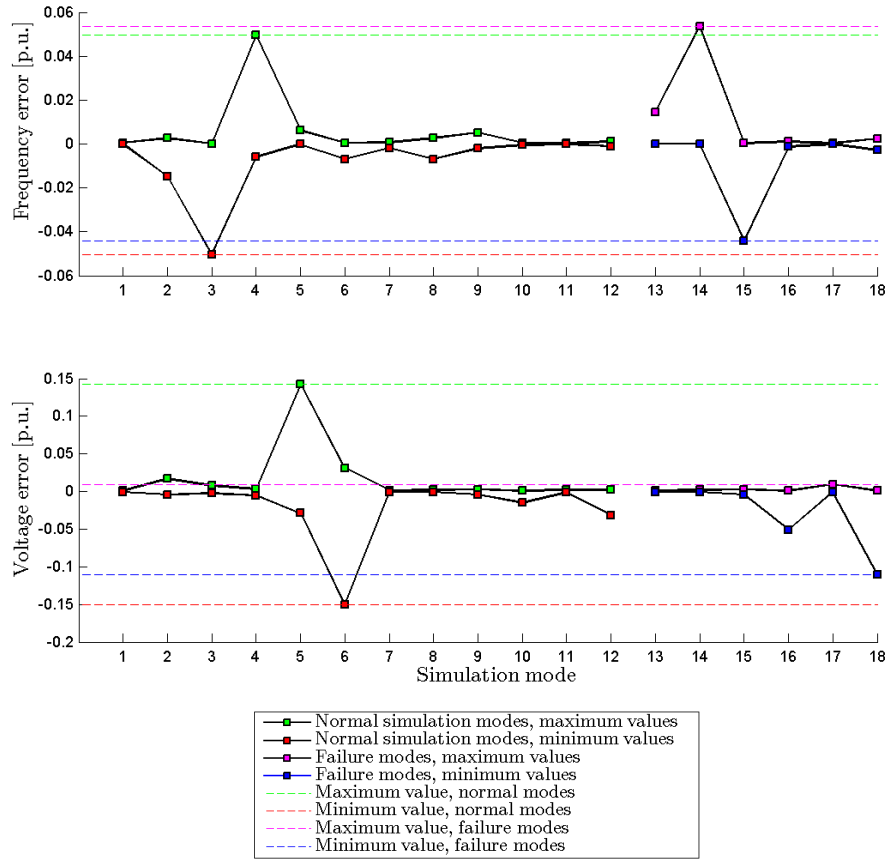
$$\begin{array}{ll} \Delta r_{v,min} \leq r_v \leq \Delta r_{v,max} & \text{No fault detected} \\ r_v \geq \Delta r_{v,max} & \text{AVR fault detected} \\ r_v \leq \Delta r_{v,min} & \text{AVR fault detected} \end{array} \quad (8.6)$$

8.2 Simulation study

In order to verify the performance of the designed AGS, it is implemented in Simulink/MATLAB, together with the simulation plant model. The system parameters and simulation scenarios, are the same as in Section 6.

8.2.1 Fault detection without exceedance duration

Figure 8.1 shows the maximum and minimum difference between actual and expected frequency and voltage, when the duration of the values are not taken into account. The plots to the left in the figure, are from the normal operation modes. In other words, these are operation modes, that the fault detection system should not act on. The plots to the right in the figure, are from the failure modes. This means, that for the fault detection system to be able to detect the faults, either the maximum or minimum values from the failure modes, must be larger than the maximum and minimum values from the normal operation modes. Based on this, it is obvious that the fault detection system without exceedance duration, is not suitable for fault detection.



Number	Simulation mode description
1	Normal operation
2	Sudden disconnection of one genset, values for healthy gensets
3	Sudden active power increase
4	Sudden active power decrease
5	Sudden reactive power increase
6	Sudden reactive power decrease
7	Governor frozen, values for healthy genset
8	Governor to minimum, values for healthy genset
9	Governor to maximum, values for healthy genset
10	AVR frozen, values for healthy genset
11	AVR to minimum, values for healthy genset
12	AVR to maximum, values for healthy genset
13	Governor frozen, values for genset with failure
14	Governor to minimum, values for genset with failure
15	Governor to maximum, values for genset with failure
16	AVR frozen, values for genset with failure
17	AVR to minimum, values for genset with failure
18	AVR to maximum, values for genset with failure

Figure 8.1: Minimum and maximum difference between actual and expected frequency and voltage, for each simulation scenario, and for all durations of the values. Values from the first 10 seconds of the simulation, are not represented.

8.2.2 Fault detection with exceedance duration

Figure 8.2 shows the error between actual and expected frequency and voltage, for simulations with two normal modes, and two failure modes. It can be seen that for both the normal modes, the reaction to the inflicted event, is a sudden spike in the error. The peak value has a relatively short duration, before the error starts approaching zero. The failure modes, however, reacts in a different way. As the inflicted event occurs, the error increases more or less suddenly, before it stabilizes at a steady error value.

Knowing this about the system behavior, it should be possible to separate the normal modes from the failure modes, by taking both the error magnitude and duration into account. Based on this, the accepted error duration time is tuned until either the maximum, or minimum error value for all failure modes, are larger than the maximum or minimum error value for all the normal simulation modes. It is however, adequately that this is satisfied for all failure modes for either the frequency error, or the voltage error. In addition, it is required that the failure mode with error closest to zero, is between 10 and 20 % larger than the closest normal operation error. The last requirement, is added in order to be able to compare the different fault detection algorithms presented in this thesis.

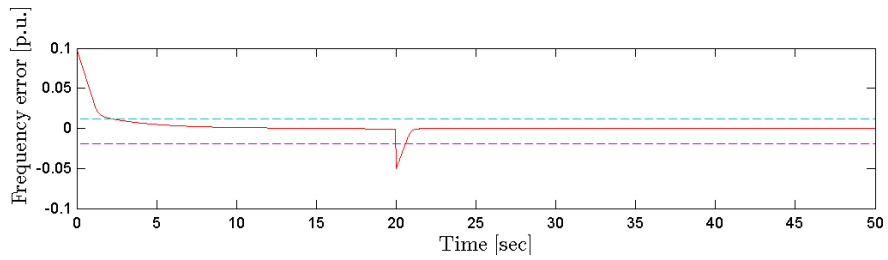
The results from this tuning are presented in Table 8.1. For both the minimum and maximum error window, two values are given. The lower value is the largest and smallest error value for all the normal simulation modes. Hence, this is the values closest to zero, that are possible to use as limit values for the fault detection system. These values are displayed in Figure 8.3 as red and green lines, and in Figure 8.2 as dotted pink and light blue lines. The highest value is the limit value furthest from zero, that can be used by the fault detection system. These values are displayed in Figure 8.3 as dotted blue and pink lines. The

	Frequency	Voltage
Δt [sec]	0.6	0.6
$\Delta r_{max,max}$	0.0145	0.0085
$\Delta r_{max,min}$	0.0122	0.0074
$\Delta r_{min,max}$	0.0440	0.0505
$\Delta r_{min,min}$	0.0190	0.0076
$\frac{\Delta r_{max,max} - \Delta r_{max,min}}{\Delta r_{min,min}}$ [%]	18.85	14.86
$\frac{\Delta r_{min,max} - \Delta r_{min,min}}{\Delta r_{min,min}}$ [%]	131.58	564.47

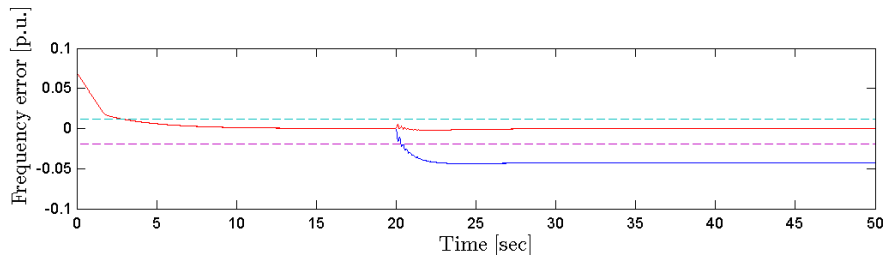
Table 8.1: Parameters for fault detection with exceedance duration.

Figure 10.1 shows the maximum and minimum errors, for all simulation scenarios, where maximum duration of the errors are as defined in Table 8.1. It can be seen that all the governor faults results

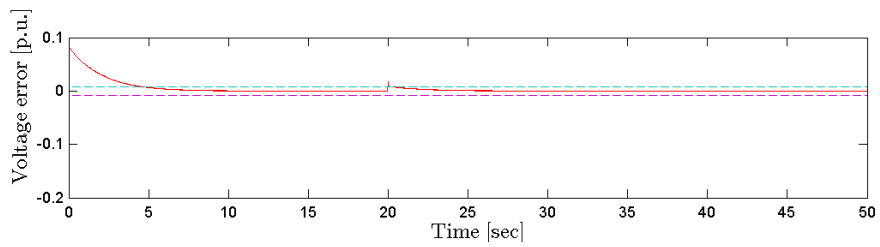
in larger frequency error values, than the normal operation modes. The same is seen to be the case for the AVR faults and voltage error. Hence, it can be concluded that the AGC is able to detect all the simulated failure modes, within 0.6 second.



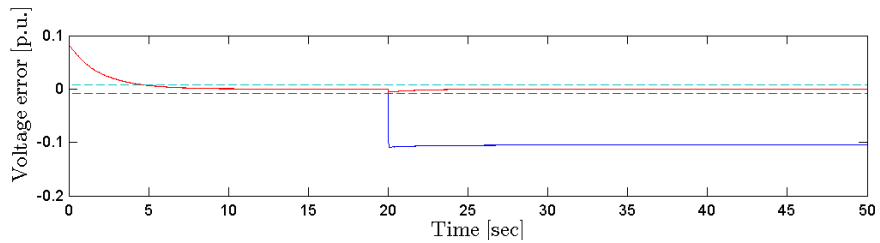
(a) Normal operation mode, sudden increase of active power.



(b) Failure mode, governor to maximum



(c) Normal operation mode, sudden increase of reactive power.



(d) Failure mode, AVR to maximum.

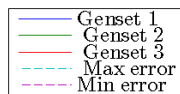
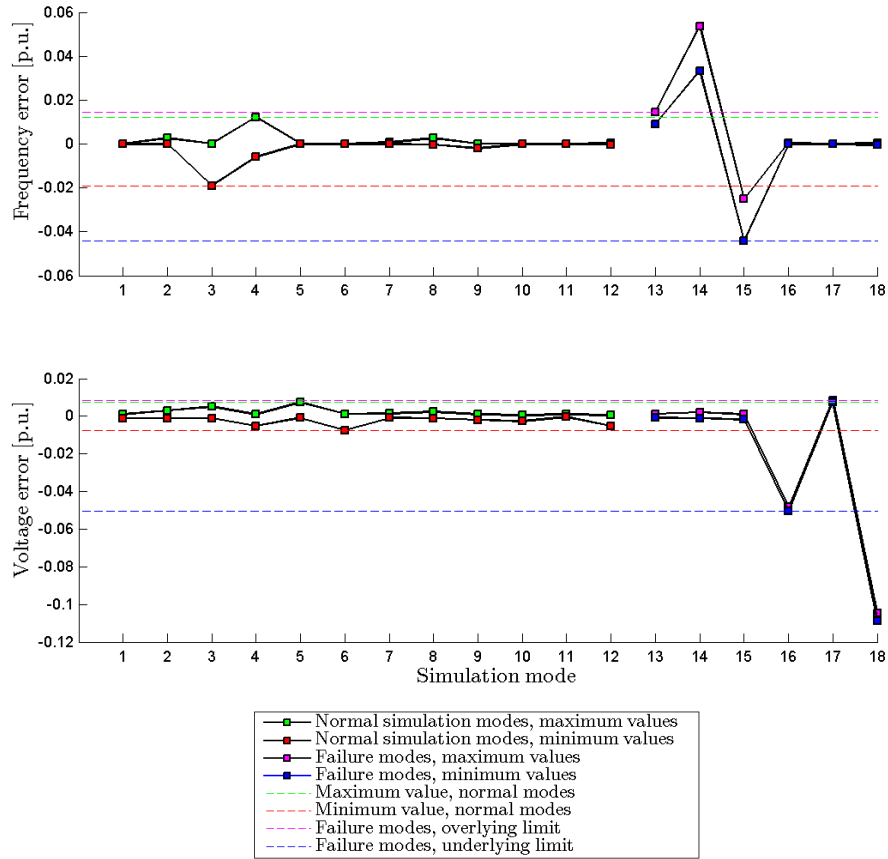


Figure 8.2: Difference between actual and expected frequency and voltage, for different simulation scenarios, with event occurring after 20 seconds. The dotted lines represent the maximum and minimum deviation values, presented in Table 8.1, the value closest to zero is used.



Number	Simulation mode description
1	Normal operation
2	Sudden disconnection of one genset, values for healthy gensets
3	Sudden active power increase
4	Sudden active power decrease
5	Sudden reactive power increase
6	Sudden reactive power decrease
7	Governor frozen, values for healthy genset
8	Governor to minimum, values for healthy genset
9	Governor to maximum, values for healthy genset
10	AVR frozen, values for healthy genset
11	AVR to minimum, values for healthy genset
12	AVR to maximum, values for healthy genset
13	Governor frozen, values for genset with failure
14	Governor to minimum, values for genset with failure
15	Governor to maximum, values for genset with failure
16	AVR frozen, values for genset with failure
17	AVR to minimum, values for genset with failure
18	AVR to maximum, values for genset with failure

Figure 8.3: Minimum and maximum difference between actual and expected frequency and voltage, for each simulation scenario, and for error durations as defined in Table 8.1. Values from the first 10 seconds of the simulation, are not represented.

8.3 Resulting fault detection system

The final fault detection system can now be formulated

$$\begin{array}{lll}
 r_\omega \geq \Delta r_{\omega,max} & \text{and} & t(r_\omega \geq \Delta r_{\omega,max}) \geq \Delta t_\omega & \text{Governor fault detected} \\
 r_\omega \leq \Delta r_{\omega,min} & \text{and} & t(r_\omega \leq \Delta r_{\omega,min}) \geq \Delta t_\omega & \text{Governor fault detected} \\
 \\
 r_v \geq \Delta r_{v,max} & \text{and} & t(r_v \geq \Delta r_{v,max}) \geq \Delta t_v & \text{AVR fault detected} \\
 r_v \leq \Delta r_{v,min} & \text{and} & t(r_v \leq \Delta r_{v,min}) \geq \Delta t_v & \text{AVR fault detected}
 \end{array}$$

where the parameters are given in Table 8.2, and the system architecture is presented in Figure 8.4. This means that the AGP is capable of detecting governor and AVR faults in 0.6 seconds.

	Frequency	Voltage
Δt [sec]	0.6	0.6
Δr_{max}	0.0145	0.0085
Δr_{min}	0.0440	0.0505

Table 8.2: Parameters for fault detection with exceedance duration.

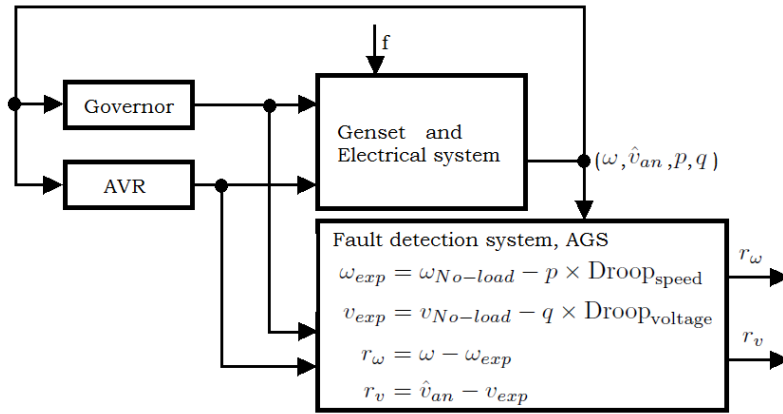


Figure 8.4: AGP block diagram

9 Analytical redundancy relation from nonlinear model

9.1 Model

The analytical redundancy relation is based on the nonlinear dynamic model described by (7.9) to (??) derived in Section 7

$$\dot{\delta} = \omega_b (\omega - \omega_0) \quad (9.1)$$

$$\dot{\omega} = \frac{1}{2H} \left(t_m - D_{fw}\omega - \frac{1}{x_s} \frac{\delta}{\omega} - \frac{r_s}{x_s^2} \frac{\delta^2}{\omega \hat{v}_l^2} - \frac{r_s}{x_s^2} \frac{(r_f \omega i_f - \hat{v}_l)^2}{\omega \hat{v}_l^2} \right) \quad (9.2)$$

$$\dot{t}_m = -\frac{1}{\tau_e} t_m + \frac{D_{fw} + 1}{\tau_e} u + \frac{D_{fw} + 1}{\tau_e} f_u \quad (9.3)$$

$$\dot{i}_f = -\frac{1}{\tau_f} i_f + \frac{1}{\tau_f r_f} v_f + \frac{1}{\tau_f r_f} f_{v_f} \quad (9.4)$$

Measurements:

$$\omega = \omega \quad (9.5)$$

$$p = \frac{1}{x_s} \delta \quad (9.6)$$

$$q = \frac{1}{x_s} (r_f \omega i_f - \hat{v}_l) \quad (9.7)$$

9.2 Theoretical background for redundancy relations

The derivation of the redundancy relations, are based on the method described by (Blanke et al, 2006). Calculation of the redundancy relations with this method, causes a so-called explosion of equations. To handle this, a Matlab program is developed to calculate the redundancy relations. Due to this, the method is only presented in a theoretical manner.

The method is based on a nonlinear system on the form

$$\dot{\mathbf{x}} = \mathbf{g}(\mathbf{x}, \mathbf{u}, \mathbf{f}) \quad (9.8)$$

$$\mathbf{y} = \mathbf{h}(\mathbf{x}, \mathbf{u}, \mathbf{f}) \quad (9.9)$$

where \mathbf{x} is the state vector, \mathbf{u} is the input vector, and \mathbf{f} is the fault vector. The system variables have the following dimensions

$$\mathbf{x} \in \mathbb{R}^{n_x} \quad \mathbf{u} \in \mathbb{R}^{n_u} \quad \mathbf{y} \in \mathbb{R}^{n_y} \quad \mathbf{f} \in \mathbb{R}^{n_f} \quad (9.10)$$

It is assumed that all functions are differentiable with respect to their variables. Then the derivative of the measurement can be calculated

$$\dot{\mathbf{y}} = \frac{\partial \mathbf{h}}{\partial \mathbf{x}}(\cdot) \dot{\mathbf{x}} + \frac{\partial \mathbf{h}}{\partial \mathbf{u}}(\cdot) \dot{\mathbf{u}} + \frac{\partial \mathbf{h}}{\partial \mathbf{f}}(\cdot) \dot{\mathbf{f}} \quad (9.11)$$

Inserting for $\dot{\mathbf{x}}$ in the above equation then gives

$$\dot{\mathbf{y}} = \frac{\partial \mathbf{h}}{\partial \mathbf{x}}(\cdot) \mathbf{g}(\mathbf{x}, \mathbf{u}, \mathbf{f}) + \frac{\partial \mathbf{h}}{\partial \mathbf{u}}(\cdot) \dot{\mathbf{u}} + \frac{\partial \mathbf{h}}{\partial \mathbf{f}}(\cdot) \dot{\mathbf{f}} \quad (9.12)$$

$$:= \mathbf{h}_1(\mathbf{x}, \mathbf{u}, \dot{\mathbf{u}}, \mathbf{f}, \dot{\mathbf{f}}) \quad (9.13)$$

Assuming the existence of the necessary further derivatives, this operation can be continued for a desired order of derivation, d . The size of d is decided from the system properties and design preferences, and will be discussed more carefully later. The resulting system of equations can then be written

$$\begin{aligned} \dot{\mathbf{y}} &= \mathbf{h}_1(\mathbf{x}, \mathbf{u}, \dot{\mathbf{u}}, \mathbf{f}, \dot{\mathbf{f}}) \\ \ddot{\mathbf{y}} &= \mathbf{h}_2(\mathbf{x}, \mathbf{u}, \dot{\mathbf{u}}, \ddot{\mathbf{u}}, \mathbf{f}, \dot{\mathbf{f}}, \ddot{\mathbf{f}}) \\ &\vdots \\ \mathbf{y}^{(d)} &= \mathbf{h}_d(\mathbf{x}, \mathbf{u}, \dot{\mathbf{u}}, \ddot{\mathbf{u}}, \dots, \mathbf{u}^{(d)}, \mathbf{f}, \dot{\mathbf{f}}, \ddot{\mathbf{f}}, \dots, \mathbf{f}^{(d)}) \end{aligned} \quad (9.14)$$

Defining the notation $\bar{\mathbf{u}}^{(d)} = (\mathbf{u}, \dot{\mathbf{u}}, \ddot{\mathbf{u}}, \dots, \mathbf{u}^{(d)})$, the above system can be written

$$\bar{\mathbf{y}}^{(d)} = \mathbf{H}^d(\mathbf{x}, \bar{\mathbf{u}}^{(d)}, \bar{\mathbf{f}}^{(d)}) \quad (9.15)$$

The variables defined by this notation have the following dimensions:

$$\bar{\mathbf{u}}^{(d)} \in \mathbb{R}^{(d+1)n_u} \quad \bar{\mathbf{y}}^{(d)} \in \mathbb{R}^{(d+1)n_y} \quad \bar{\mathbf{f}}^{(d)} \in \mathbb{R}^{(d+1)n_f} \quad (9.16)$$

To continue the derivation of the redundancy relations, the following assumptions must be satisfied

$$(d+1)n_y > n_x \quad \text{and} \quad \text{rank} \left(\frac{\partial \mathbf{H}^d(\cdot)}{\partial \mathbf{x}} \right) = n_x \quad (9.17)$$

Together, these assumptions ensures that the order of differentiation (d) is high enough to establish a suitable (9.15), and that it is possible to derive one or more redundancy relations for the system. When these conditions are satisfied, (9.15) can be decomposed into

$$\bar{\mathbf{y}}_{\mathbf{x}}^{(d)} = \mathbf{H}_{\mathbf{x}}^d(\mathbf{x}, \bar{\mathbf{u}}^{(d)}, \bar{\mathbf{f}}^{(d)}) \quad (9.18)$$

$$\bar{\mathbf{y}}_{\mathbf{r}}^{(d)} = \mathbf{H}_{\mathbf{r}}^d(\mathbf{x}, \bar{\mathbf{u}}^{(d)}, \bar{\mathbf{f}}^{(d)}) \quad (9.19)$$

where (9.18) is of dimension n_x . (9.18) can now be used to solve for \mathbf{x}

$$\mathbf{x} = \phi(\bar{\mathbf{y}}^{(d)}, \bar{\mathbf{u}}^{(d)}, \bar{\mathbf{f}}^{(d)}) \quad (9.20)$$

By inserting (9.20) for \mathbf{x} in (9.19), and subtracting with $\mathbf{H}_{\mathbf{r}}^d$ on both sides, the redundancy relations for the system can be derived

$$\mathbf{r} = \bar{\mathbf{y}}_{\mathbf{r}}^{(d)} - \mathbf{H}_{\mathbf{r}}^d \left(\phi(\bar{\mathbf{y}}^{(d)}, \bar{\mathbf{u}}^{(d)}, \bar{\mathbf{f}}^{(d)}), \bar{\mathbf{u}}^{(d)}, \bar{\mathbf{f}}^{(d)} \right) \quad (9.21)$$

9.3 Resulting redundancy relations

From (9.1) to (9.7) it is seen that at least one derivation is needed to derive a redundancy relation for the control plant model. This is obvious since there are four states (δ , ω , t_m , and i_f) and three measurements (ω , p , and q). Hence, differentiating the measurements once, results in six equations that can be used for solving for four unknown variables and two redundancy relations. To ensure the quality of the redundancy relations, the measurements are differentiated two times, and hence, $d = 2$.

As two derivation steps are performed, several redundancy relations can be derived from the system. For a redundancy relation to be suitable for fault detection it has to satisfy some requirements. Further, different properties of the redundancy relation will have influence on the fault detection properties.

For a redundancy relation to be suitable for fault detection, it must be a function of the modeled faults, in this case f_u and f_{v_f} . In addition, it is an advantage if the redundancy relation is only a function of one modeled fault. In this case, the relation can not only be used to detect a fault, it can also be used to diagnosis the fault. For the nonlinear dynamic model in (??) to (??), it is therefore desired to derive at least two redundancy relations, one dependent of f_u and independent of f_{v_f} , and one dependent of f_{v_f} and independent of f_u . Further, the derivatives a redundancy relation is a function of, should be of as low degree as possible. This is because each derivation increases the uncertainties caused by measurement noise and differences between the real system and the model. To base fault detection on a redundancy relation that is only a function of a differentiation of the modeled fault, will not be as good as to base it on the actual modeled fault.

With $d = 2$, at least five different redundancy relations can be derived. More than five relations can be found by using different equations of $\bar{y}^{(2)}$, to calculate the states, which causes that there are possible to derive several different expressions for each state. This will of course, lead to more than five redundancy relations. It is desired to use the redundancy relations that are of as high quality as possible. Therefore, the equations in $\bar{y}^{(2)}$ with the lowest differentiation degree as possible, are used to derive the state expressions. Further, the resulting redundancy relations are checked for dependency of f , \dot{f} , and \ddot{f} .

In order to estimate the system states, we set $\bar{\mathbf{y}}_{\mathbf{x}}^{(d)} = [\mathbf{y} \quad \dot{\mathbf{y}}(1)]^T = [\omega \quad p \quad q \quad \dot{\omega}]^T$. This gives the following solution for the states

$$\delta = x_s p \tag{9.22}$$

$$\omega = \omega \tag{9.23}$$

$$t_m = 2H\dot{\omega} + D_{fw}\omega + \frac{p}{\omega} + r_s \frac{p^2 + q^2}{\omega \hat{v}_{ll}^2} \tag{9.24}$$

$$i_f = \frac{x_s q + \hat{v}_{ll}}{r_f \omega} \tag{9.25}$$

This means that the redundancy relations must be calculated from $\bar{\mathbf{y}}_{\mathbf{r}}^{(d)} = [\dot{\mathbf{y}}(2) \quad \dot{\mathbf{y}}(3) \quad \ddot{\mathbf{y}}]^T = [\dot{p} \quad \dot{q} \quad \ddot{\omega} \quad \ddot{p} \quad \ddot{q}]$. Since the resulting redundancy relations are very large, all except one, are not presented here. However, Table 9.1 to 9.3, shows how the redundancy relations are dependent on

the different system variables.

From Table 9.1 it is seen that from $\dot{\mathbf{y}}$ there is only one redundancy relation worth to consider, namely the one derived from \dot{q} , since it is the only one dependent on \mathbf{f} . The equation for this redundancy relation is

$$r_{\dot{q}} = -\frac{\omega\hat{v}_{ll} - f_{v_f}\omega^2 - \omega^2v_f + \tau_f\dot{v}_{ll}\omega - \tau_f\dot{\omega}\hat{v}_{ll} + \omega qx_s - \tau_f\dot{\omega}qx_s + \tau_f\dot{q}\omega x_s}{\tau_f\omega x_s} \quad (9.26)$$

It can be seen that the relation is only dependent on f_{v_f} . Since it is derived from $\dot{\mathbf{y}}$, the highest degree of differentiation of any variable is one. $r_{\dot{q}}$ should therefore be well suited for fault detection.

Further, it is seen that there are two more redundancy relations, $r_{\ddot{\omega}}$ and $r_{\ddot{q}}$. Both redundancy relations, are dependent on both governor and AVR faults. $r_{\ddot{q}}$ is also dependent on \dot{f}_{v_f} , and is therefore expected to be best at detecting AVR faults. This is especially true, since the differentiation is expected to magnify the fault.

From Table 9.2 and 9.3, it is seen that both redundancy relations are dependent on both first and second derivatives. They are therefore expected to be more noisy than $r_{\dot{q}}$. $r_{\ddot{q}}$ is expected to be the most noisy redundancy relation, since it has the highest dependency on both first and second derivatives.

Redundancy relation	f_u	f_{v_f}	\dot{f}_u	\dot{f}_{v_f}	\ddot{f}_u	\ddot{f}_{v_f}
$r_{\ddot{\omega}}$						
$r_{\ddot{p}}$						
$r_{\dot{q}}$		1				
$r_{\ddot{\omega}}$	1	1				
$r_{\ddot{p}}$						
$r_{\ddot{q}}$	1	1		1		

Table 9.1: First and second derivative redundancy relations' dependencies on faults. 1 means that there is a dependency.

Redundancy relation	ω	p	q	$\dot{\omega}$	\dot{p}	\dot{q}	$\ddot{\omega}$	\ddot{p}	\ddot{q}
$r_{\ddot{\omega}}$	1	1	1	1			1		
$r_{\ddot{p}}$				1				1	
$r_{\ddot{q}}$	1	1	1	1					1

Table 9.2: Second derivative redundancy relations' dependencies on measurements.

Redundancy relation	ω_0	\hat{v}_l	u	v_f	$\dot{\omega}_0$	$\dot{\hat{v}}_l$	\dot{u}	\dot{v}_f	$\ddot{\omega}_0$	$\ddot{\hat{v}}_l$	\ddot{u}	\ddot{v}_f
$r_{\ddot{\omega}}$	1	1	1	1		1						
$r_{\ddot{p}}$					1							
$r_{\ddot{q}}$	1	1	1	1		1		1		1		

Table 9.3: Second derivative redundancy relations' dependencies on inputs.

9.4 Redundancy relation testing and validation

All redundancy relations are quite complex, and the behavior is therefore difficult to analyze analytically. In addition, it is desired to verify that the redundancy relations are calculated correctly. Therefore, the redundancy relations are run against the control plant model they are based on. In order to do this, a simulator based on (9.1) to (9.7) is implemented in Simulink/Matlab. The estimated states (in 9.22 to 9.25), and the derived redundancy relations are then implemented in the simulator. The governor and AVR used in the simulator, are identical to the ones used in the simulation plant model in Section 6. Also, all controller gains and system parameters are the same as for the simulator plant model, and can be found in Table 6.2 to 6.4. The control plant simulator is run with the same combination of simulation modes and loads as the simulation plant model, further details about this is therefore not presented here, but can be found in Section 6. All simulation results are presented here, or in Appendix D.1.

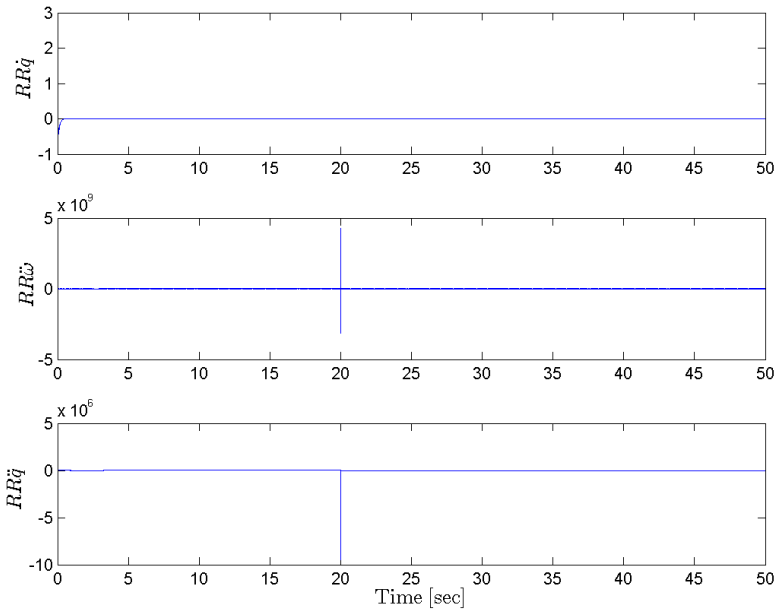
Figure ?? and ?? show the simulation results for the redundancy relations and estimated states, run against the control plant model. In Figure ??, the failure mode governor to maximum is simulated, while the failure mode AVR to maximum is simulated in Figure ?. For both simulation modes, the failure is inflicted after 20 seconds.

From the figures it can be seen that all states are quite well predicted. The estimation error for the load angle, frequency and field current, is zero for all simulation modes. However, the mechanical torque estimation error is quite noisy and has a clear negative deviation from zero, even though it is quite low. In addition, it reacts to the governor faults by a short and sudden spike. From (9.24) it is seen that the mechanical torque is derived from $\dot{\omega}$, and is therefore the only state dependent on a differentiated variable. Differentiation is known to increase errors, and it is therefore not unexpected that the mechanical torque is more noisy than the other states. The estimation error for the mechanical torque, is therefore considered acceptable. Based on this it is concluded that this method for estimating states, works satisfactory.

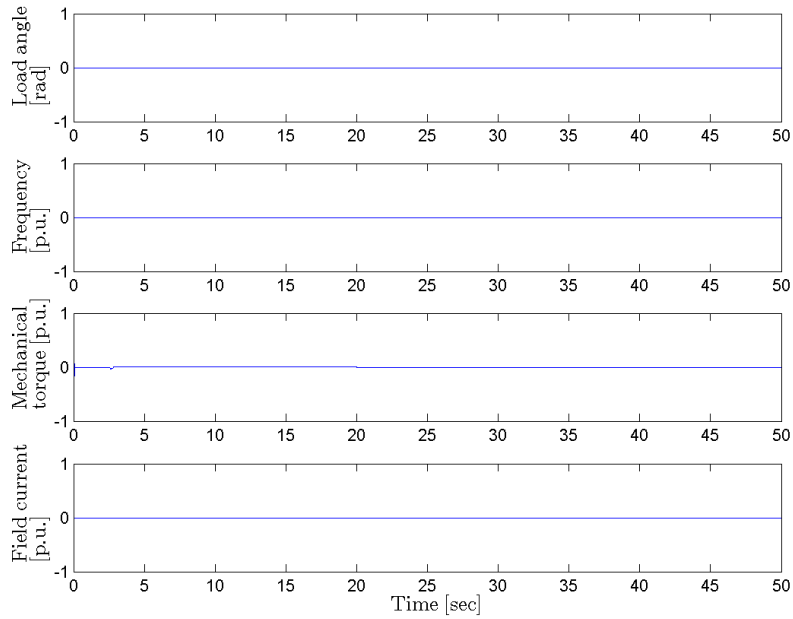
After initiation, all redundancy relations stabilizes around zero. It can be seen that all signals contains some noise, which is probably due to the differentiated variables. For normal simulation modes, the redundancy relations perform satisfactory.

When the different failure modes are introduced, the redundancy relations has reactions. For the governor faults, it is seen that $r_{\ddot{\omega}}$ and $r_{\ddot{q}}$ both have large reactions, while $r_{\ddot{p}}$ barely has any reaction. However, while $r_{\ddot{\omega}}$ responds with a large drop, and then stays on a steady value, $r_{\ddot{q}}$ drops and then slowly moves back toward zero. For the AVR failure modes $r_{\ddot{q}}$ and $r_{\ddot{p}}$ both have large

responses, while r_{ω} barely has any response. Both $r_{\dot{q}}$ and $r_{\ddot{q}}$, reacts to the AVR failures with a large increase or decrease, before they stay at a steady value. It is also seen, that the response of $r_{\ddot{q}}$, to the AVR failure modes are much larger than the response to the governor failure modes. It can therefore be concluded that r_{ω} is well suited for detecting governor faults, while $r_{\dot{q}}$ and $r_{\ddot{q}}$ are well suited for for detecting AVR faults.

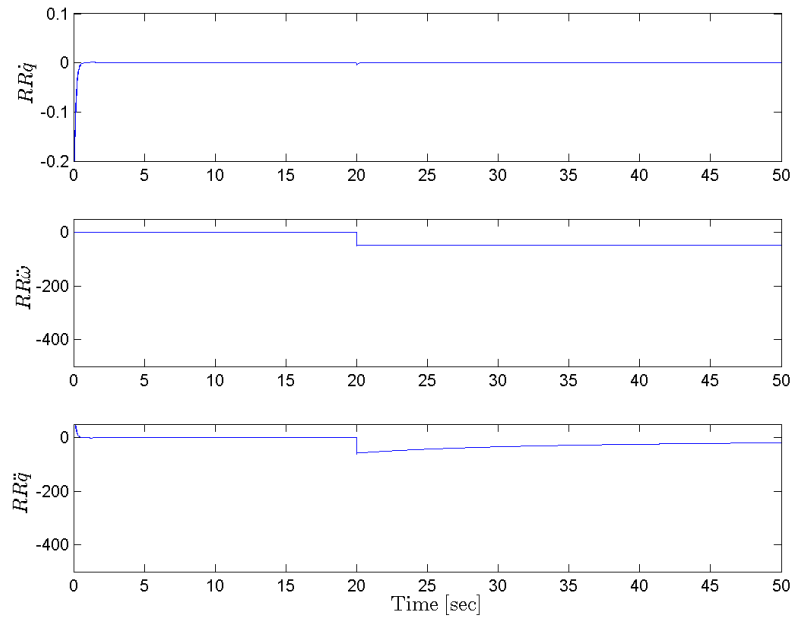


(a) Redundancy relation, Governor to maximum

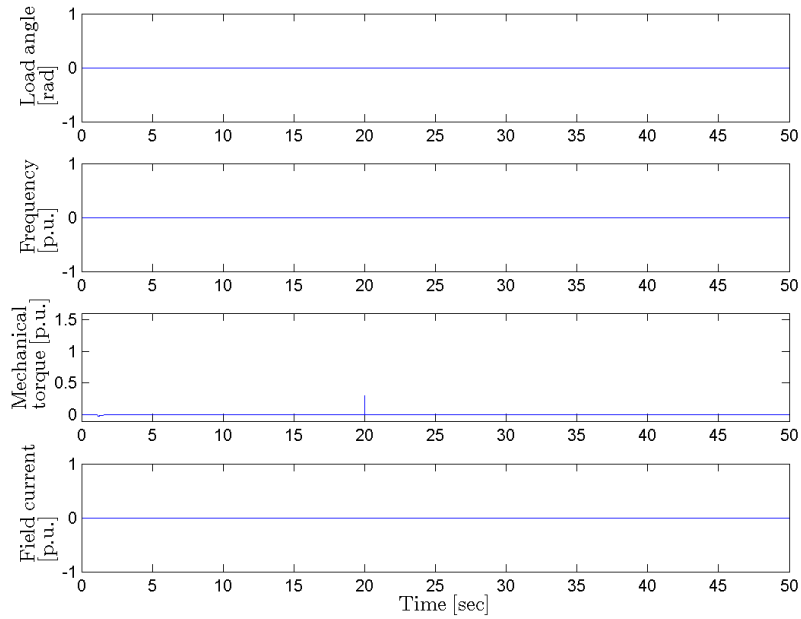


(b) State estimation error, Governor to maximum

Figure 9.1: Nonlinear redundancy relations and state estimation error, run against nonlinear control plant model, with sudden active load increase occurring after 20 seconds

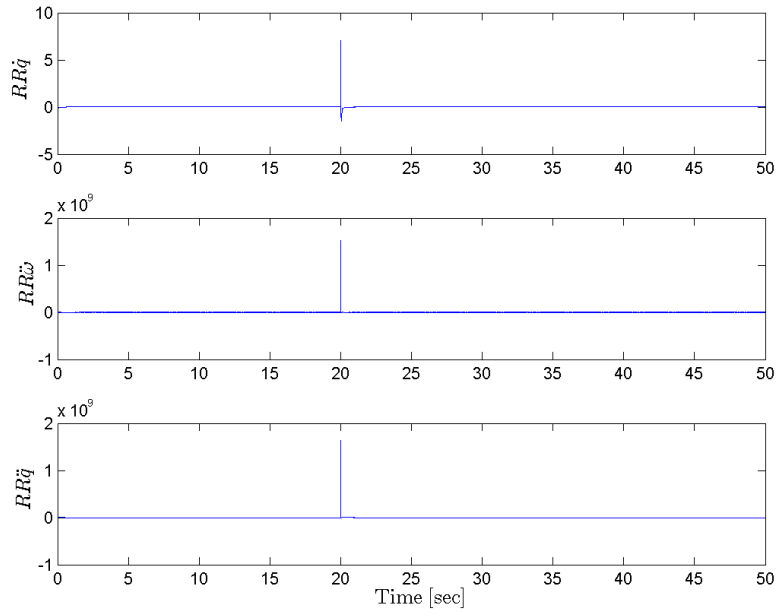


(a) Redundancy relation, Governor to maximum

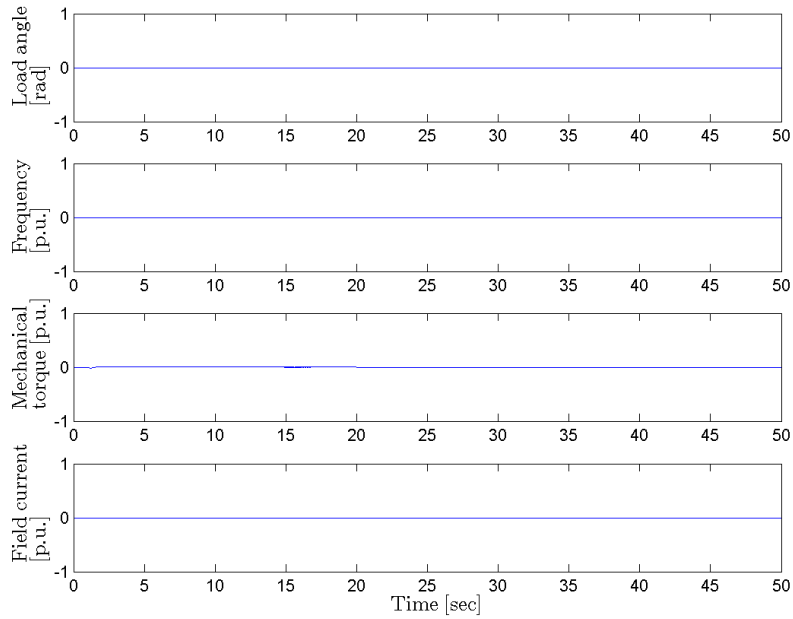


(b) State estimation error, Governor to maximum

Figure 9.2: Nonlinear redundancy relations and state estimation error, run against nonlinear control plant model, with Governor to maximum occurring after 20 seconds

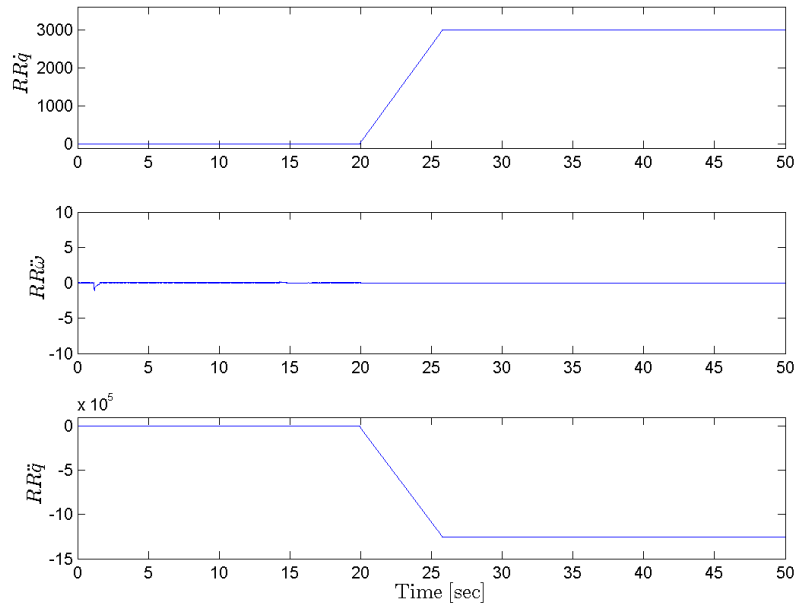


(a) Redundancy relation, AVR to maximum

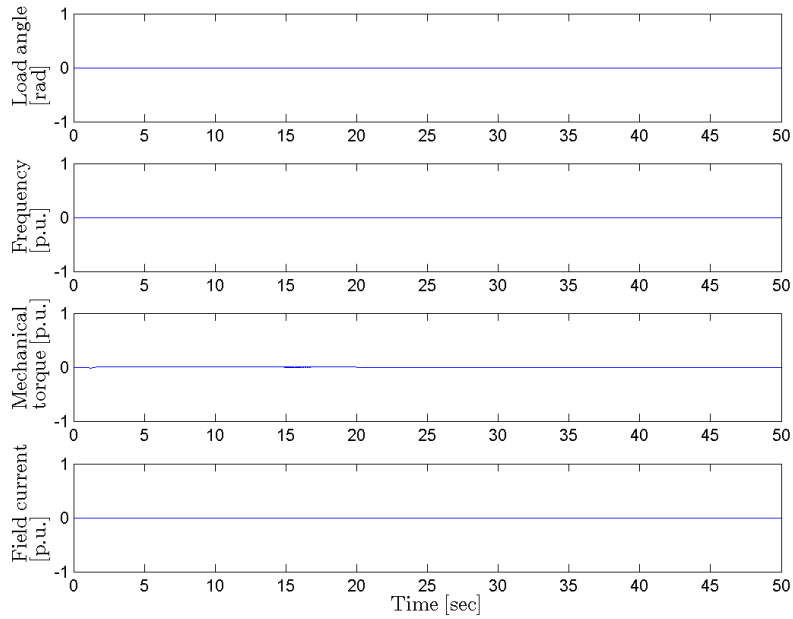


(b) State estimation error, AVR to maximum

Figure 9.3: Nonlinear redundancy relations and state estimation error, run against nonlinear control plant model, with sudden reactive load increase occurring after 20 seconds



(a) Redundancy relation, AVR to maximum



(b) State estimation error, AVR to maximum

Figure 9.4: Nonlinear redundancy relations and state estimation error, run against nonlinear control plant model, with AVR faults occurring after 20 seconds

9.5 Resulting fault detection system

Based on the discussion in Section 9.4, it is clear how the different redundancy relations can be used to detect governor and AVR faults. In the same way as for the AGP, the redundancy relations must be tolerant to noise, sudden load changes, and other scenarios that can occur in normal operation modes. Therefore the parameters, Δr_{min} and Δr_{max} are defined for each redundancy relation, to allow acceptable small deviations from zero. The redundancy relations with limitations, are then

$$\begin{aligned} \Delta r_{\dot{q},min} \leq r_{\dot{q}} \leq \Delta r_{\dot{q},max} & \quad \text{No fault detected} & (9.27) \\ r_{\dot{q}} \geq \Delta r_{\dot{q},max} & \quad \text{AVR fault detected} \\ r_{\dot{q}} \leq \Delta r_{\dot{q},min} & \quad \text{AVR fault detected} \end{aligned}$$

$$\begin{aligned} \Delta r_{\ddot{\omega},min} \leq r_{\ddot{\omega}} \leq \Delta r_{\ddot{\omega},max} & \quad \text{No fault detected} & (9.28) \\ r_{\ddot{\omega}} \geq \Delta r_{\ddot{\omega},max} & \quad \text{Governor fault detected} \\ r_{\ddot{\omega}} \leq \Delta r_{\ddot{\omega},min} & \quad \text{Governor fault detected} \end{aligned}$$

$$\begin{aligned} \Delta r_{\ddot{q},min} \leq r_{\ddot{q}} \leq \Delta r_{\ddot{q},max} & \quad \text{No fault detected} & (9.29) \\ r_{\ddot{q}} \geq \Delta r_{\ddot{q},max} & \quad \text{AVR fault detected} \\ r_{\ddot{q}} \leq \Delta r_{\ddot{q},min} & \quad \text{AVR fault detected} \end{aligned}$$

9.6 Simulation results, simulation plant model

In order to define the values of Δr_{min} and Δr_{max} , and to prove the performance of fault detection system, the redundancy relations must be run against the process plant, for which they are to perform fault detection. The redundancy relations are therefore run against the simulation plant model, developed in Section 6. In addition, the estimated states are included in the simulation. The state estimation error is mainly included for analysis purposes, it gives a better understanding of the basis for the redundancy relations, and has no practical purpose in the fault detection system.

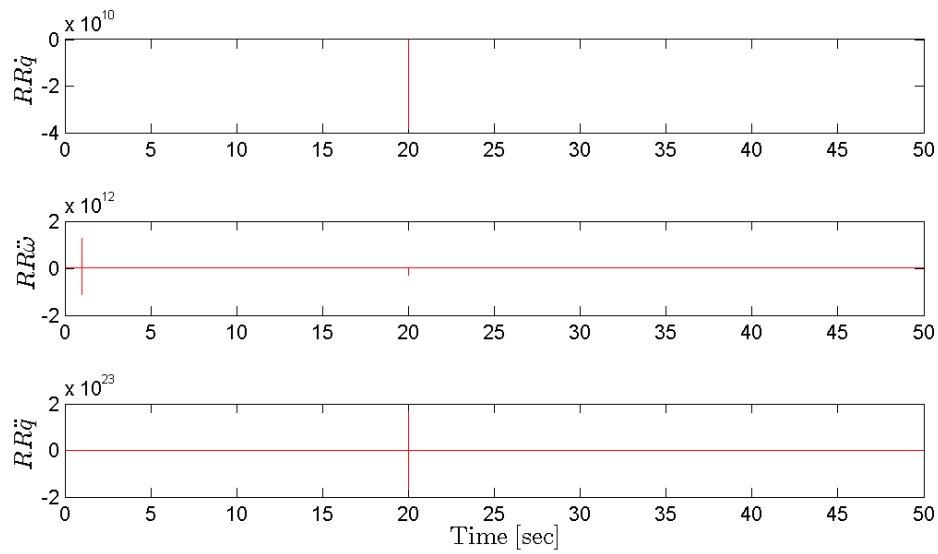
Figure 9.5 shows the redundancy relations and state estimation performance when run against the simulation plant, with a sudden load decrease occurring after 20 seconds. It is seen that before the load decrease, the mechanical torque and frequency estimation error is zero. Hence, these states are well predicted.

The load angle and field current, both have a steady deviation from zero. The prediction of these states clearly have a bias. When the load change occur, the load angle makes a sudden step up to a new steady value. The other values stay about the same, except from some short-lasting reactions due to the dependency on differentiated variables. From (9.22) it is seen that the estimated load angle is proportional to the active power. This simplification is probably the reason for the load angle bias, and the sudden bias step. The estimated field current bias is probably also caused by the simplifications in the control plant model model (see (9.25)). As long as this deviation stays at about the same value for all normal simulation modes, and both before and after a normal simulation mode event occurs, the bias should not have any effect on the fault detection performance. This is obvious, since the fault detection system is based on that the redundancy relations should stay within certain predefined limits during normal operation mode. Hence, the step occurring for

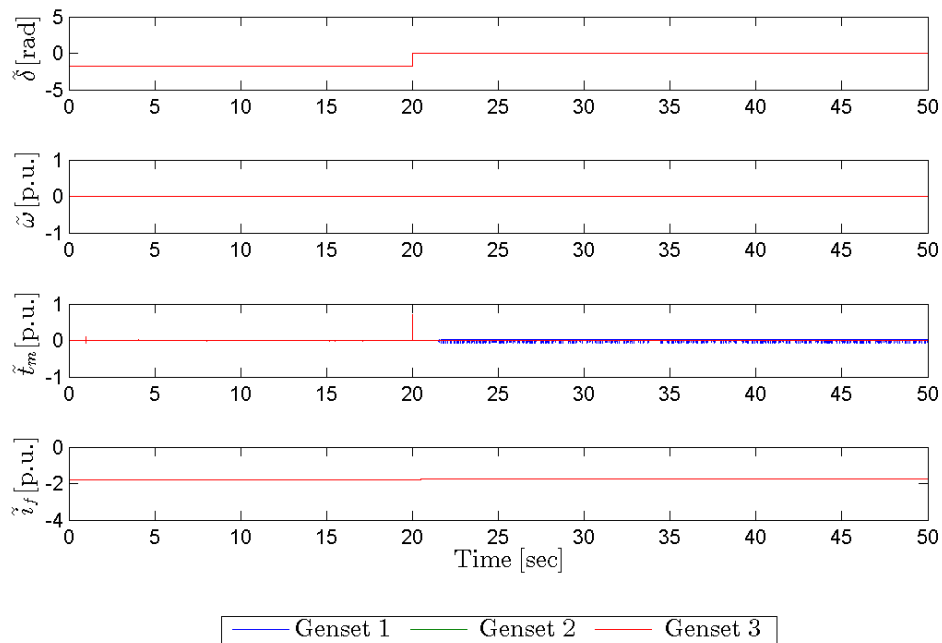
the load angle might cause the redundancy relations to be less effective. From (9.26) and Table 9.2 it is seen that this might be an issue for $r_{\dot{\omega}}$ and $r_{\dot{q}}$, since they are dependent on the active power (due to the method used to derive the redundancy relations, dependency on the load angle leads to dependency of the active power).

In Figure 9.5a, it is seen that after initiation, the redundancy relations stay at a steady value both before and after the load increase. The change in load angle bias can therefore be concluded to not have a significant effect on the fault detection capabilities of the redundancy relations. When the load change occur, it is seen that the redundancy relations respond with a very short and high, spike. This can be concluded that is caused by the differentiation terms; the spike is very high and short lasting, which is typical behavior for a parameter that undergoes a sudden change is differentiated. This can also be concluded since the magnitude of the spike increases with the redundancy relation's dependency on derivatives (see (9.26) and Table 9.2 and 9.3).

Since the redundancy relations stays at about the same value both before and after the load change, it can be concluded that the redundancy relations should be possible to use for fault detection. However, in order to do this, the redundancy relation's results for the different simulation modes, must be further analyzed.



(a) Redundancy relations



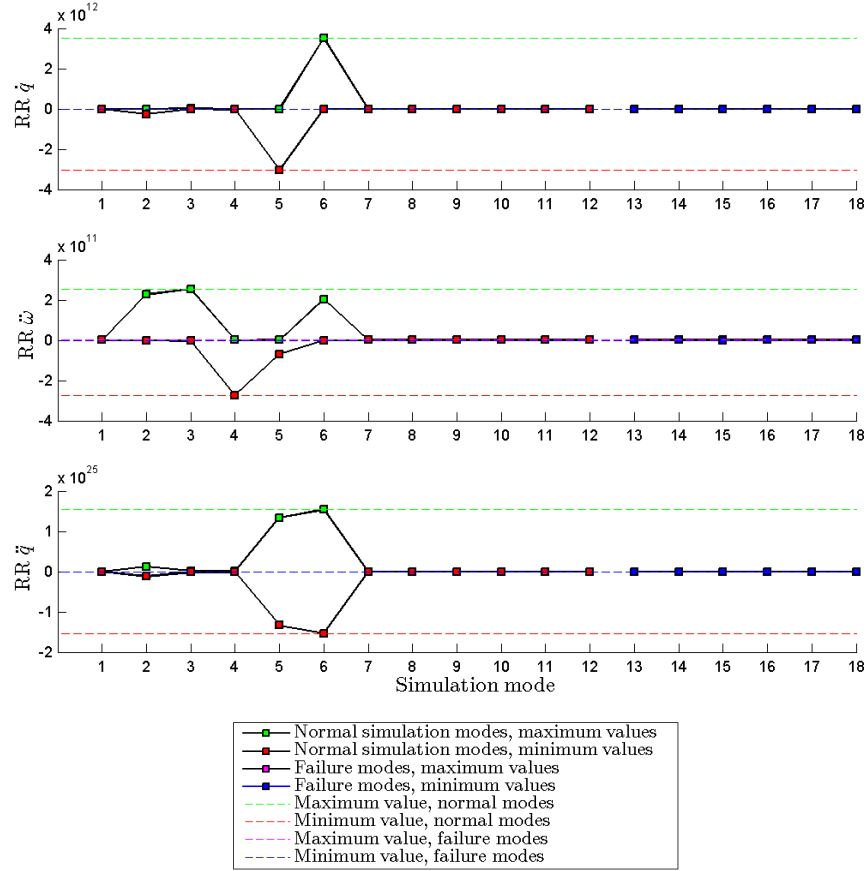
(b) State estimation error

Figure 9.5: Nonlinear redundancy relations and state estimation error, run against control plant model, with sudden active load decrease occurring after 20 seconds.

9.6.1 Fault detection without exceedance duration

Figure 10.1 shows the maximum and minimum values of the redundancy relations, for the different simulation modes. The plots to the left in the figure (1 to 12), are the values for the normal simulation modes. This also includes the values for the healthy gensets, in the failure modes. It is important that these are included in the analysis, since it is crucial that the fault detection system only disconnects the faulty genset when a failure mode occurs. The graphs to the right in the figure (13 to 18), are the values for the faulty gensets, for the failure modes.

From Figure 10.1, it is clear that the redundancy relations are not capable of detecting the failure modes. This can be seen, since several of the values on the left-side graph (the normal simulation modes), are larger than any of the values on the right-side graph (the failure modes). This is clearly not in accordance with the functionality of the fault detection system, described in (9.27), (9.28) and (9.29).



Number	Simulation mode description
1	Normal operation
2	Sudden disconnection of one genset, values for healthy gensets
3	Sudden active power increase
4	Sudden active power decrease
5	Sudden reactive power increase
6	Sudden reactive power decrease
7	Governor frozen, values for healthy genset
8	Governor to minimum, values for healthy genset
9	Governor to maximum, values for healthy genset
10	AVR frozen, values for healthy genset
11	AVR to minimum, values for healthy genset
12	AVR to maximum, values for healthy genset
13	Governor frozen, values for genset with failure
14	Governor to minimum, values for genset with failure
15	Governor to maximum, values for genset with failure
16	AVR frozen, values for genset with failure
17	AVR to minimum, values for genset with failure
18	AVR to maximum, values for genset with failure

Figure 9.6

9.6.2 Fault detection with exceedance duration

From the previous results for the fault detection system, it is clear that it is not capable of detecting faults based on the redundancy relation values alone. Therefore the duration of the redundancy relation values are also taken into consideration. This means that the redundancy relation limit values (Δr_{min} and Δr_{max}), are set so that for no normal simulation modes these limits are exceeded for a duration higher than a preset limit, Δt . The fault detection system in (9.27), (9.28) and (9.29), is then extended to

$$\begin{aligned} r \geq \Delta r_{max} \quad \text{and} \quad t(r \geq \Delta r_{max}) \geq \Delta t & \quad \text{Fault detected} & (9.30) \\ r \leq \Delta r_{min} \quad \text{and} \quad t(r \leq \Delta r_{min}) \geq \Delta t & \quad \text{Fault detected} \end{aligned}$$

where $t(r \leq \Delta r)$ is defined as the duration of the situation $r \leq \Delta r$.

From Figure 9.7, it can be seen that this method might make the redundancy relations suitable for fault detection. The figure illustrates the behavior of the redundancy relations when active and reactive load is increased, and when governor and AVR faults occur. It can be seen that when the active or reactive power is increased, the redundancy relations respond with a high peak with very short duration. When the failure modes are inflicted to the system, the response is a sudden and lasting change in value. The change in value caused by the failure modes, is much lower than for the normal simulation modes. This clearly demonstrates that the duration of the exceedance must be included in the fault detection system.

Figure 9.8 displays plots of the maximum and minimum redundancy relation values, that have a duration higher than Δt . The plots to the left in the figure (simulation mode 1 to 12), are the normal operation modes, while the plots to the right in the figure (simulation mode 13 to 18), are the failure modes. The allowed duration times are tuned, so that r_{ω} for the governor failure modes (simulation mode 13 to 15), deviates more from zero than r_{ω} for the normal simulation modes (simulation mode 1 to 12). The same is done with $r_{\dot{q}}$ and $r_{\ddot{q}}$ for the AVR failure modes. Based on the results of this tuning, the lowest possible value of Δr_{max} , and the highest possible value of Δr_{min} , can be decided for each redundancy relation. These values are presented in Figure 9.8 as a dotted green and red lines, respectively. In the following, these values are denoted $\Delta r_{max,min}$ and $\Delta r_{min,min}$, respectively.

In the tuning of Δt , it is also set a higher requirement for the duration. This requirement is that the highest possible value of Δr_{max} , and the lowest possible value of Δr_{min} , is between 10 and 20 % higher/lower than $r_{max,min}$ and $\Delta r_{min,min}$, respectively. In the following, these values are denoted $\Delta r_{max,max}$ and $\Delta r_{min,max}$, respectively. These values, are displayed in Figure 9.8 as dotted pink lines for $\Delta r_{max,max}$, and dotted blue lines for $\Delta r_{min,max}$.

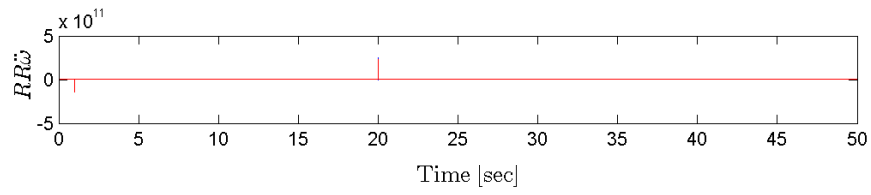
The reason last requirement, is that it makes it possible to compare the different fault detection systems. However, for the redundancy relations, this requirement is not met. Due to the short

duration of the redundancy relation spikes that occur for normal operation events (see Figure 9.7), it is possible to set Δt to be very small. Δt is therefore restricted to not be lower than 0.001, as Δt can not be lower than the step size used in the simulator.

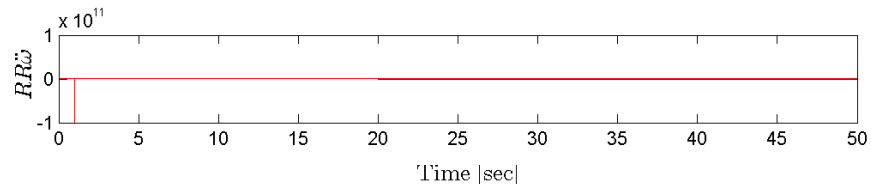
The numerical results for the fault detection system are displayed in Table 9.4. These are the values obtained in accordance with the above described requirements.

	$r_{\dot{q}}$	$r_{\ddot{\omega}}$	$r_{\ddot{q}}$
Δt [sec]	0.001	0.001	0.001
$\Delta r_{max,max}$	-40.2571	36.9756	6.5173×10^5
$\Delta r_{max,min}$	-272.2272	23.1585	4.0423×10^5
$\Delta r_{min,max}$	-1.5589×10^3	-24.0442	1.7261×10^4
$\Delta r_{min,min}$	-953.5123	-4.2183	1.1603×10^5
$\frac{\Delta r_{max,max} - \Delta r_{max,min}}{\Delta r_{min,min}}$ [%]	-0.8521	0.5966	0.6123
$\frac{\Delta r_{min,max} - \Delta r_{min,min}}{\Delta r_{min,min}}$ [%]	0.6349	4.7000	-0.8512

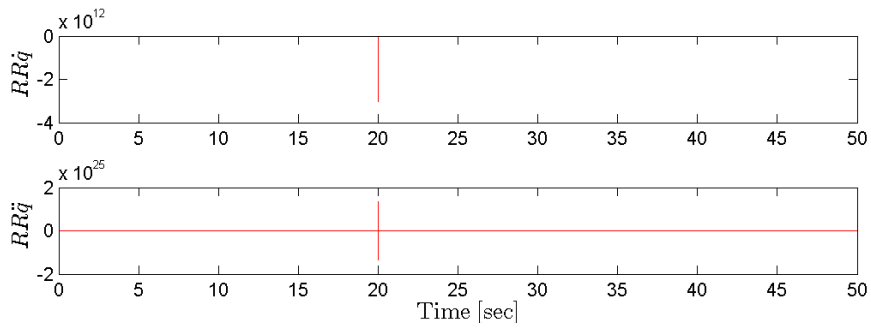
Table 9.4: Parameters for fault detection with exceedance duration.



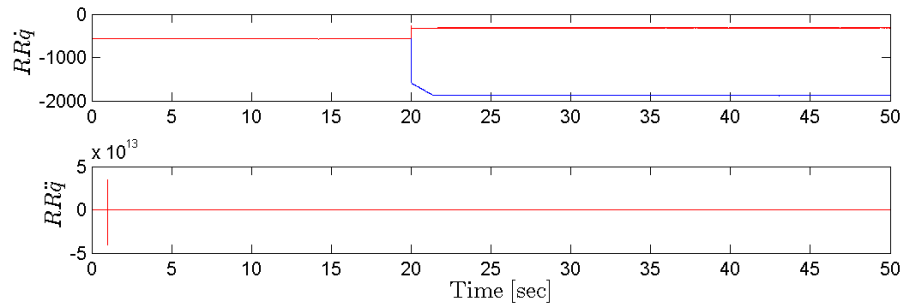
(a) Sudden increase in active power.



(b) Failure mode, governor to maximum

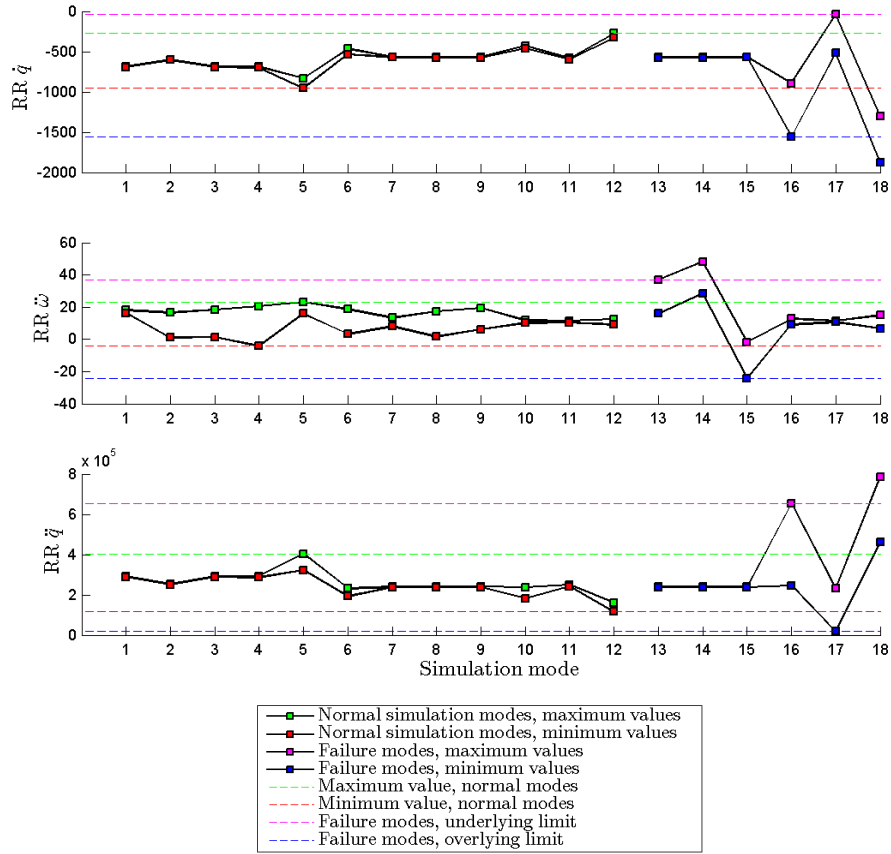


(c) Sudden increase in reactive power.



(d) Failure mode, AVR to maximum.

Figure 9.7: Measurement estimation errors, for observer run against simulation plant model, events occurring after 20 seconds.



Number	Simulation mode description
1	Normal operation
2	Sudden disconnection of one genset, values for healthy gensets
3	Sudden active power increase
4	Sudden active power decrease
5	Sudden reactive power increase
6	Sudden reactive power decrease
7	Governor frozen, values for healthy genset
8	Governor to minimum, values for healthy genset
9	Governor to maximum, values for healthy genset
10	AVR frozen, values for healthy genset
11	AVR to minimum, values for healthy genset
12	AVR to maximum, values for healthy genset
13	Governor frozen, values for genset with failure
14	Governor to minimum, values for genset with failure
15	Governor to maximum, values for genset with failure
16	AVR frozen, values for genset with failure
17	AVR to minimum, values for genset with failure
18	AVR to maximum, values for genset with failure

Figure 9.8: Minimum and maximum values of redundancy relations, for each simulation scenario, and with maximum duration of the values 0.001 second.

9.7 Resulting fault detection system

The final fault detection system can now be formulated

$$\begin{array}{lll}
 r_{\dot{q}} \geq \Delta r_{\dot{q},max} & \text{and} & t(r_{\dot{q}} \geq \Delta r_{\dot{q},max}) \geq \Delta t_{\dot{q}} & \text{AVR fault detected} \\
 r_{\dot{q}} \leq \Delta r_{\dot{q},min} & \text{and} & t(r_{\dot{q}} \leq \Delta r_{\dot{q},min}) \geq \Delta t_{\dot{q}} & \text{AVR fault detected} \\
 \\
 r_{\ddot{\omega}} \geq \Delta r_{\ddot{\omega},max} & \text{and} & t(r_{\ddot{\omega}} \geq \Delta r_{\ddot{\omega},max}) \geq \Delta t_{\ddot{\omega}} & \text{Governor fault detected} \\
 r_{\ddot{\omega}} \leq \Delta r_{\ddot{\omega},min} & \text{and} & t(r_{\ddot{\omega}} \leq \Delta r_{\ddot{\omega},min}) \geq \Delta t_{\ddot{\omega}} & \text{Governor fault detected} \\
 \\
 r_{\ddot{q}} \geq \Delta r_{\ddot{q},max} & \text{and} & t(r_{\ddot{q}} \geq \Delta r_{\ddot{q},max}) \geq \Delta t_{\ddot{q}} & \text{AVR fault detected} \\
 r_{\ddot{q}} \leq \Delta r_{\ddot{q},min} & \text{and} & t(r_{\ddot{q}} \leq \Delta r_{\ddot{q},min}) \geq \Delta t_{\ddot{q}} & \text{AVR fault detected}
 \end{array}$$

where the parameter values are given in Table 9.5, and with system architecture as showed in Figure 9.9. This means that the fault detection system based on nonlinear redundancy relations, is able to detect governor faults and AVR faults after 0.001 seconds.

	$r_{\dot{q}}$	$r_{\ddot{\omega}}$	$r_{\ddot{q}}$
Δt [sec]	0.001	0.001	0.001
Δr_{max}	-40.2571	36.9756	6.5173×10^5
Δr_{min}	-1.5589×10^3	-24.0442	1.7261×10^4

Table 9.5: Parameters for fault detection system based on redundancy relations.

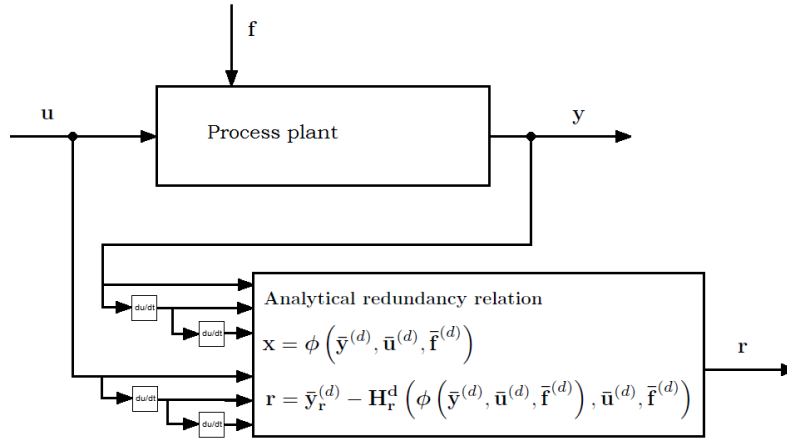


Figure 9.9: Block diagram for fault detection based on redundancy relations

10 Observer based fault detection system

10.1 Theoretical background

The observer based fault detection system, is based on the nonlinear Luenberger-type observer derived in Section 7. For the observer based fault detection, the measurement estimation error is used as fault detection algorithm

$$\mathbf{r} = \mathbf{y} - \hat{\mathbf{y}} \quad (10.1)$$

where

$$\mathbf{r} = [r_\omega \quad r_p \quad r_q]^T = [\tilde{\omega} \quad \tilde{p} \quad \tilde{q}]^T \quad (10.2)$$

In order to take modeling errors into account, it is required that \mathbf{r} is inside of a predefined window, $\Delta\mathbf{r}$, before a deviation from zero is considered a fault.

Based on the measurement estimation error in (7.31), the fault detection algorithms dependencies of the states can be found; $r_\omega(\tilde{\omega})$, $r_p(\tilde{\delta})$, and $r_q(\tilde{\omega}, \tilde{i}_f)$. Using the state estimation error in (7.30), it is clear that the input dependencies are; $r_\omega(u)$, $r_p(u)$, and $r_q(u, v_f)$. Hence, it is known how the different failure modes can be detected by the different parts of the fault detection algorithm. This system can be written

$$\begin{aligned} \Delta r_{\omega, \min} \leq r_\omega \leq \Delta r_{\omega, \max} & \quad \text{No fault detected} & (10.3) \\ r_\omega \leq \Delta r_{\omega, \min} & \quad \text{Governor fault detected} \\ r_\omega \geq \Delta r_{\omega, \max} & \quad \text{Governor fault detected} \end{aligned}$$

$$\begin{aligned} \Delta r_{p, \min} \leq r_p \leq \Delta r_{p, \max} & \quad \text{No fault detected} & (10.4) \\ r_p \leq \Delta r_{p, \min} & \quad \text{Governor fault detected} \\ r_p \geq \Delta r_{p, \max} & \quad \text{Governor fault detected} \end{aligned}$$

$$\begin{aligned} \Delta r_{q, \min} \leq r_q \leq \Delta r_{q, \max} & \quad \text{No fault detected} & (10.5) \\ r_q \leq \Delta r_{q, \min} & \quad \text{Governor and AVR fault detected} \\ r_q \geq \Delta r_{q, \max} & \quad \text{Governor and AVR fault detected} \end{aligned}$$

10.2 Simulation study

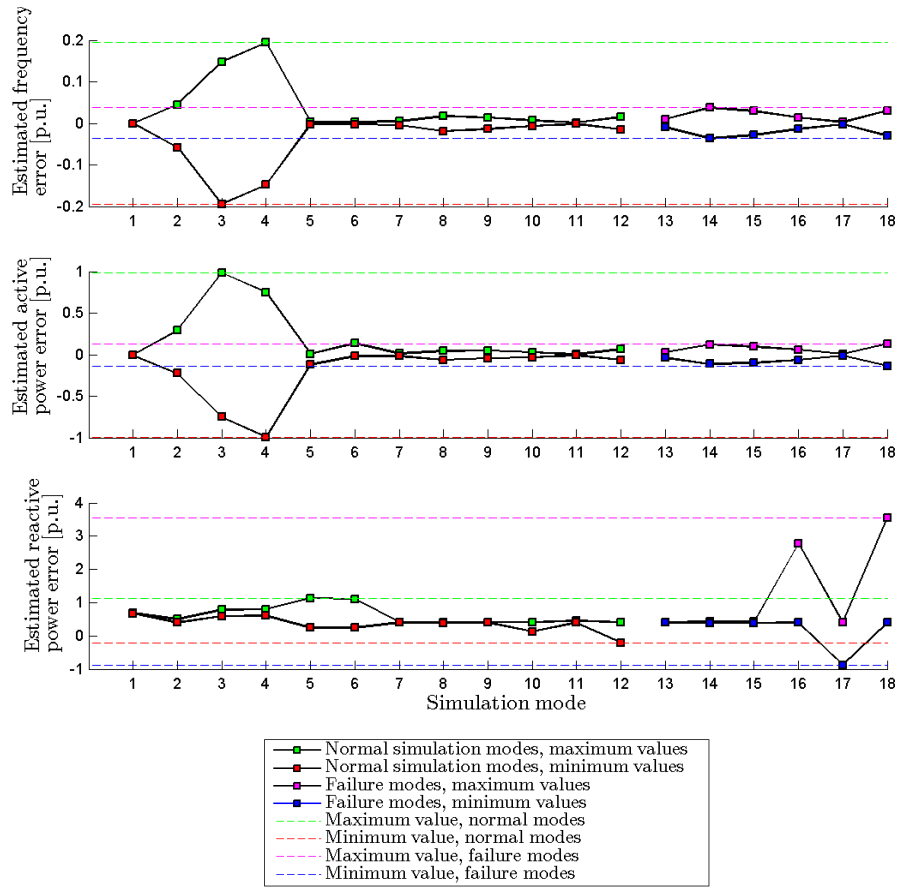
The performance of the nonlinear Luenberger-type observer, is verified in Section 7.

From the simulation results with the control plant model it can be seen that the frequency and active power estimation errors, are affected by the governor faults. This is in accordance with the fault detection system in (10.3) to (10.4). In accordance with the fault detection system in (10.5), the reactive power estimation error is the only fault detection algorithm affected by the AVR faults. However, response of the reactive power estimation error to the governor failures, is quite weak. The fault detection algorithm should therefore not be used for detection of governor faults. This is also in accordance with the results from the simulations of the observer with the simulation plant model, in Section 7.4.

10.2.1 Fault detection without exceedance duration

Figure 10.1 shows the maximum and minimum measurement estimation error, for the different simulation scenarios. The plots to the left (simulation mode 1 to 12), are the results for the normal operation modes, while the plots to the right (simulation mode 13 to 18), are the failure modes.

From the figure it is clear that the governor failures can not be detected by the system described in (10.3) and (10.4). It is therefore concluded that in order to be able to detect the governor failure modes, the exceedance duration must be included in the fault detection system. When it comes to the AVR failure modes, it is clearly seen that they are detected by the fault detection system in (10.5). The exceedance duration, is therefore not necessary to find for r_q .



Number	Simulation mode description
1	Normal operation
2	Sudden disconnection of one genset, values for healthy gensets
3	Sudden active power increase
4	Sudden active power decrease
5	Sudden reactive power increase
6	Sudden reactive power decrease
7	Governor frozen, values for healthy genset
8	Governor to minimum, values for healthy genset
9	Governor to maximum, values for healthy genset
10	AVR frozen, values for healthy genset
11	AVR to minimum, values for healthy genset
12	AVR to maximum, values for healthy genset
13	Governor frozen, values for genset with failure
14	Governor to minimum, values for genset with failure
15	Governor to maximum, values for genset with failure
16	AVR frozen, values for genset with failure
17	AVR to minimum, values for genset with failure
18	AVR to maximum, values for genset with failure

Figure 10.1

10.2.2 Fault detection with exceedance duration

Figure 10.2 shows the simulation results for the fault detection algorithms, for two different normal simulation modes, and two failure modes. It is seen that for the estimated active power and frequency error, have a quite similar reaction to a sudden change in active power, and a governor failure mode (Figure 10.2a and 10.2b). However, when the events occur, the normal operation modes leads to higher spikes than for the failure modes. This is in accordance with the observations in Figure 10.1. It is also seen that after the occurrence of the events, the error for the normal operation modes, settle at the same value as before the event. For the failure modes, however, the faulty genset clearly settles at a new steady value. For both scenarios, the duration before settlement on a steady value, is quite long. This leads to the conclusion, that the failure modes should be possible to detect with this system. However, the detection time is probably relatively long.

Figure 10.2c and 10.2d shows the behavior of the estimated reactive power error, when a reactive power increase, and a AVR failure mode occur. For both scenarios the fault detection algorithm's response is a sudden change in value. For both simulation modes, the estimation error stays at a new steady value. Luckily, the response to the failure mode is larger, than for the normal simulation mode. This is clearly the reason why the AVR failure modes can be detected without considering the exceedance duration. This however, introduces a concern for the quality of the fault detection algorithm. Since the the reactive power estimation error, experiences a step in value for both normal simulation modes, and failure modes, it is dependent on that the step for all failure modes is larger than for all normal modes. For the failure modes investigated in this thesis, this is the case. However, further analysis with different failure modes should be performed.

In order to take the exceedance duration into account, the variable Δt is defined so that $t(r \leq \Delta r)$ is the duration of the situation $r \leq \Delta r$. Δt is then tuned so that all maximum and minimum values of the frequency and active power estimation error, are further from zero for simulation mode 13 to 15, than for simulation mode 1 to 12. The simulation mode numbers are as defined in Figure 10.1 and 10.3. Based on the results of this tuning, the lowest possible value of Δr_{max} , and the highest possible value of Δr_{min} , can be decided for each measurement estimation error. These values are presented in Figure 10.3 as a dotted green and red lines, respectively. In the following, these values are denoted $\Delta r_{max,min}$ and $\Delta r_{min,min}$, respectively.

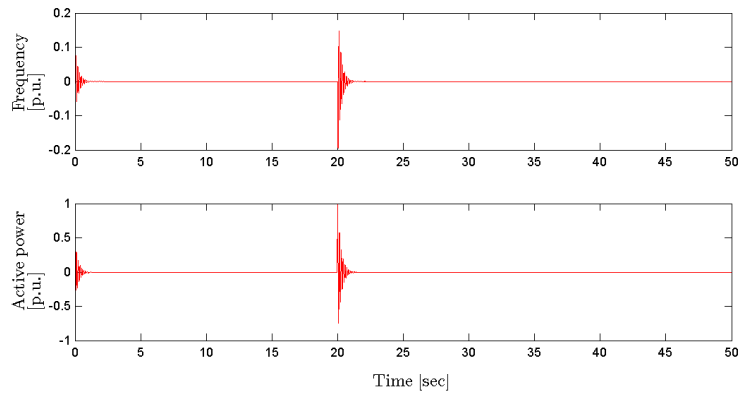
As for the two other fault detection systems, the value of Δt is restricted so that that the highest possible value of Δr_{max} , and the lowest possible value of Δr_{min} , is between 10 and 20 % higher/lower than $r_{max,min}$ and $\Delta r_{min,min}$, respectively. In the following, these values are denoted $\Delta r_{max,max}$ and $\Delta r_{min,max}$, respectively. These values, are displayed in Figure 9.8 as dotted pink lines for $\Delta r_{max,max}$, and dotted blue lines for $\Delta r_{min,max}$. This last requirement is not satisfied for the reactive power estimation error, as the exceedance duration is not used for this fault detection

algorithm.

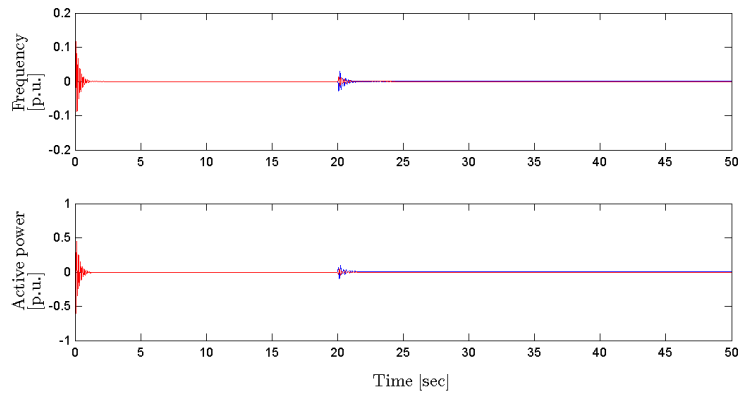
The maximum and minimum measurement estimation errors, when the exceedance duration is taken into account, is displayed in Figure 10.3. It is clear that this system is capable of detecting all failure modes. The numerical results for the fault detection system, can be found in Table 10.1.

	Frequency	Active power	Reactive power
Δt [sec]	3.0	1.535	Immediately
$\Delta r_{max,max}$	9.6529×10^{-5}	0.0110	2.7680
$\Delta r_{max,min}$	6.4219×10^{-5}	0.0035	1.1370
$\Delta r_{min,max}$	-2.2859×10^{-4}	-0.0108	-0.8780
$\Delta r_{min,min}$	-1.2811×10^{-4}	-0.0092	-0.2036
$\frac{\Delta r_{max,max} - \Delta r_{max,min}}{\Delta r_{min,min}}$ [%]	50.31	197.38	143.44
$\frac{\Delta r_{min,max} - \Delta r_{min,min}}{\Delta r_{min,min}}$ [%]	10.32	17.51	331.16

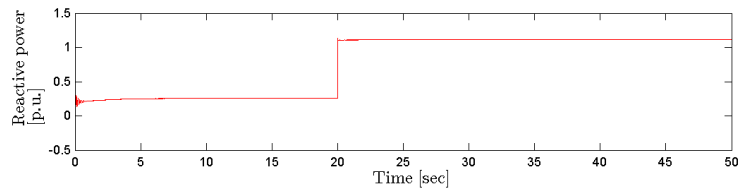
Table 10.1: Parameters for fault detection with exceedance duration.



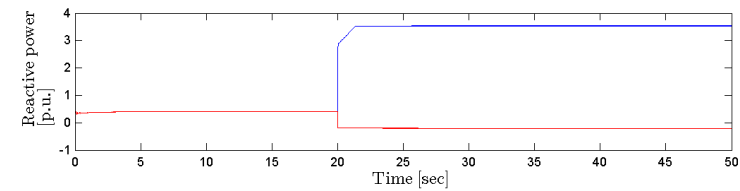
(a) Sudden increase in active power.



(b) Failure mode, governor to maximum

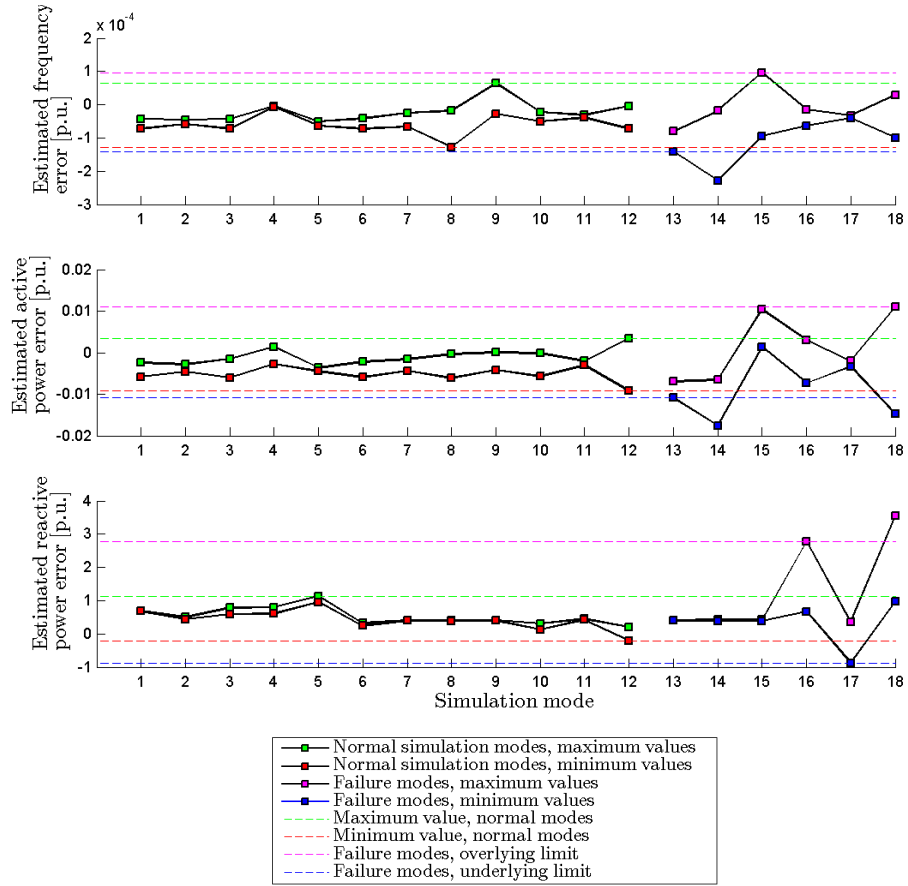


(c) Sudden increase in reactive power.



(d) Failure mode, AVR to maximum.

Figure 10.2: Measurement estimation errors, for observer run against simulation plant model, events occurring after 20 seconds. The failure modes are implemented in Genset 1.



Number	Simulation mode description
1	Normal operation
2	Sudden disconnection of one genset, values for healthy gensets
3	Sudden active power increase
4	Sudden active power decrease
5	Sudden reactive power increase
6	Sudden reactive power decrease
7	Governor frozen, values for healthy genset
8	Governor to minimum, values for healthy genset
9	Governor to maximum, values for healthy genset
10	AVR frozen, values for healthy genset
11	AVR to minimum, values for healthy genset
12	AVR to maximum, values for healthy genset
13	Governor frozen, values for genset with failure
14	Governor to minimum, values for genset with failure
15	Governor to maximum, values for genset with failure
16	AVR frozen, values for genset with failure
17	AVR to minimum, values for genset with failure
18	AVR to maximum, values for genset with failure

Figure 10.3

10.3 Resulting fault detection system

The final fault detection system can now be formulated

$$\begin{aligned} r_\omega \geq \Delta r_{\omega,max} \quad \text{and} \quad t(r_\omega \geq \Delta r_{\omega,max}) \geq \Delta t_\omega & \quad \text{Governor fault detected} & (10.6) \\ r_\omega \leq \Delta r_{\omega,min} \quad \text{and} \quad t(r_\omega \leq \Delta r_{\omega,min}) \geq \Delta t_\omega & \quad \text{Governor fault detected} \end{aligned}$$

$$\begin{aligned} r_p \geq \Delta r_{p,max} \quad \text{and} \quad t(r_p \geq \Delta r_{p,max}) \geq \Delta t_p & \quad \text{Governor fault detected} & (10.7) \\ r_p \leq \Delta r_{p,min} \quad \text{and} \quad t(r_p \leq \Delta r_{p,min}) \geq \Delta t_p & \quad \text{Governor fault detected} \end{aligned}$$

$$\begin{aligned} r_q \leq \Delta r_{q,min} & \quad \text{AVR fault detected} & (10.8) \\ r_q \geq \Delta r_{q,max} & \quad \text{AVR fault detected} \end{aligned}$$

where the parameter values are given in Table 10.2, and with system architecture as showed in Figure 10.4. This means that the fault detection system based on nonlinear redundancy relations, is able to detect governor faults after 1.535 seconds and AVR faults immediately after the fault occurs.

	Frequency	Active power	Reactive power
Δt [sec]	3.0	1.535	Immediately
Δr_{max}	9.6529×10^{-5}	0.0110	2.7680
Δr_{min}	-2.2859×10^{-4}	-0.0108	-0.8780

Table 10.2: Parameters for fault detection with exceedance duration.

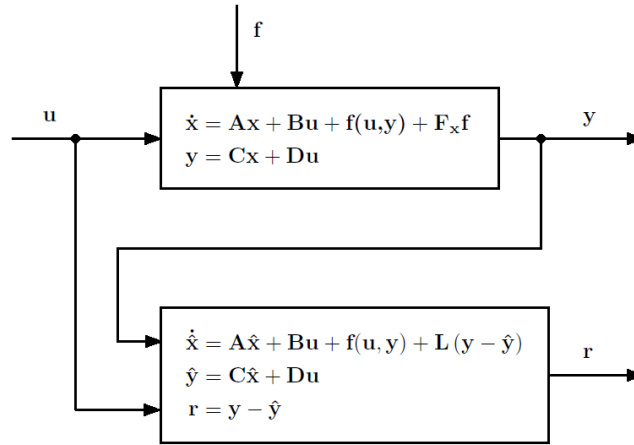


Figure 10.4: State-space implementation of nonlinear Luenberg-type observer based fault detection

11 Comparison of fault detection systems

In this theses three different fault detection systems are derived, and their performance is demonstrated. The AGP is presented in Section 8, fault detection based on redundancy relations is presented in Section 9, and observer based fault detection is presented in Section 10. Table 11.1 shows the shortest possible fault detection times for governor and AVR faults, for the three fault detection systems.

	Governor faults	AVR faults
Δt , AGP [sec]	0.6	0.6
Δt , Redundancy relations [sec]	0.001	0.001
Δt , Observer based [sec]	1.535	Immediately

Table 11.1: Shortest possible fault detection times for the three fault detection systems.

It is seen, that the redundancy relation based fault detection system, has the overall best performance. The big weakness of this method, the differentiation of the parameters, might have turned out to be an advantage. Differentiation is known to increase noise, and hence also modeling differences. But it also increases the errors introduced by the failure modes and makes the faults easier to detect. However, it is difficult to conclude if this method would work satisfactory for a real system. After all, the simulation plant model and the control plant model, are still quite similar. A real power system, also have noisy sensor signals. This would probably result in quite noisy redundancy relation values, and it is uncertain if it would be possible for the failure modes to "stand out".

The observer based fault detection system is the best at detecting AGP faults, but the slowest at detecting governor faults. This is most likely due to the observer design. It is obvious that the AVR failures have a larger effect on the reactive power estimation error, than on the frequency and active power estimation error. There are several methods for improving the observer, that could make the observer based fault detection system better. More extensive tuning of the observer, is possible, for example by using optimization to find the observer gains. An other possibility is to change the control plant model. There might be simplifications or extensions, that would make the control plant model more suitable for the observer design. Regardless of this, the performance of the observer based fault detection system's capability of detecting AVR faults, proves that it is possible to develop well functioning observer based fault detection systems.

The AGP is proven to give relatively quick detection of the failure modes. The main advantage of the method is that it is simple and robust. It does not need extensive knowledge about the power system, and can be implemented for all power systems as long as they are run in droop.

In order to fully conclude on the performance of the fault detection systems, more testing of the systems should be performed. In this thesis, the fault detection systems are tested against a process plan model with no sensor noise, and for a limited number of simulation scenarios. In order to fully verify the performance, more extensive testing should be performed. Simulation scenarios with

oscillating loads, and a wider range of values for frozen governor and AVR, are examples of relevant simulation scenarios that should be tested.

12 Concluding remarks

12.1 Conclusion

In this thesis three fault detection systems for a marine power plant are presented. Two of the fault detection systems are model based while one is not model based. based on the droop curves of the load sharing system. The method that is not model based, is called Advanced Generator Protection and is a system commonly used for marine power systems. The two developed model based fault detection algorithms, are both based on the same nonlinear state model, but two slightly different models for the measurements. One of the methods uses analytical redundancy relations calculated from the nonlinear state and measurement model. The last method uses the nonlinear state model, and the linearized measurement model, to develop an observer for the power plant. The observer measurement estimation error, is then used as fault detection system.

In order to verify the performance of the fault detection systems, they are simulated together with a simulation plant model. The simulation plant model is a more complex model of a marine power plant. Simulations are then run for several normal operation modes, and some failure modes of interest. The failure modes of interest, are governor and AVR actuator failures. In order for a fault detection system to detect the failure modes, it must be able to separate a faulty situation from a normal operation mode.

It is found that for most of the fault detection algorithms, it is necessary to limit both the value of the fault detection algorithm, and the duration of the values. Since it is desired to detect a faulty situation quickly, the duration of the exceedance is desired to be as low as possible. This also makes it possible to compare the different fault detection systems.

It is found that all of the fault detection systems are capable of detecting the simulated faults. They are also capable of separating the governor failures from the AVR failures. The main difference between the methods are therefore the detection time, and the systems' individual properties.

The Advanced Generator Protection is able to detect both governor and AVR failures in 0.6 seconds. The main advantage with this method is that it is simple. It can be implemented in most marine power systems, and is not dependent on extensive knowledge of the system parameters. The only requirement is that the power plant is run in droop mode.

The fault detection system based on redundancy relations, is capable of detecting all governor and AVR failure modes within 0.001 seconds, is therefore the best performing fault detecting system. A disadvantage with this system is that it is dependent on several system parameters, and it is very sensitive to noise. Since the simulations are performed with the assumption that there are no measurement noise, this weakness of the fault detection system is not fully investigated.

The observer based fault detection system, is capable of detecting governor faults in 1.535 seconds, and the AVR faults immediately after it occurred. Actually, the fault detection system is the only that does not have a limitation in time in order to detect faults. However, this is only the case for AVR faults. The fault detection system is dependent on several system parameters and tuning in order to work. In addition the capabilities for detecting governor faults is not very impressive.

However, the good results for AVR fault detection, indicates that observer based fault detection is worth further investigation. Better tuning of the observer, a better observer design, or an other model to base the observer design on, might result in fault detection system with very good capabilities. An other advantage with an observer based fault detection system, is that it probably will handle sensor noise and modeling differences well. An observer based fault detection system might therefor be very suitable for fault detection for a real marine power plant.

12.2 Suggestions for further work

All the presented fault detection systems have capabilities to be improved. First of all, more extensive testing of the systems must be performed. This includes both further tests with the simulator, and on a real system. More extensive testing with different load scenarios, and for more failure modes, should be performed with the simulator. In addition noise should be modeled into the simulator.

It is also possible to further develop the model based fault detection systems. The fault detection system based on redundancy relations, can be extended so that the differentiated inputs are estimated by an observer, and not by numerical differentiation. This might result in less noisy results. For the observer based fault detection system, more extensive tuning might give better results. It would also be interesting to test different types of observers.

References

- ABB Simulation and Test (n.d.) (2012). Excitation Systems & Combined Solutions - Simulation and Test <http://www.abb.com/product/us/9aac100578.aspx>. Online; 19-November-2012
- Arcak, M., Kokotovic, P. (2001). Nonlinear Observers: A Circle Criterion Design. Automatica, volume 37, pages 1923–1930, December 2001
- Batzel, T. D. (2006). Observer-based monitoring of synchronous generator winding health 2006 IEEE/PES Power Systems Conference and Exposition October 2006
- Blanke, M., Kinnaert, M., Lunze, J., Staroswiecki, M. (2006). Diagnosis and Fault-Tolerant Control, Second Edition OSpringer-Verlag, Berlin Heidelberg, 2006
- Bø, T. I. (2012). Dynamic Model Predictive Control for Load Sharing in Electric Power Plants for Ships Master's thesis, Norwegian University of Science and Technology
- Bø, T. I. (2011). Development of a diesel-electric simulation model and nonlinear control of power load-sharing Project thesis, Norwegian University of Science and Technology
- Cargill, S. (2007). A Novel Solution to Common Mode Failures in DP Class 2 Power Plant Dynamic Positioning Conference, October 2007
- Chen, C. T. (2009). Linear System Theory and Design, Third Edition Oxford University Press, Inc., New York, 2009
- Dassanke, S. K., Balas, G. L., Bokor, J. (2000). Using unknown input observers to detect and isolate sensor faults in a turbofan engine. 19th Digital Avionics System Conference, October 2000
- Flem, B. L. (2012). Development of real-time simulator of a diesel-electric power plant. Master's thesis, Norwegian University of Science and Technology
- Guzzella, L., Onder, C. (2009). Introduction to Modeling and Control of Internal Combustion Engine Systems Springer-Verlag, Berlin Heidelberg, 2010
- Hansen, J. F. (2000). Modelling and Control of Marine Power Systems. PhD thesis, Norwegian University of Science and Technology
- Hansen, J. F., Ådnes, A. F. (2009). Blackout Prevention & Recovery. Dynamic Positioning Conference, October 2009
- IMCA (2010). A Guide to DP Electrical Power Control Systems, International Marine Contractors Association (IMCA) <http://www.imca-int.com/documents/publications.html>. Online; accessed 05-11-2012; IMCA M 206
- Johannessen, P., Mathiesen, E. (2009) Advanced Failure Detection and Handling in Power Management System. Dynamic Positioning Conference, October 2009
- Khalil, H. K. (1996). Nonlinear Systems Pearson Education International Inc., New Jersey, 1996.

- Krause, P. C., Wasynczuk, O., Sudhoff, S. D. (2002). Analysis of electric machinery and drive systems. The Institute of Electrical and Electronics Engineers Inc., 2002
- Kyriakides, E., Heydt, G. T., Vittal, V. (2006). On-line estimation of synchronous Generator parameters using damper current observer and a graphic user interface. IEEE Transactions on Energy Conversion, volume 19, pages 499–507, September 2004
- Laila, D. S., Gruenbacher, E. (2008) Discrete-time nonlinear observer and output feedback design for a combustion test bench. 2008 47th IEEE Conference on Decision and Control December 2008
- Mathiesen, E. (2012) Presentation of Kongsberg Maritime's Power Management System Guest lecture in TMR4290, Norwegian University of Science and Technology, October 2012
- Nord, T. (2006) Voltage Stability in an Electric Propulsion System for Ships. Master's thesis, Royal Institute of Technology in Sweden
- Ouroua, A., Domaschk, L., Beno, J. H. (2005). Electric Ship Power System Integration Analysis Through Modeling and Simulation. IEEE Electric Ship Technologies Symposium, 2005
- Pedersen, T. A. (2009) Bond Graph Modeling of Marine Power Systems. PhD thesis, Norwegian University of Science and Technology
- Radan, D. (2008) Integrated Control of Marine Electrical Power Systems. PhD thesis, Norwegian University of Science and Technology
- Rizzoni, G. (2007). Principles and Applications of Electrical Engineering, Fifth Edition Mc Graw Hil, 2007
- IPP Consulting AS (2005). PMS-HL Testing, Failure Mode Description Electric System. Report Rev. C, Marine Cybernetics AS
- Skjetne, R., Egeland, O. (2006). Hardware-in-the-loop testing of marine control systems. Modeling, Identification and Control, volume 27, pages 239–258, 2006
- Skjetne, R. (2012b). Modeling a diesel-generator power plant. Lecture note TMR4290 at NTNU
- Veksler, A., Johansen, T. A., Skjetne, R. (2012) Transient power control in dynamic positioning - governor feedforward and dynamic thrust allocation. Manoeuvring and Control of Marine Craft, 9th IFAC Conference on., September 2012
- Woodward (2004). Governing Fundamentals and Power Management, Woodward. <http://www.woodward.com/enginescontrolsystems.aspx>. Online; accessed 20-10-2012; Manual 26260
- Xiros, N. (2002). Robust Control of Diesel Ship Propulsion, First Edition Springer-Verlag London Limited, 2002
- Ådnanes, A. K. (2003). Maritime Electrical Installations And Diesel Electric Propulsion. Department of Marine Technology, NTNU

A Power plant systems

The main systems where faults can occur are (IPP Consulting, 2005):

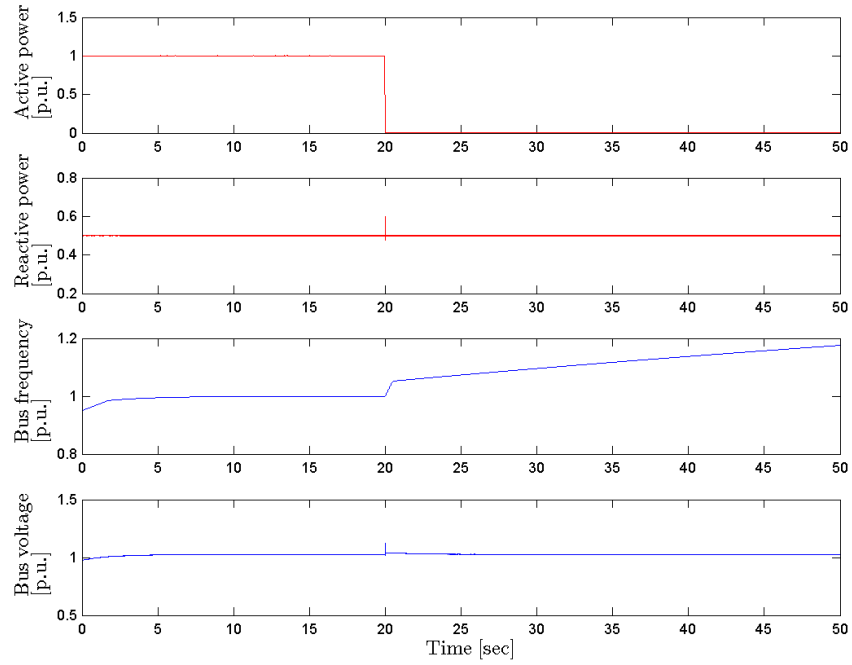
- Diesel engines
 - The actual engine with controls and sensors
 - Auxiliary systems, with associated sensors and control systems; fuel system, turbocharger, exhaust system, cooling system and lubrication system
 - Governor with controls, sensors, actuators, load sharing line and UPS
 - Safety systems with controls and sensors
- Generators
 - The actual generator with windings and sensors
 - Auxiliary systems, with associated sensors and controls; excitation system, cooling system, bearings and lubrication system
 - AVR with sensors and UPS
 - I/O to the automation system
- Main switchboards (generation and distribution)
 - Actual switchboard with bus bars and sensors
 - Circuit breakers, contactors, protection relays and UPS or battery backup
 - Synchronizing units (only for generation switchboard)
 - I/O to the automation system
- Distribution transformer
 - Actual transformer with windings, yoke and sensors
 - Auxiliary systems with sensors and controls; cooling system (fans, heat exchanger with sensors and starters) and pre-charging circuits
 - Interface to automation system
- Motors
 - Actual motor with stator, rotor, bearings and sensors
 - Cooling system and exciter system with control system (if synchronous)
- Variable speed drives
 - Motors with sensors and controls
 - Auxiliary systems; transformer with subsystems, frequency converter, cooling system and braking resistor
 - Sensors
 - Control systems, sensors and UPS/battery backup

- Communication to IAS
- Fixed speed drives
 - Motor with stator, rotor, housing, bearings and sensors
 - Starting arrangements, DOL, Y-D, auto trafo and soft starter
- Interface to PMS system

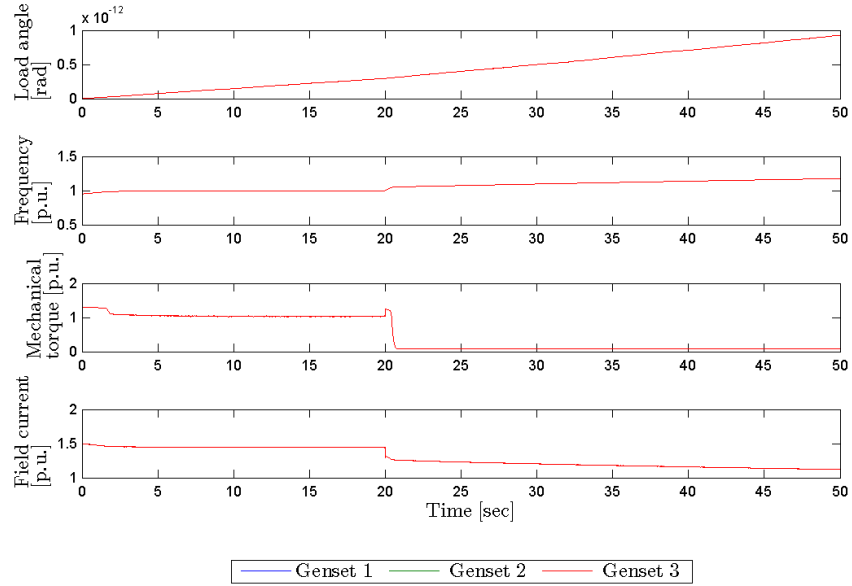
B Simulation study plots

B.1 Load change

On the following pages the simulation results for the simulation plant model are presented. The simulation parameters are defined in Section 6.

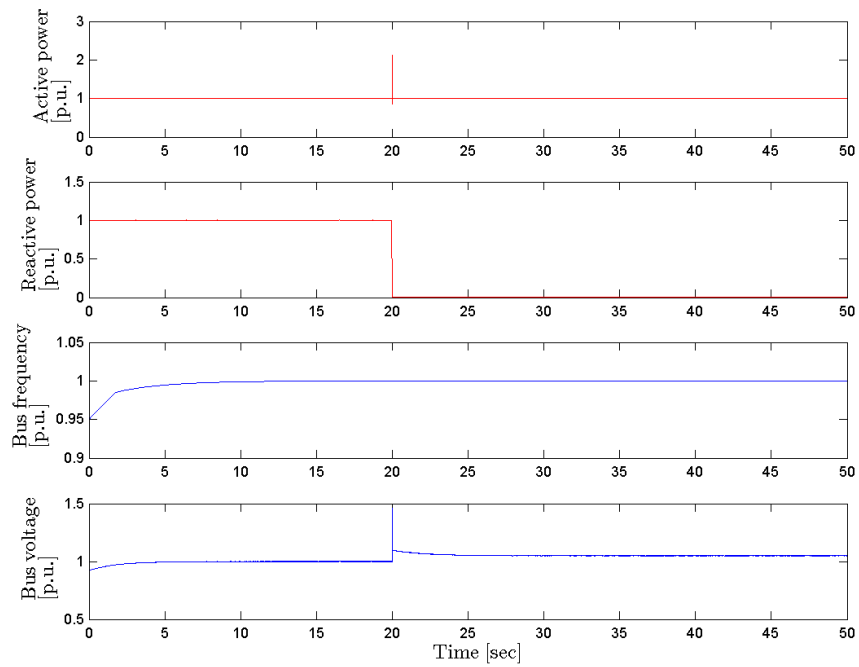


(a) Genset produced power and electrical parameters

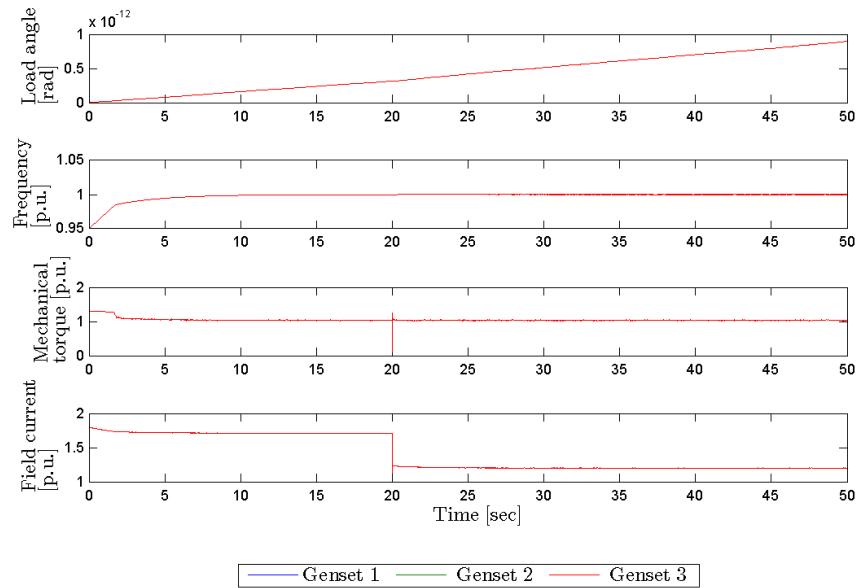


(b) Genset states

Figure B.1: Results from simulation with sudden active load decrease occurring after 20 seconds.

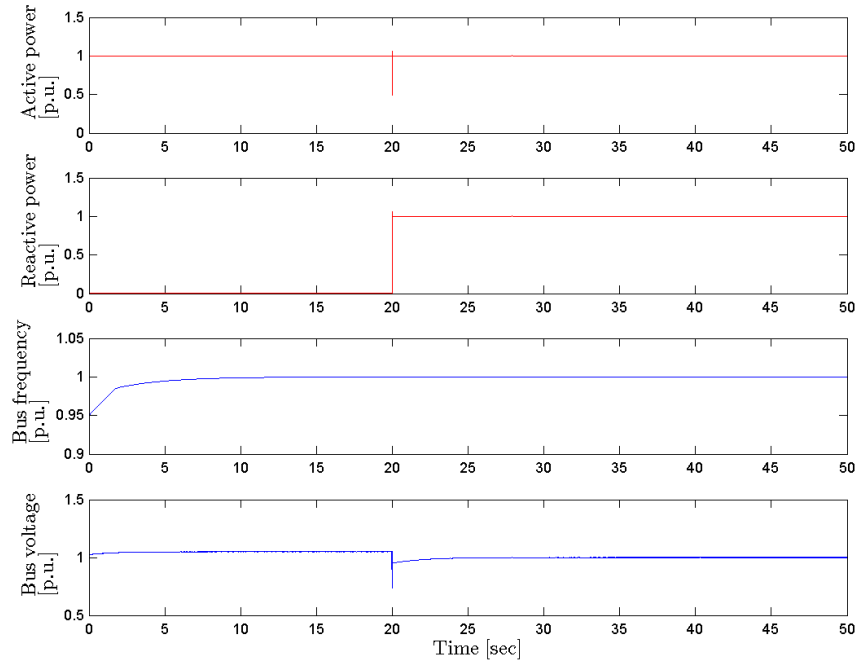


(a) Genset produced power and electrical parameters

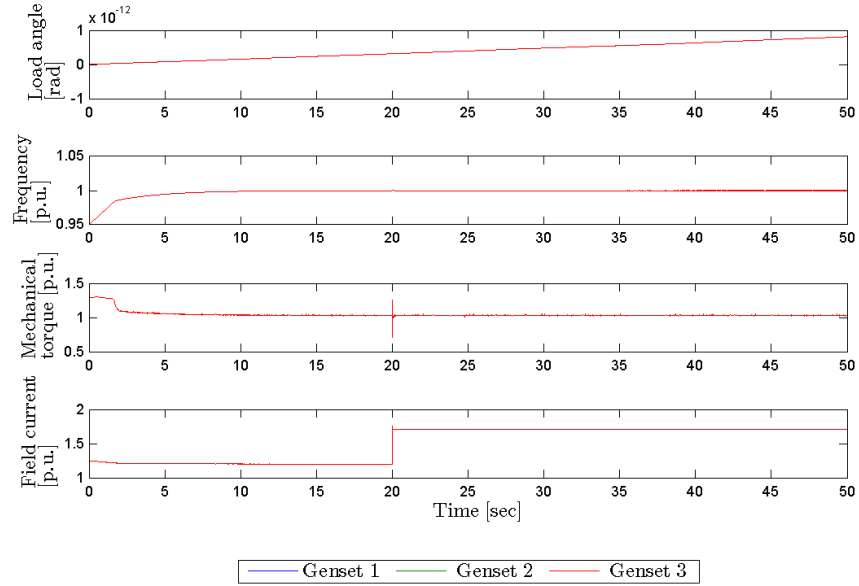


(b) Genset states

Figure B.2: Results from simulation with sudden reactive load increase occurring after 20 seconds.



(a) Genset produced power and electrical parameters



(b) Genset states

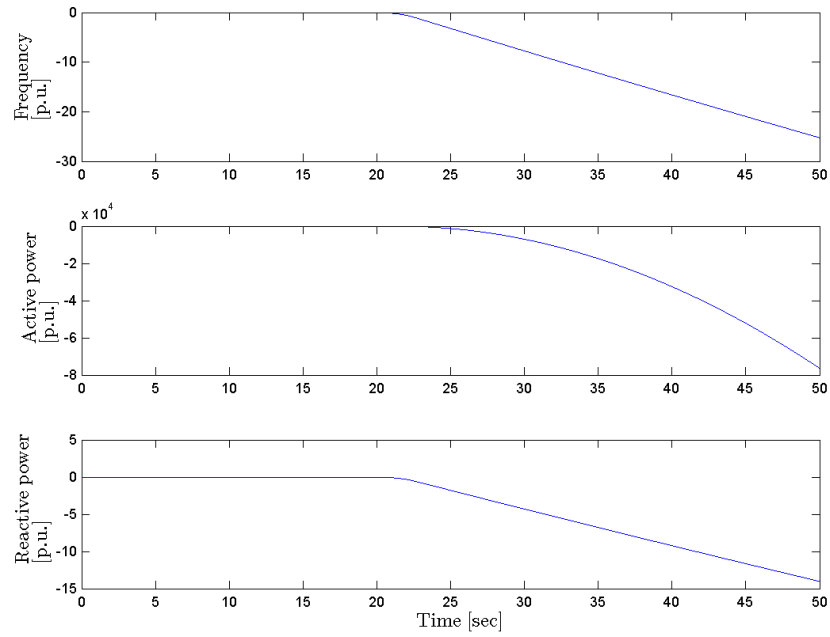
Figure B.3: Results from simulation with sudden reactive load decrease occurring after 20 seconds.

C Simulation results for observer

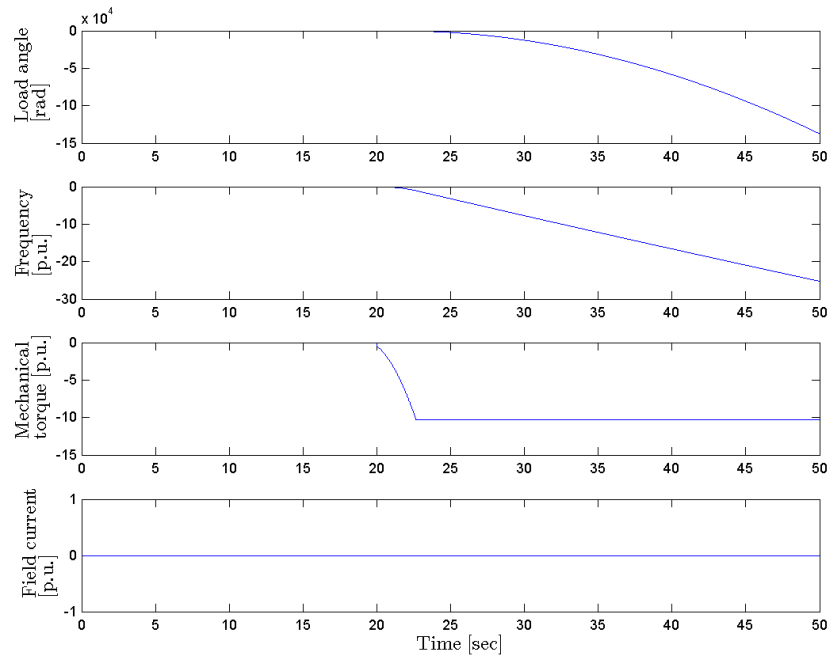
C.1 Simulation against control plant model

On the following pages, the simulation results for the nonlinear Luenberger-type observer, run against the control plant model, with different normal and faulty simulation modes. All simulation parameters are the same as in Section 6.

C.1.1 Governor failure modes

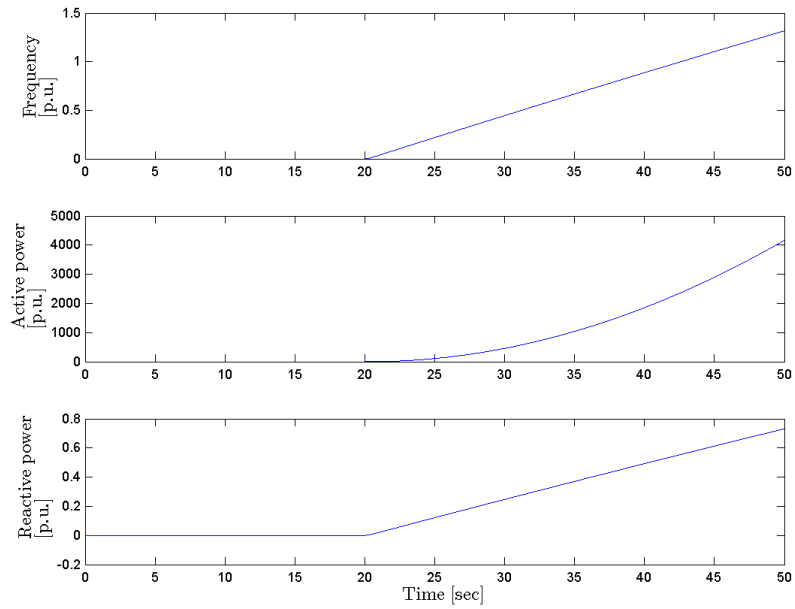


(a) Measurement estimation error.

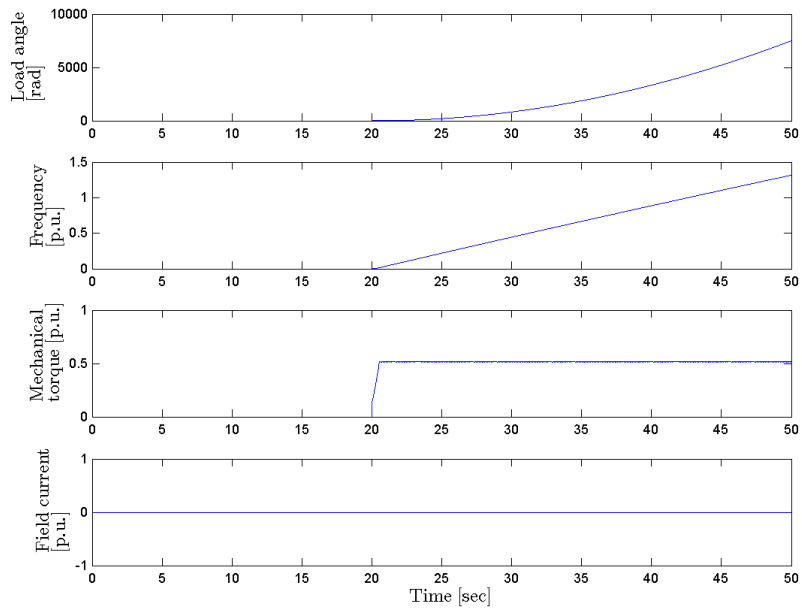


(b) State estimation error.

Figure C.1: Measurement and state errors, for observer run against control plant model, Governor to minimum occurring after 20 seconds



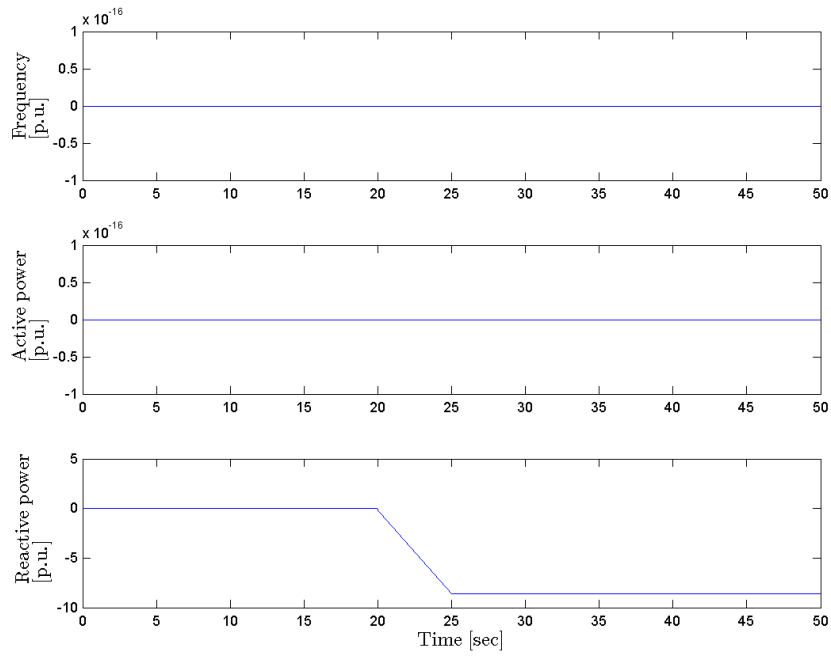
(a) Measurement estimation error.



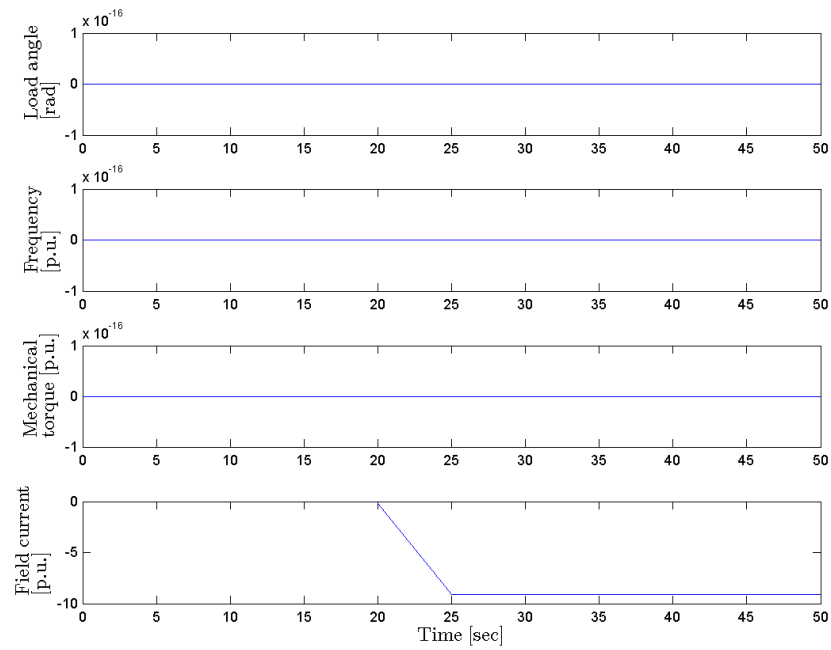
(b) State estimation error.

Figure C.2: Measurement and state errors, for observer run against control plant model, Governor frozen occurring after 20 seconds

C.1.2 AVR failure modes

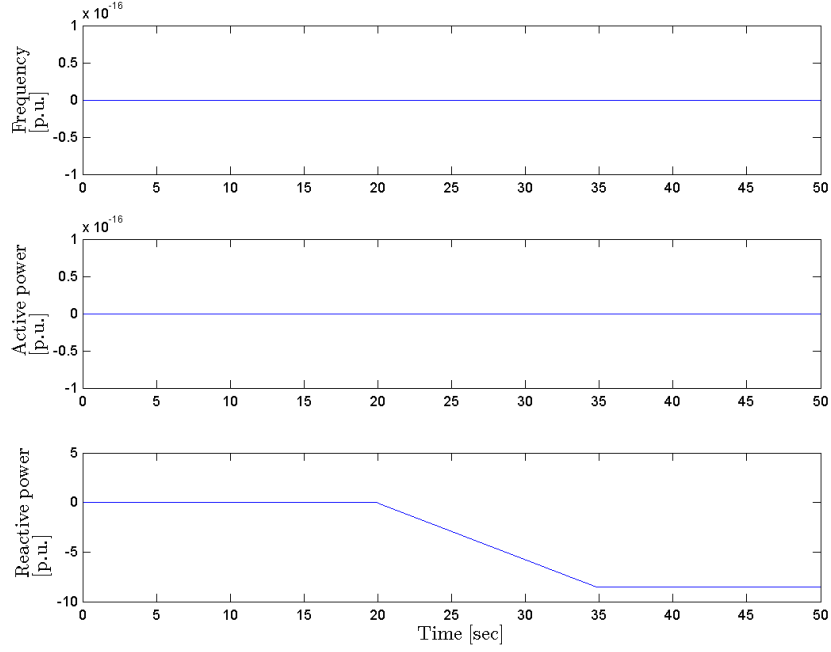


(a) Measurement estimation error, AVR to minimum

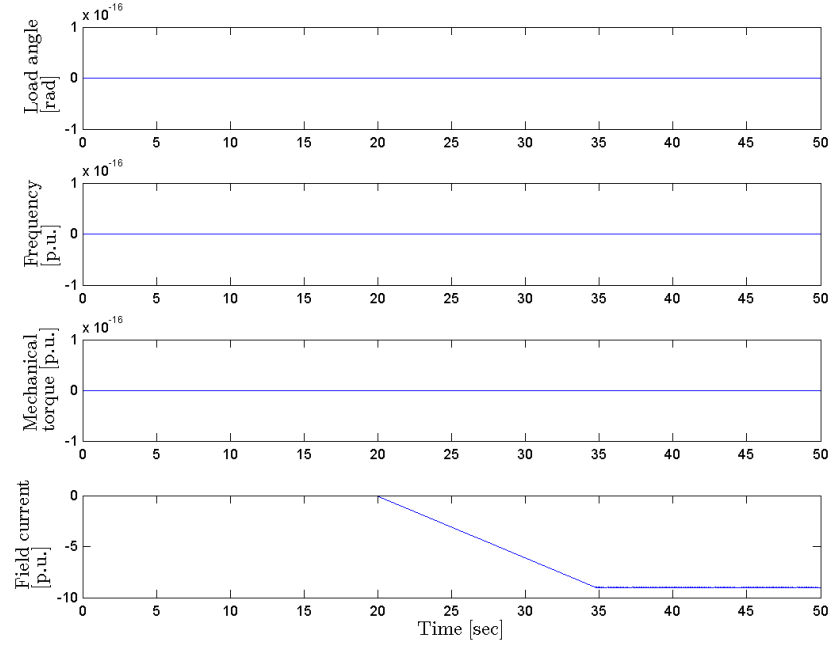


(b) State estimation error, AVR to minimum

Figure C.3: Measurement and state errors, for observer run against control plant model, AVR to min occurring after 20 seconds



(a) Measurement estimation error, AVR frozen



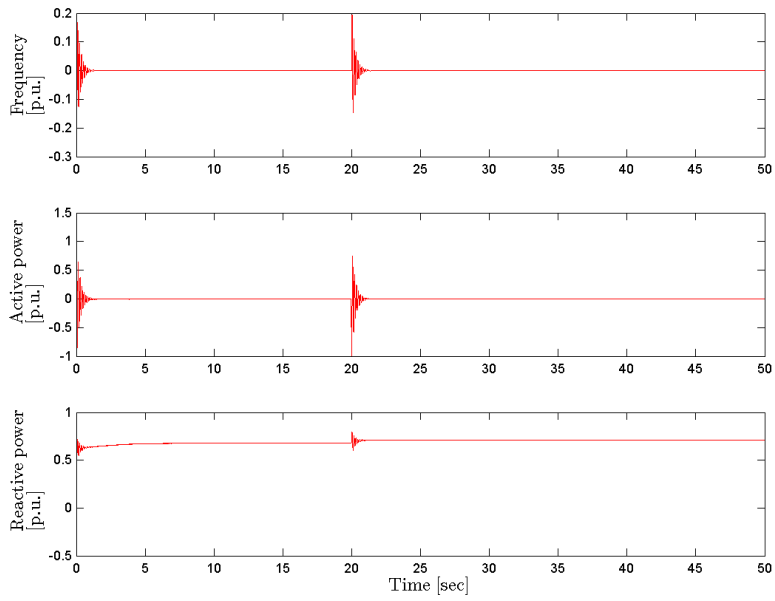
(b) State estimation error, AVR frozen

Figure C.4: Measurement and state errors, for observer run against control plant model, AVR frozen occurring after 20 seconds

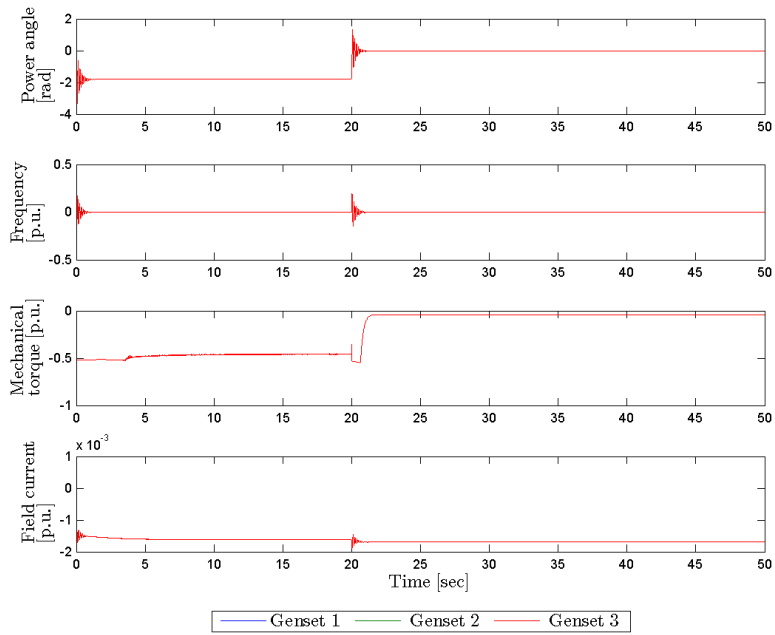
C.2 Simulation against simulation plant model

On the following pages, the simulation results for the nonlinear Luenberger-type observer, run against the simulation plant model, with different normal and faulty simulation modes. All simulation parameters are the same as in Section 6.

C.2.1 Normal simulation modes

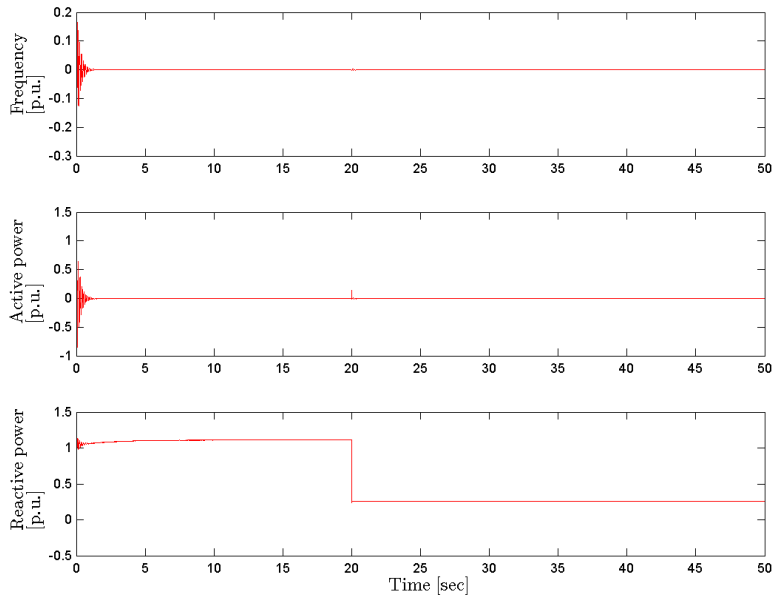


(a) Measurement estimation error.

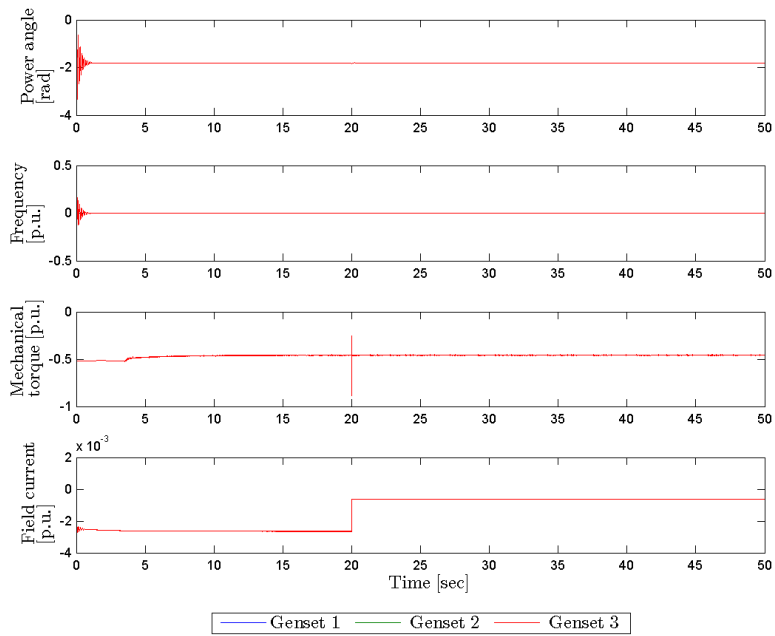


(b) State estimation error.

Figure C.5: Measurement and state errors, for observer run against control plant model, Sudden active load decrease occurring after 20 seconds.

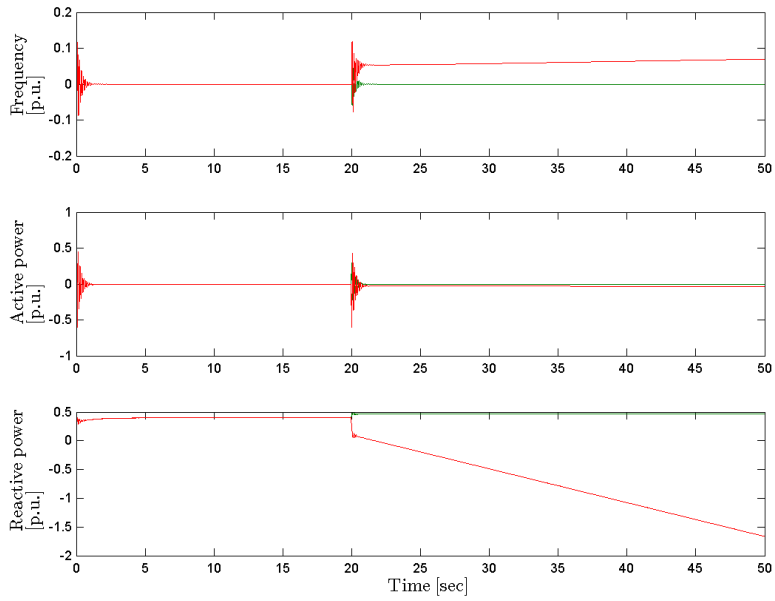


(a) Measurement estimation error.

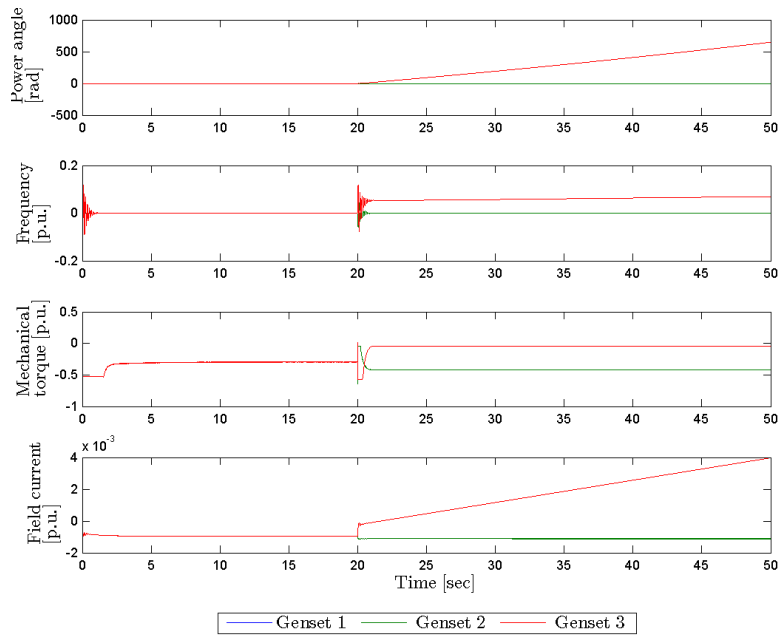


(b) State estimation error.

Figure C.6: Measurement and state errors, for observer run against control plant model, sudden reactive load decrease occurring after 20 seconds.



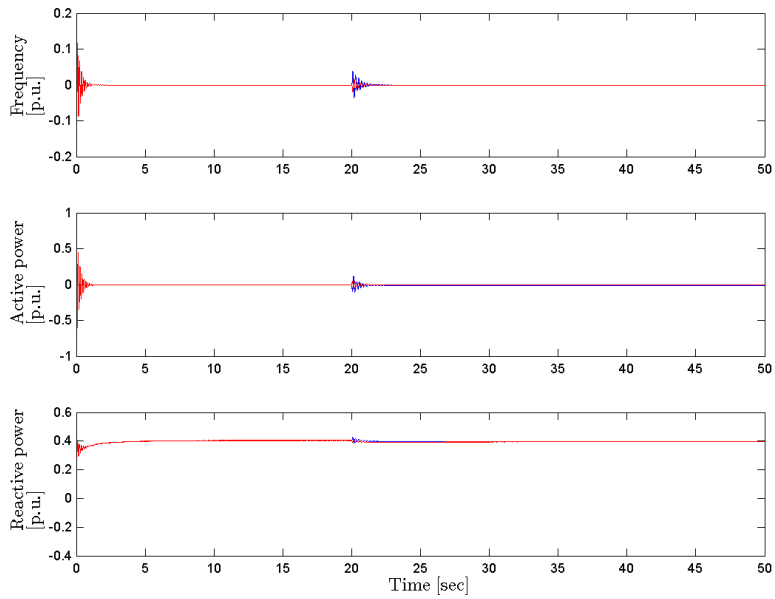
(a) Measurement estimation error.



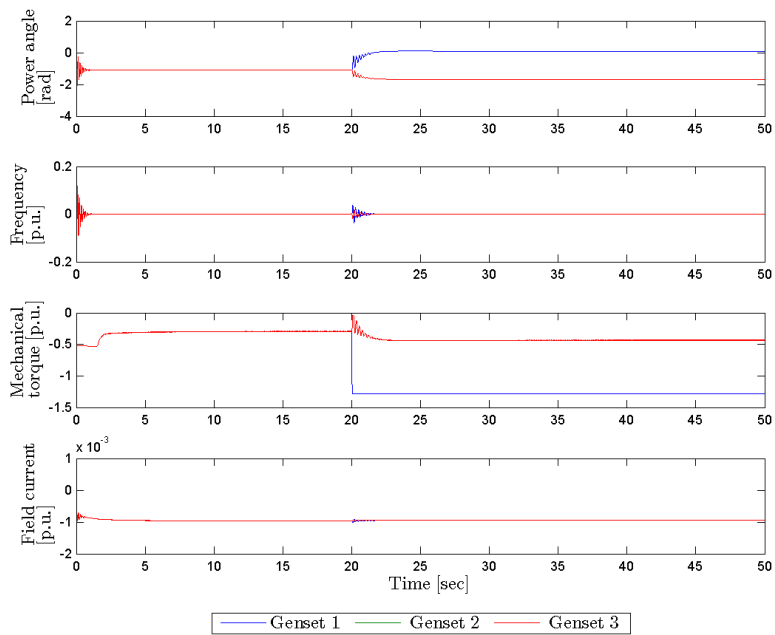
(b) State estimation error.

Figure C.7: Measurement and state errors, for observer run against control plant model, suddendisconnection of Genset 3, occurring after 20 seconds.

C.2.2 Governor failure modes

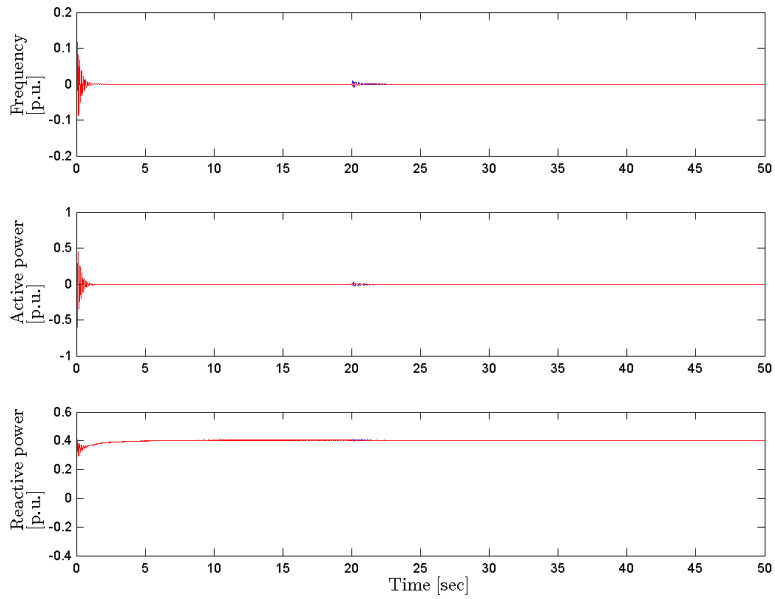


(a) Measurement estimation error.

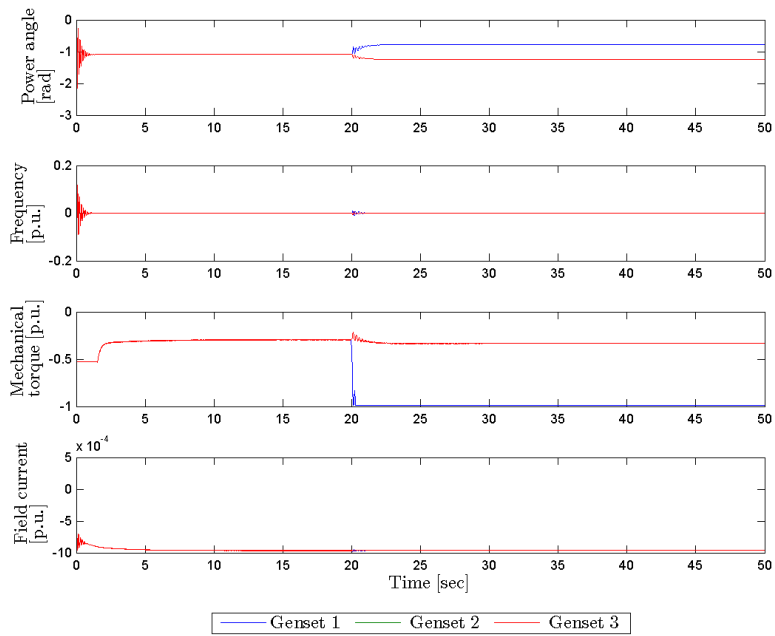


(b) State estimation error.

Figure C.8: Measurement and state errors, for observer run against simulation plant model, Governor to minimum occurring after 20 seconds. Failure implemented in Genset 1.



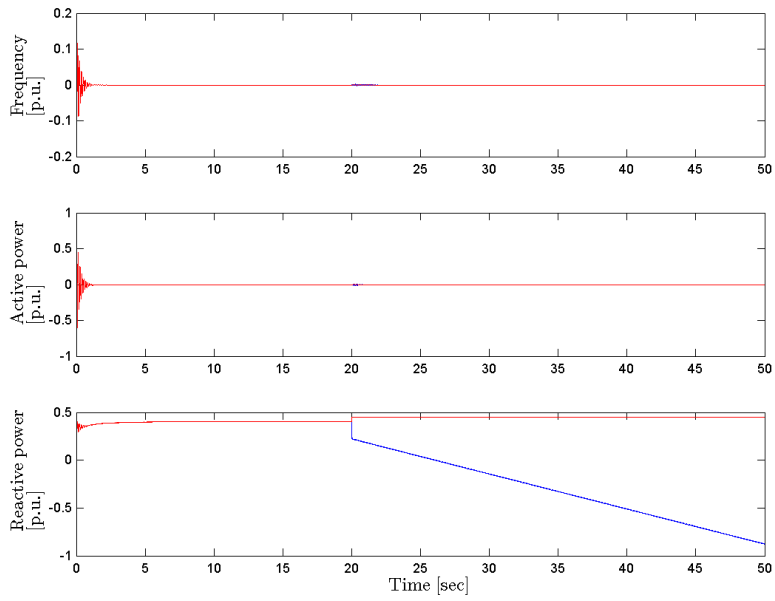
(a) Measurement estimation error.



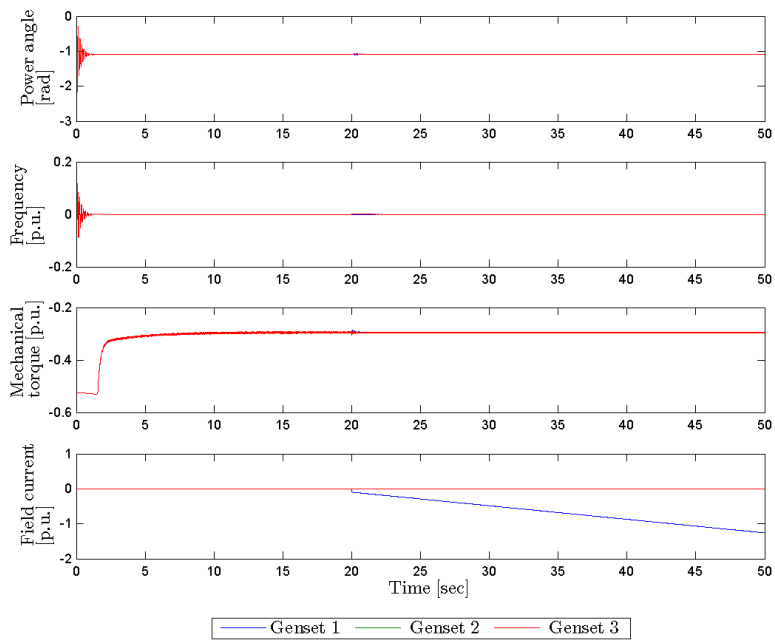
(b) State estimation error.

Figure C.9: Measurement and state errors, for observer run against simulation plant model, Governor frozen occurring after 20 seconds. Failure implemented in Genset 1.

C.2.3 AVR failure modes

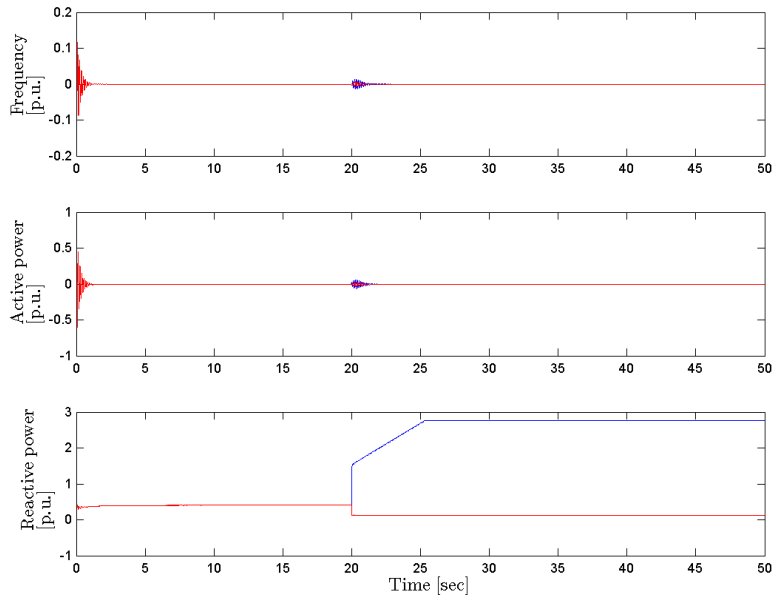


(a) Measurement estimation error.

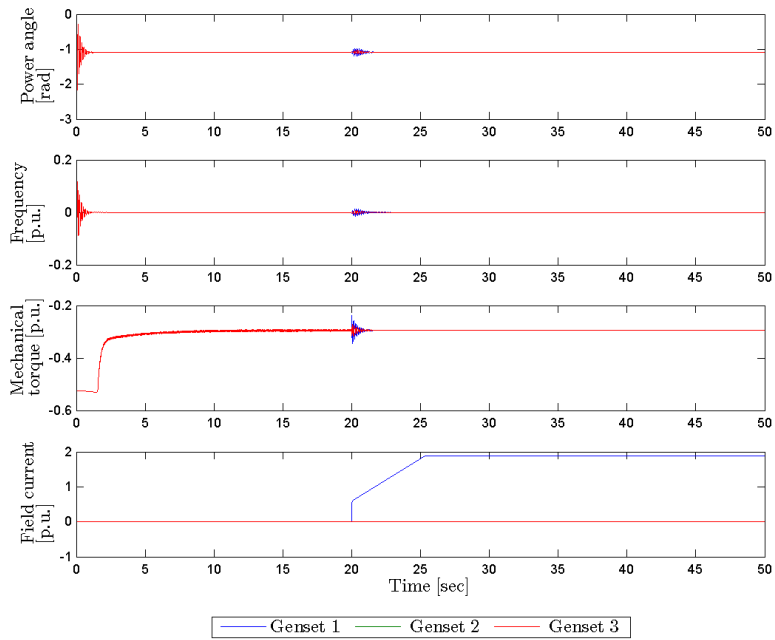


(b) State estimation error.

Figure C.10: Measurement and state errors, for observer run against simulation plant model, AVR to minimum occurring after 20 seconds. Failure implemented in Genset 1.



(a) Measurement estimation error.



(b) State estimation error.

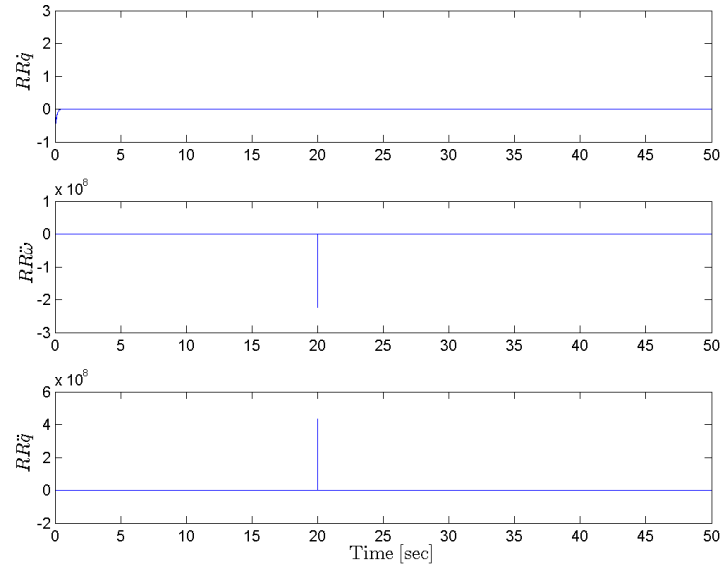
Figure C.11: Measurement and state errors, for observer run against simulation plant model, AVR frozen occurring after 20 seconds. Failure implemented in Genset 1.

D Simulation results for analytical redundancy relation from nonlinear model

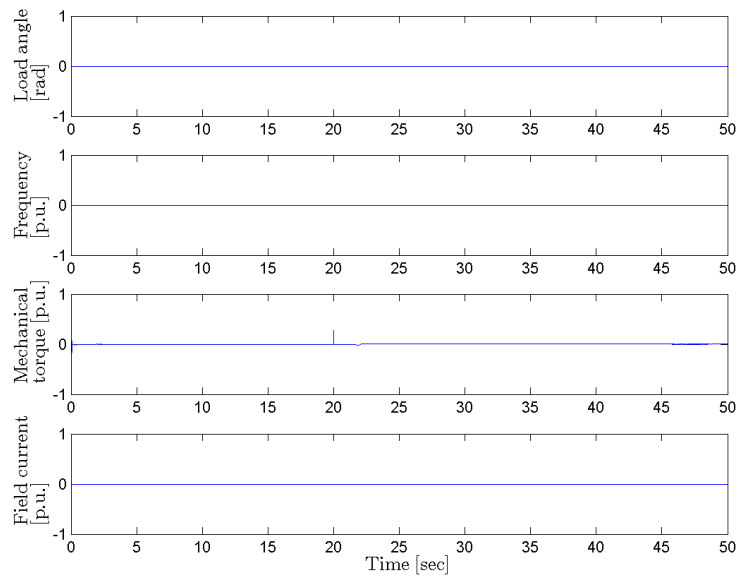
D.1 Simulation against control plant model

On the following pages the simulation results for the state estimation error and redundancy relations, run against the control plant model, with different normal and faulty simulation modes. All simulation parameters are the same as used in Section 6.

D.1.1 Sudden load change

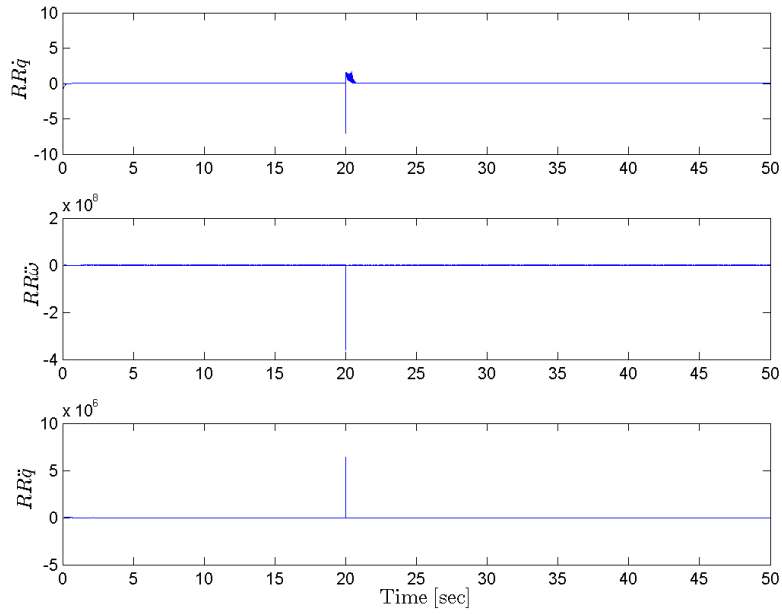


(a) Redundancy relation.

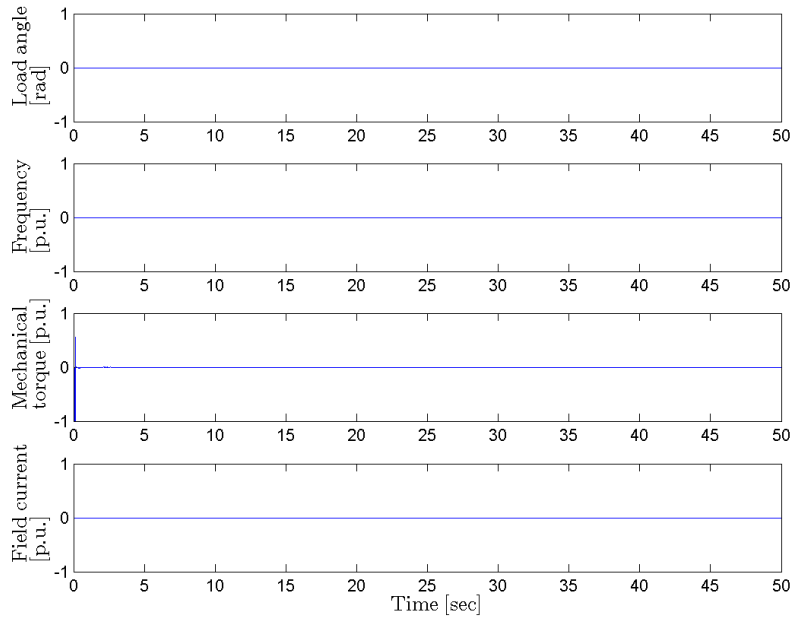


(b) State estimation error.

Figure D.1: Nonlinear redundancy relations and state estimation error, run against nonlinear control plant model, with sudden active load decrease occurring after 20 seconds



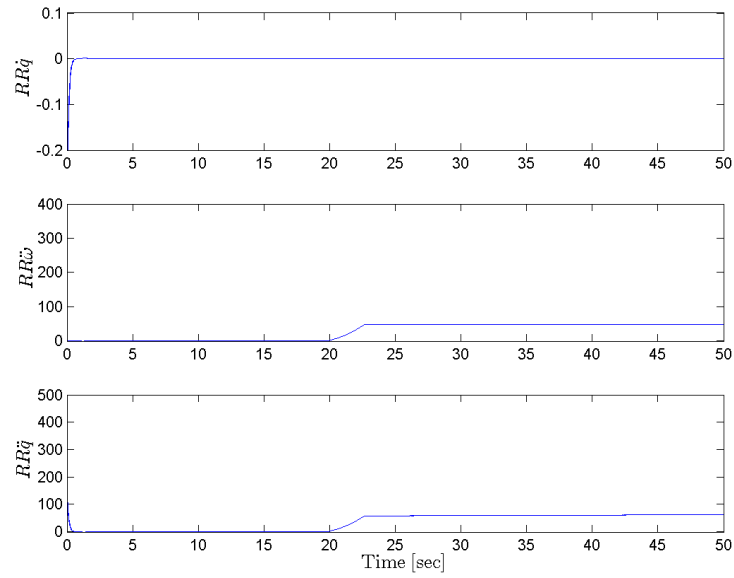
(a) Redundancy relation.



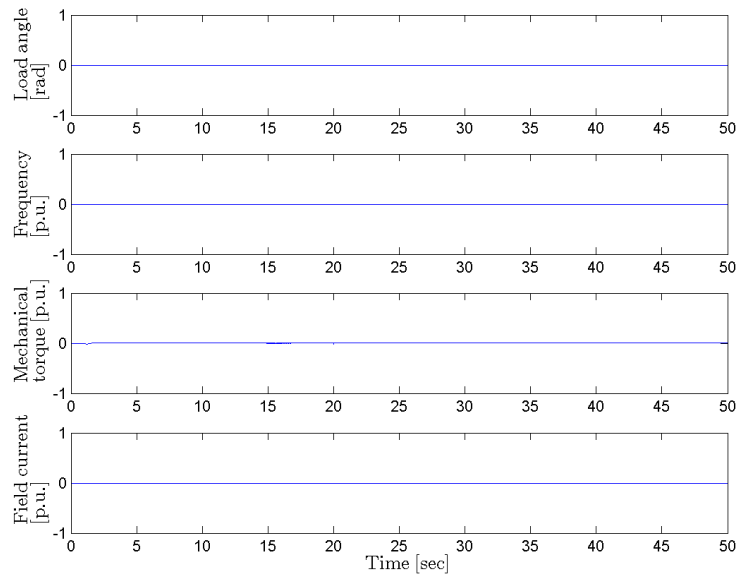
(b) State estimation error.

Figure D.2: Nonlinear redundancy relations and state estimation error, run against nonlinear control plant model, with sudden reactive load decrease occurring after 20 seconds

D.1.2 Governor failure modes

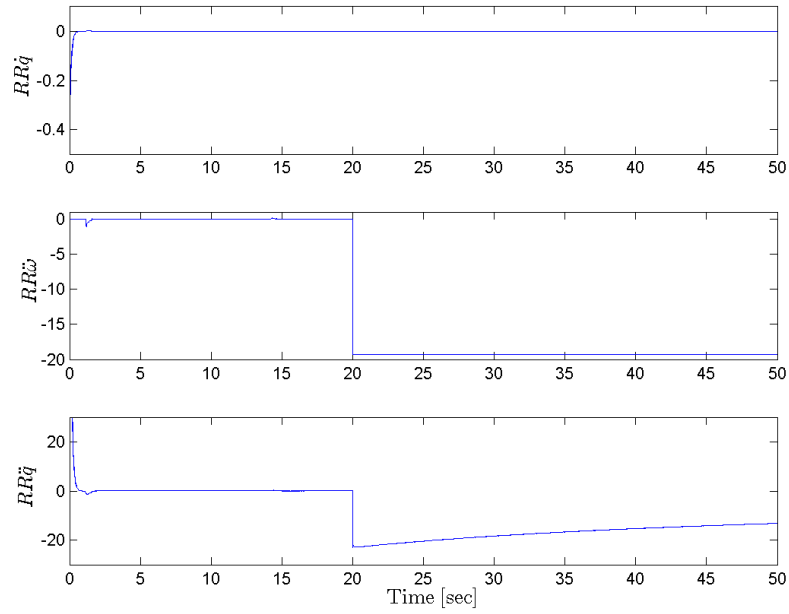


(a) Redundancy relation.

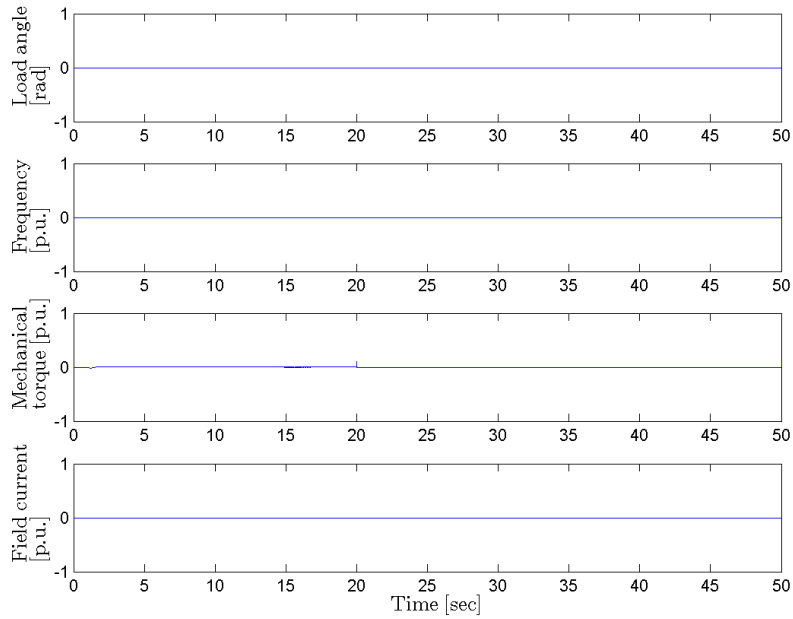


(b) State estimation error.

Figure D.3: Nonlinear redundancy relations and state estimation error, run against nonlinear control plant model, with Governor to minimum occurring after 20 seconds



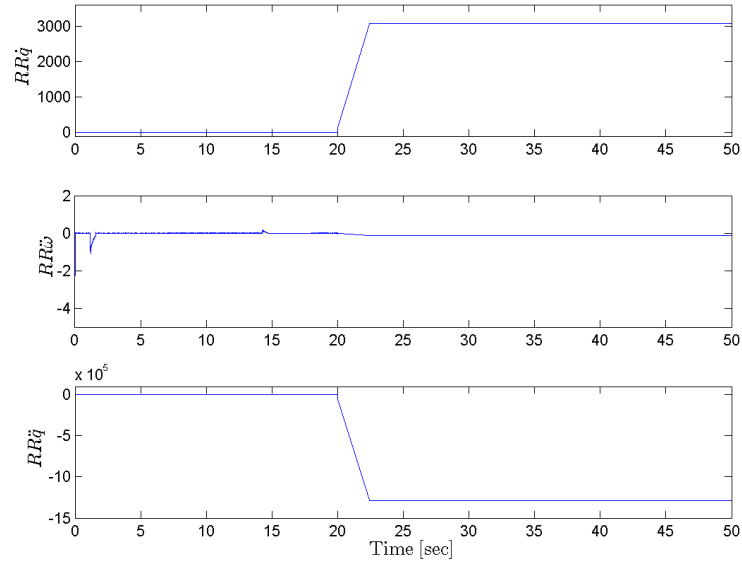
(a) Redundancy relation.



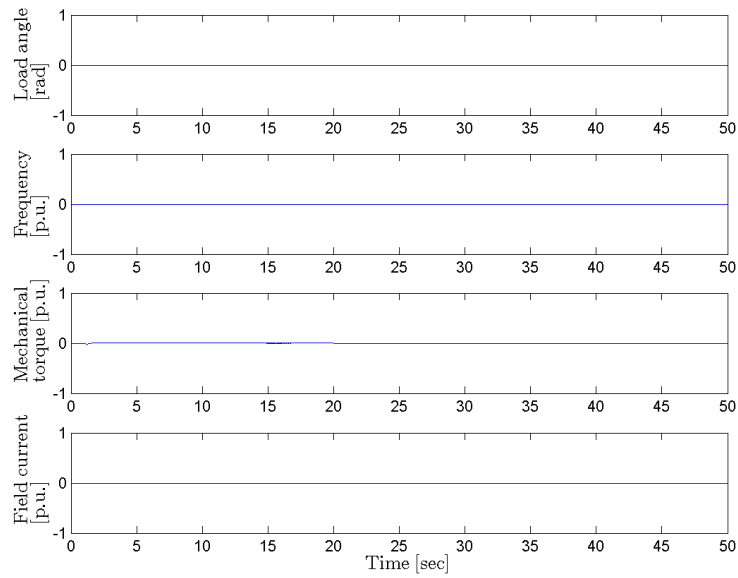
(b) State estimation error.

Figure D.4: Nonlinear redundancy relations and state estimation error, run against nonlinear control plant model, with Governor frozen occurring after 20 seconds

D.1.3 AVR failure modes

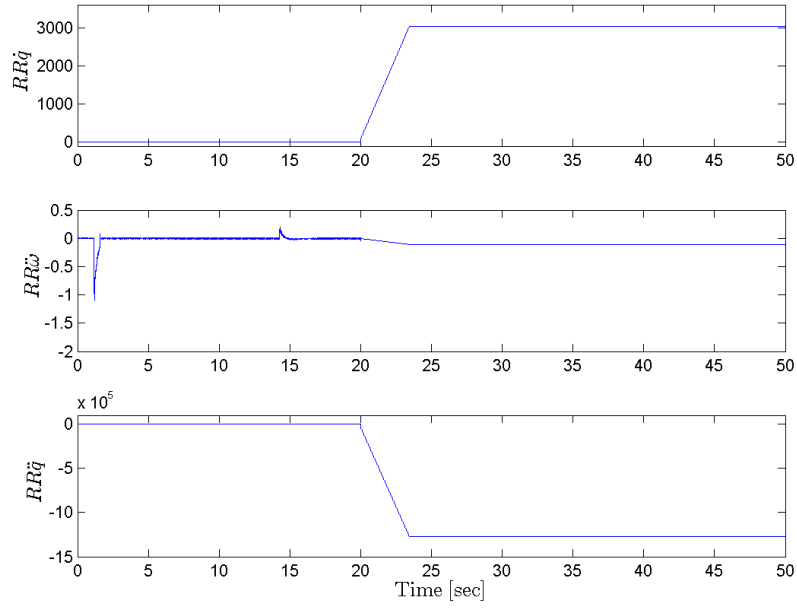


(a) Redundancy relation.

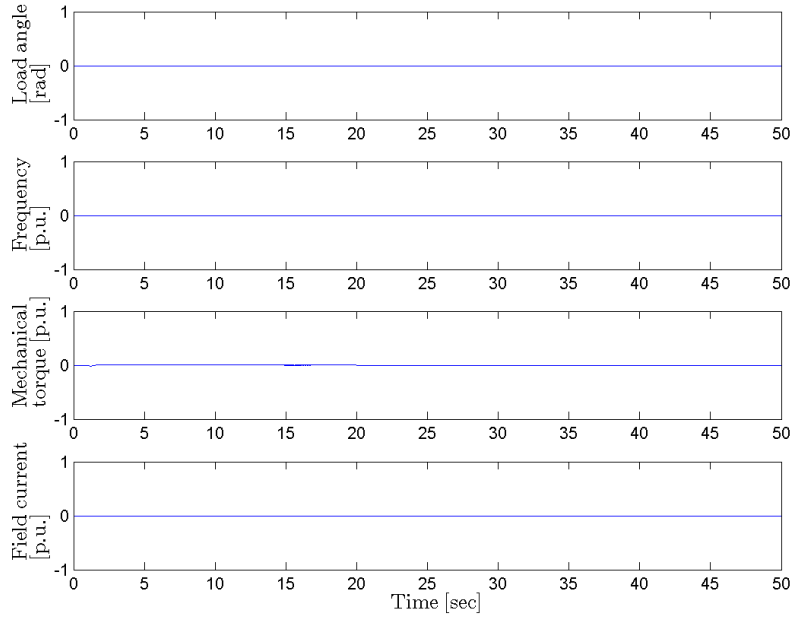


(b) State estimation error.

Figure D.5: Nonlinear redundancy relations and state estimation error, run against nonlinear control plant model, with AVR to minimum occurring after 20 seconds



(a) Redundancy relation.



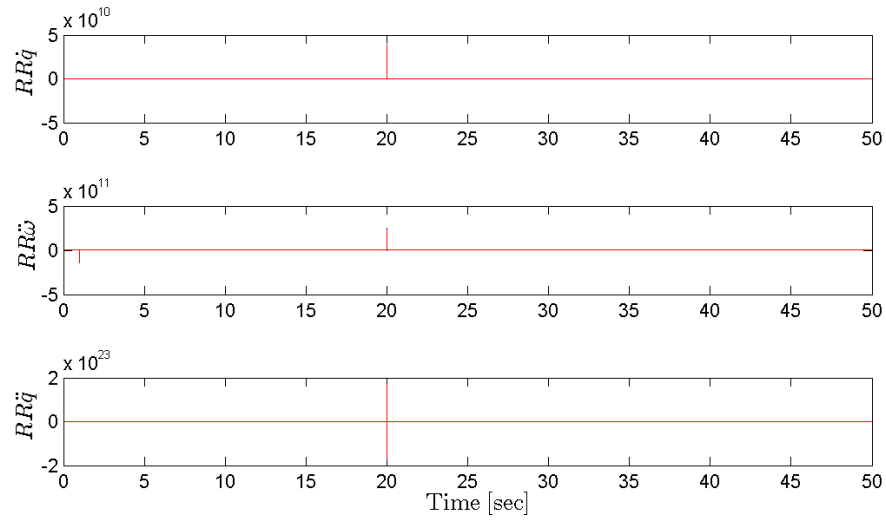
(b) State estimation error.

Figure D.6: Nonlinear redundancy relations and state estimation error, run against nonlinear control plant model, with AVR frozen occurring after 20 seconds

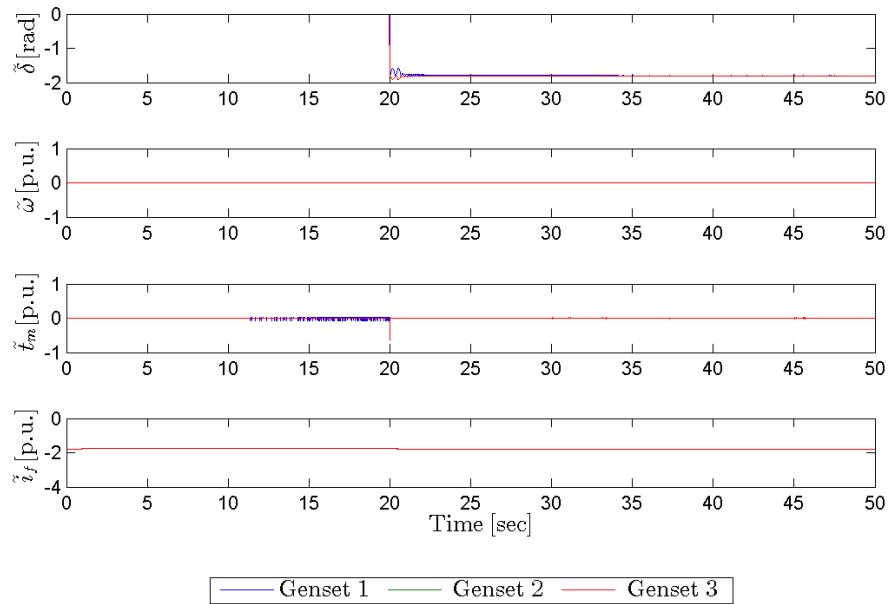
D.2 Simulation against simulation plant model

On the following pages the simulation results for the state estimation error and redundancy relations, run against the simulation plant model, with different normal and faulty simulation modes. All simulation parameters are the same as used in Section 6.

D.2.1 Normal simulation modes

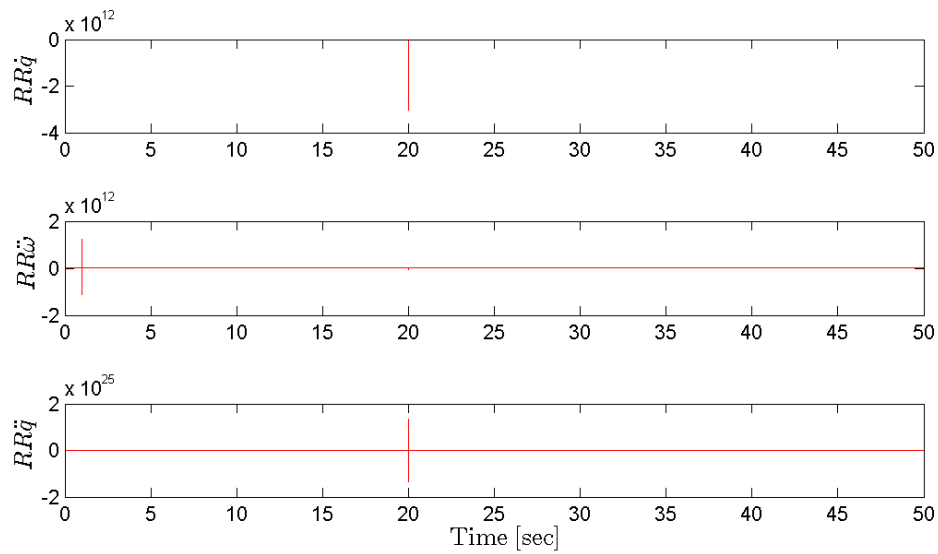


(a) Redundancy relations

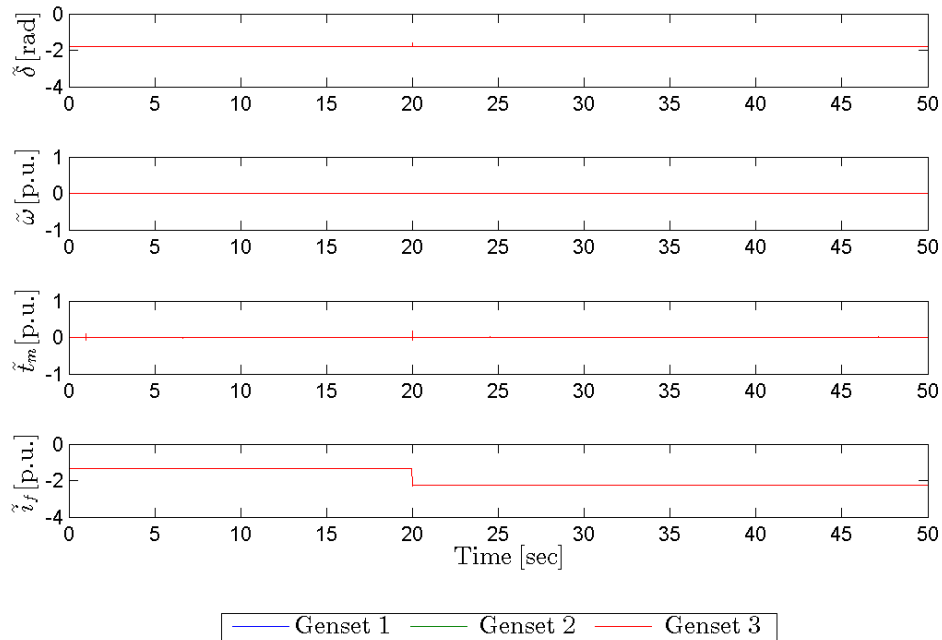


(b) State estimation error

Figure D.7: Nonlinear redundancy relations and state estimation error, run against control plant model, with sudden active load increase occurring after 20 seconds.

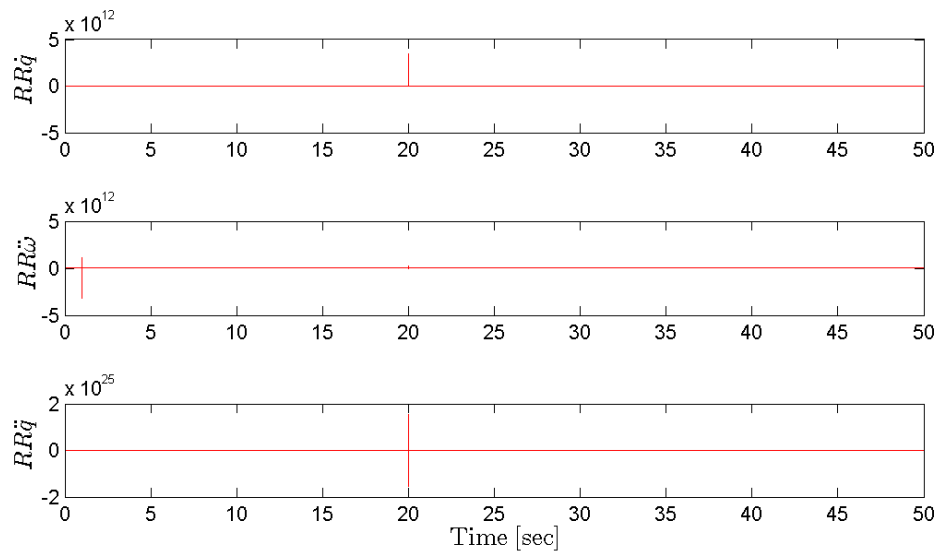


(a) Redundancy relations

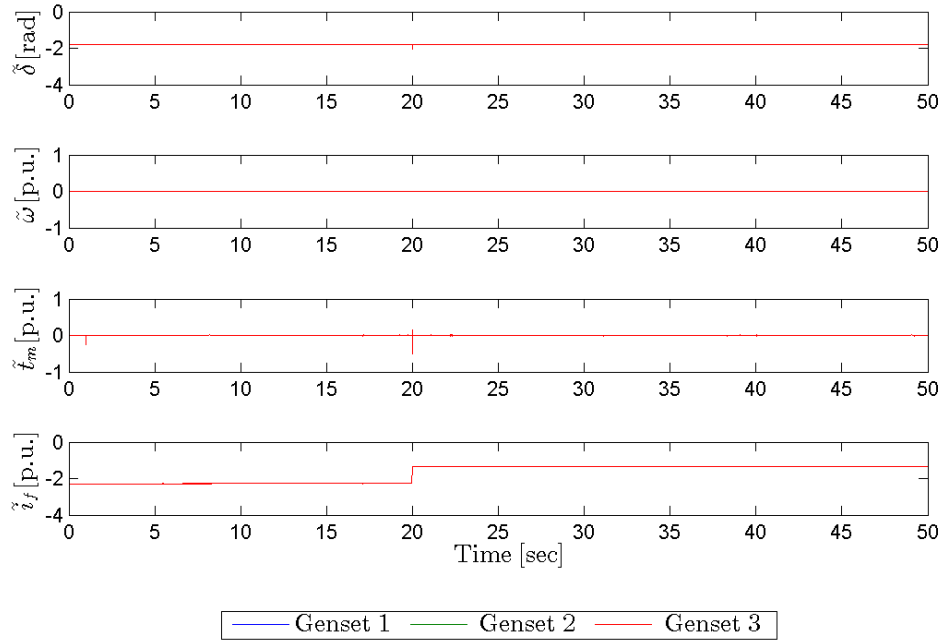


(b) State estimation error

Figure D.8: Nonlinear redundancy relations and state estimation error, run against control plant model, with sudden reactive load increase occurring after 20 seconds.

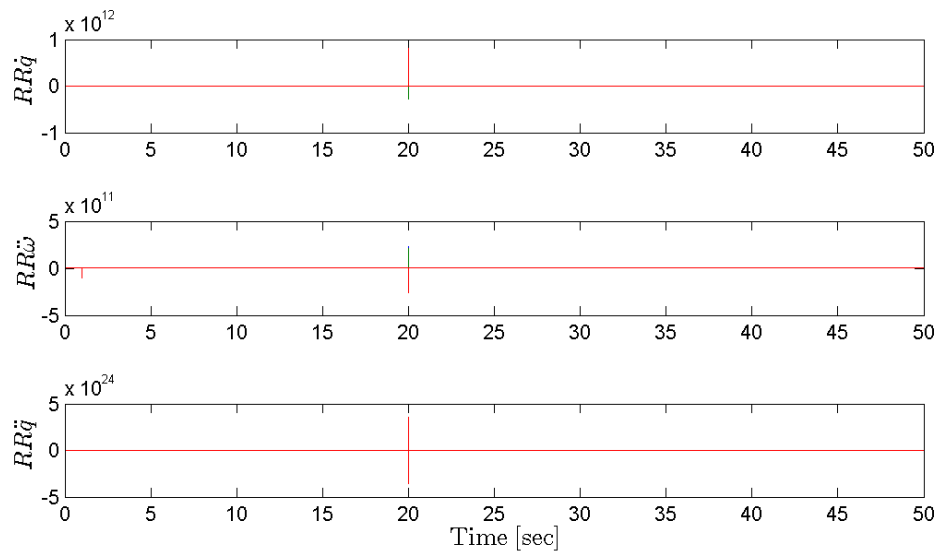


(a) Redundancy relations

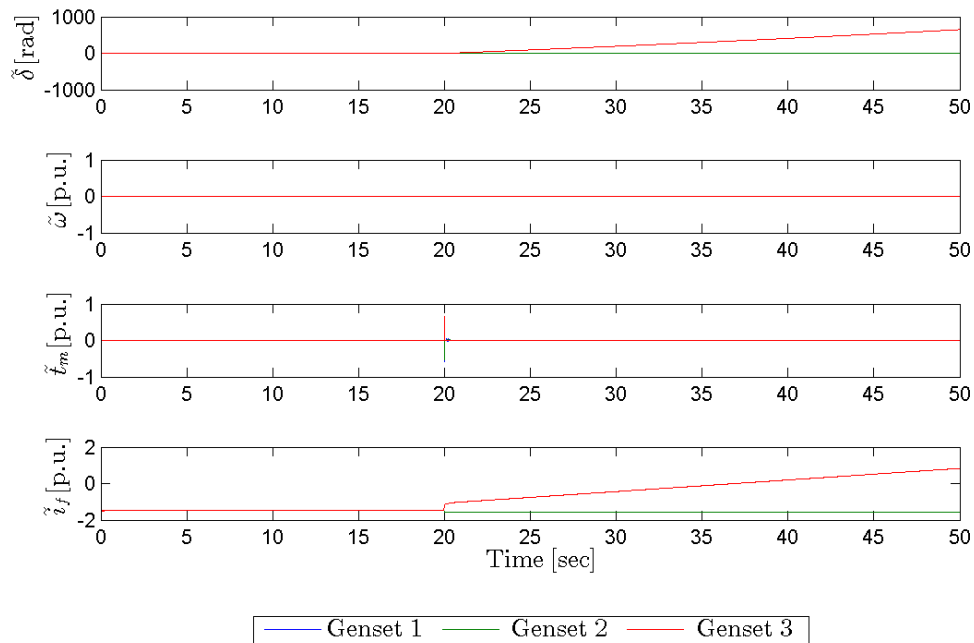


(b) State estimation error

Figure D.9: Nonlinear redundancy relations and state estimation error, run against control plant model, with sudden reactive load decrease occurring after 20 seconds.



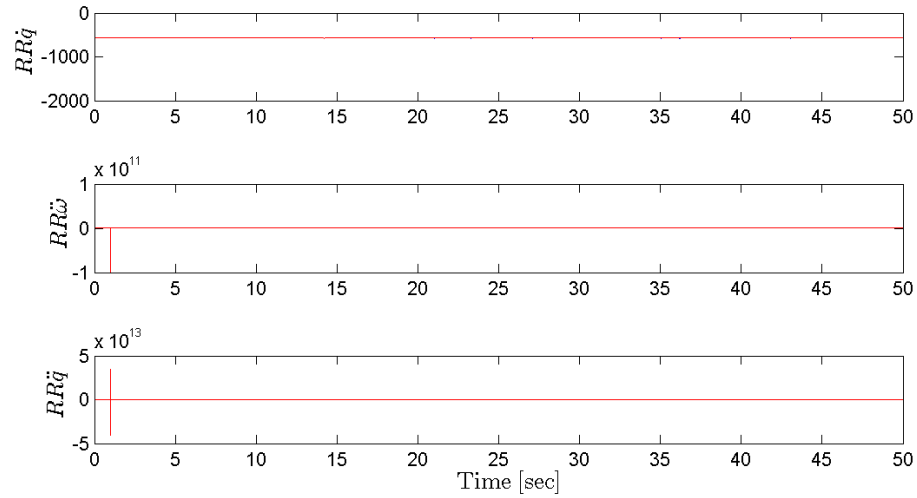
(a) Redundancy relations



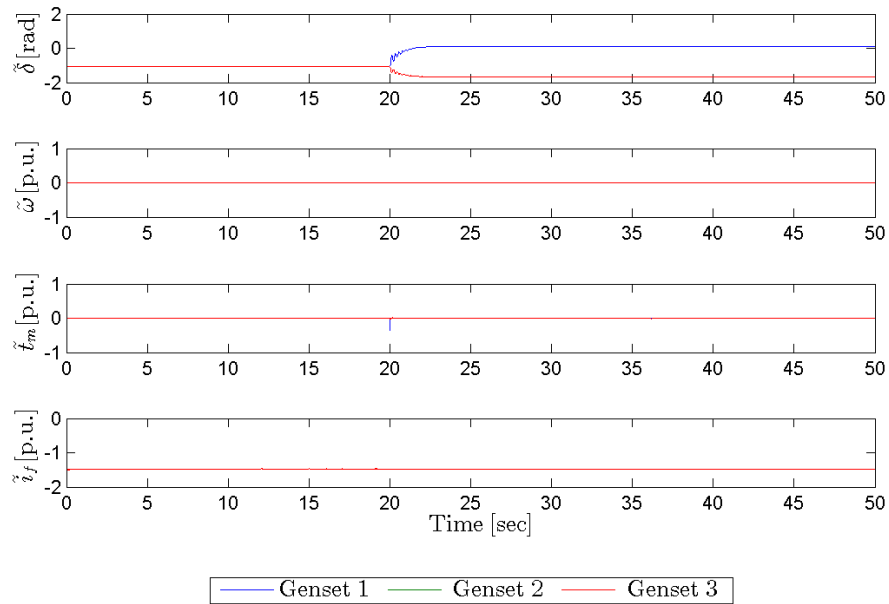
(b) State estimation error

Figure D.10: Nonlinear redundancy relations and state estimation error, run against control plant model, with sudden disconnection of Genset 3 occurring after 20 seconds.

D.2.2 Governor failure modes

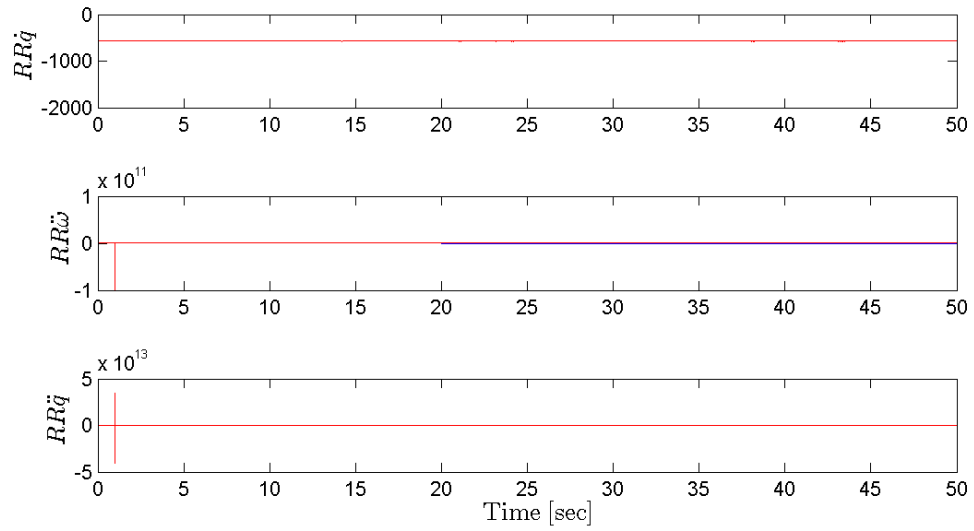


(a) Redundancy relations

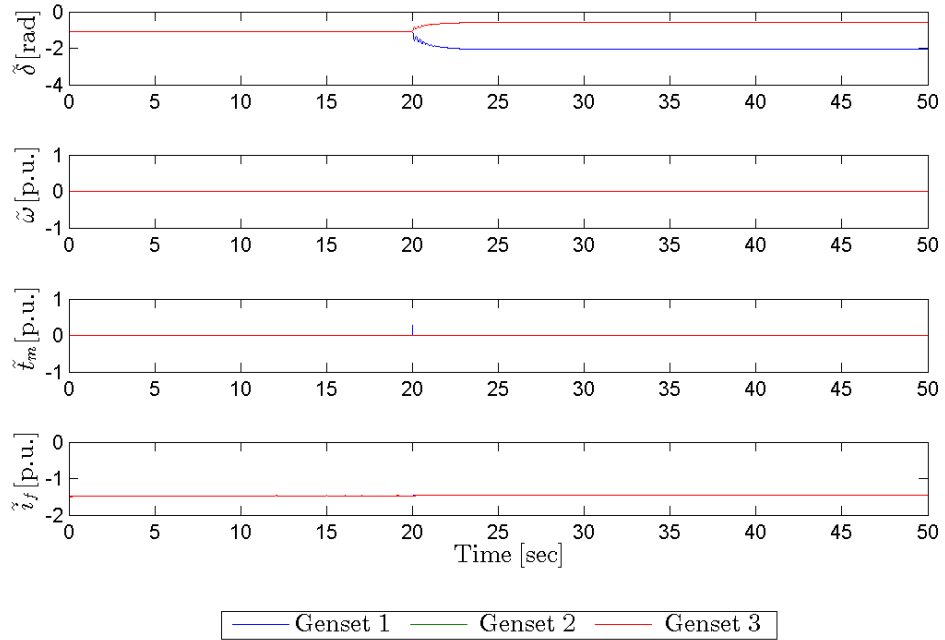


(b) State estimation error

Figure D.11: Nonlinear redundancy relations and state estimation error, run against control plant model, with failure Governor to minimum occurring after 20 seconds.

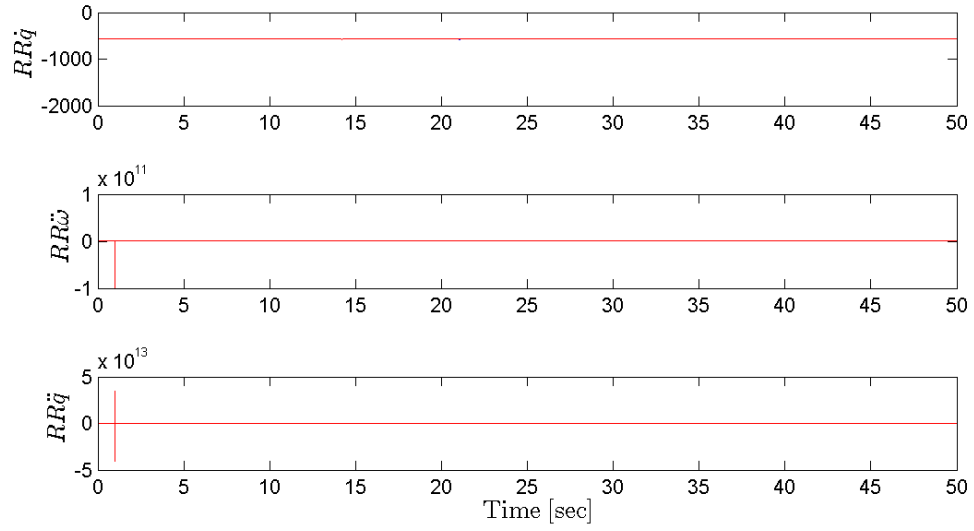


(a) Redundancy relations

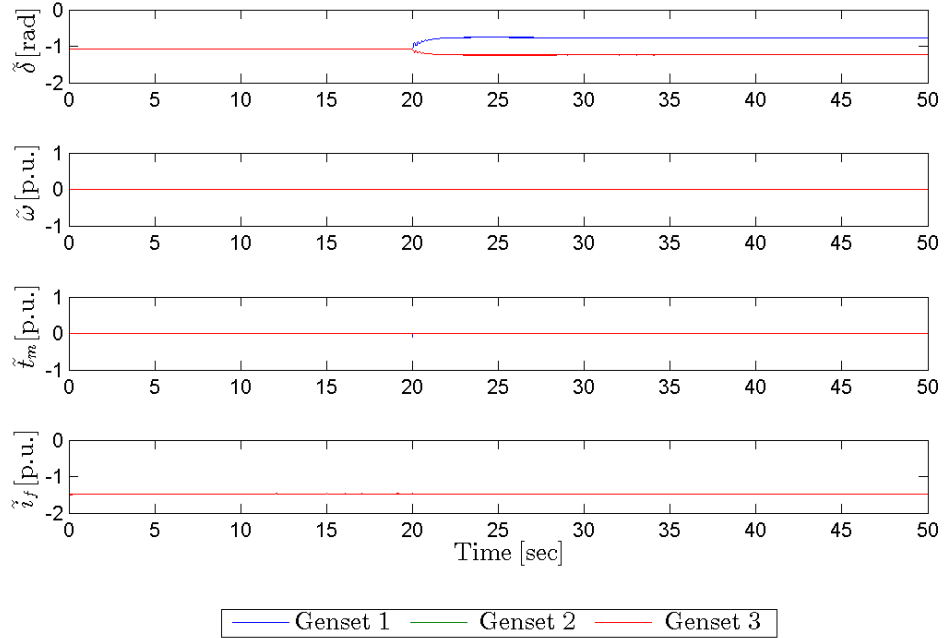


(b) State estimation error

Figure D.12: Nonlinear redundancy relations and state estimation error, run against control plant model, with failure Governor to maximum occurring after 20 seconds.



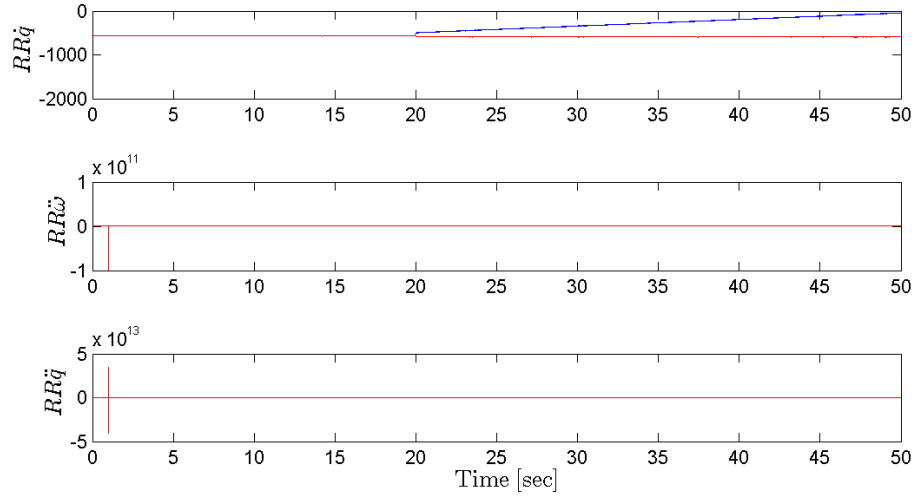
(a) Redundancy relations



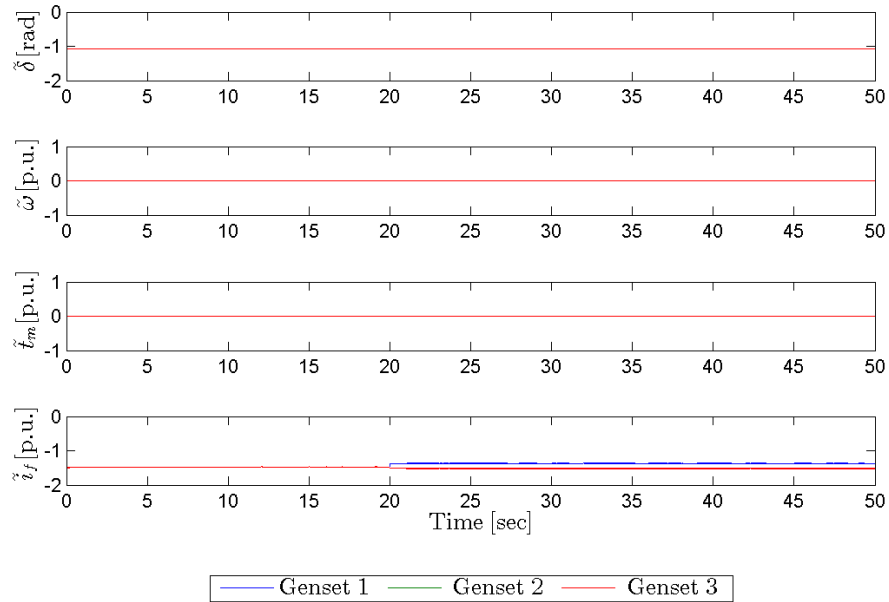
(b) State estimation error

Figure D.13: Nonlinear redundancy relations and state estimation error, run against control plant model, with failure Governor frozen occurring after 20 seconds.

D.2.3 AVR failure modes

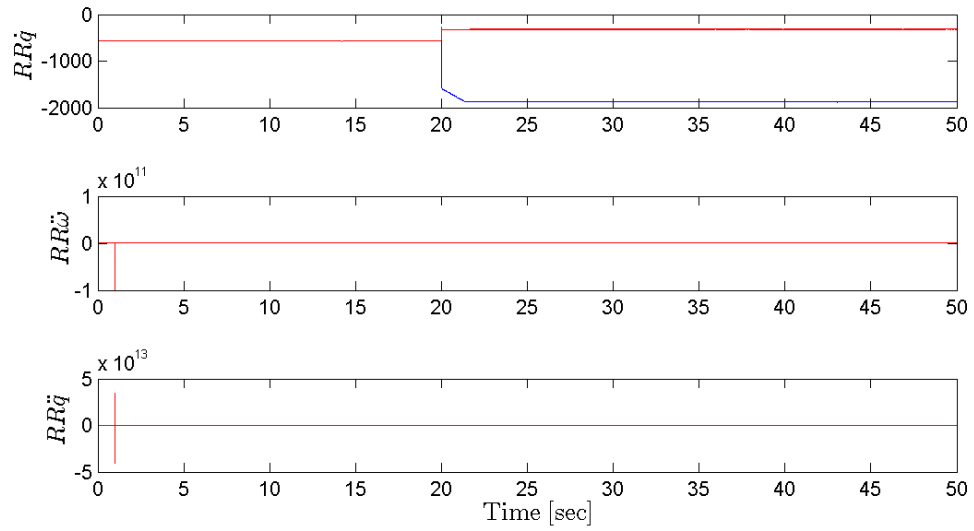


(a) Redundancy relations

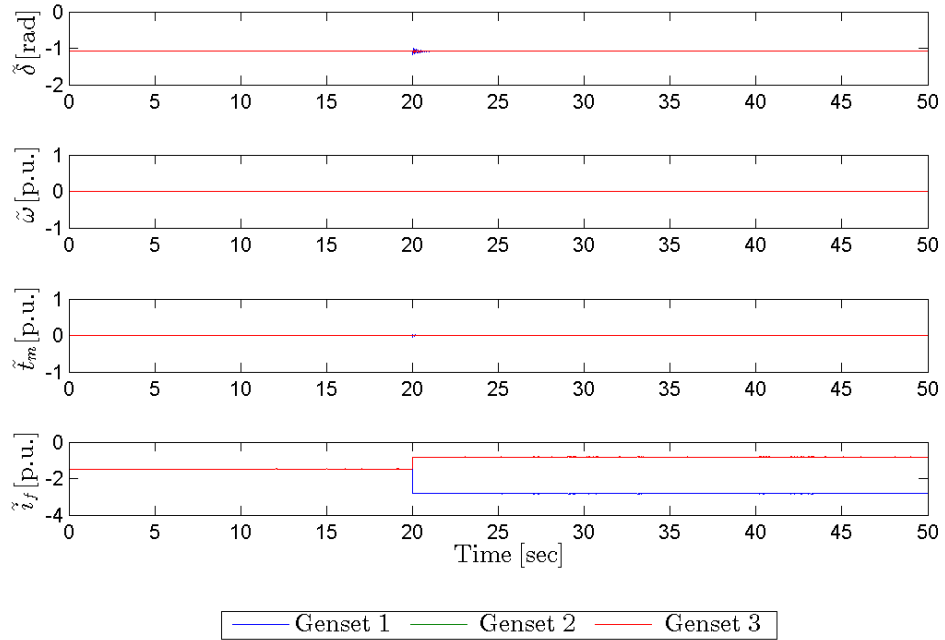


(b) State estimation error

Figure D.14: Nonlinear redundancy relations and state estimation error, run against control plant model, with failure AVR to minimum occurring after 20 seconds.

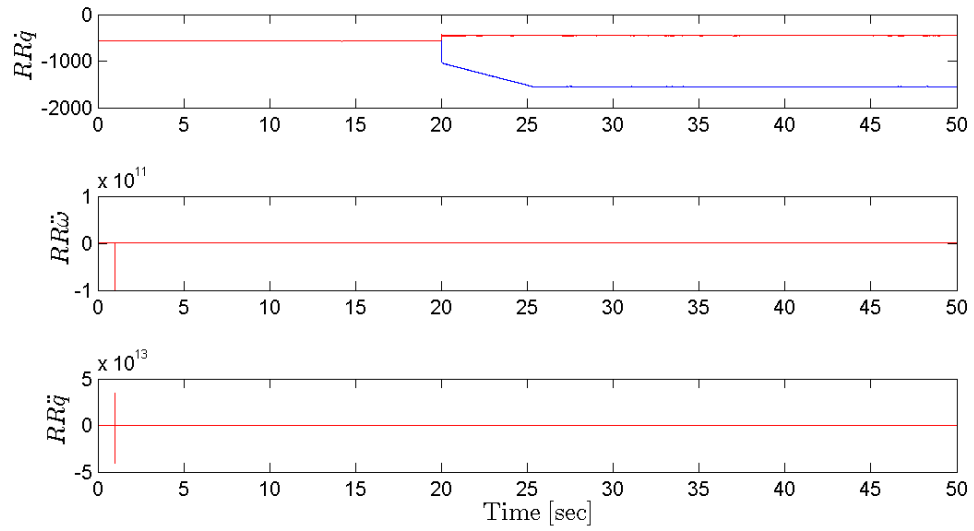


(a) Redundancy relations

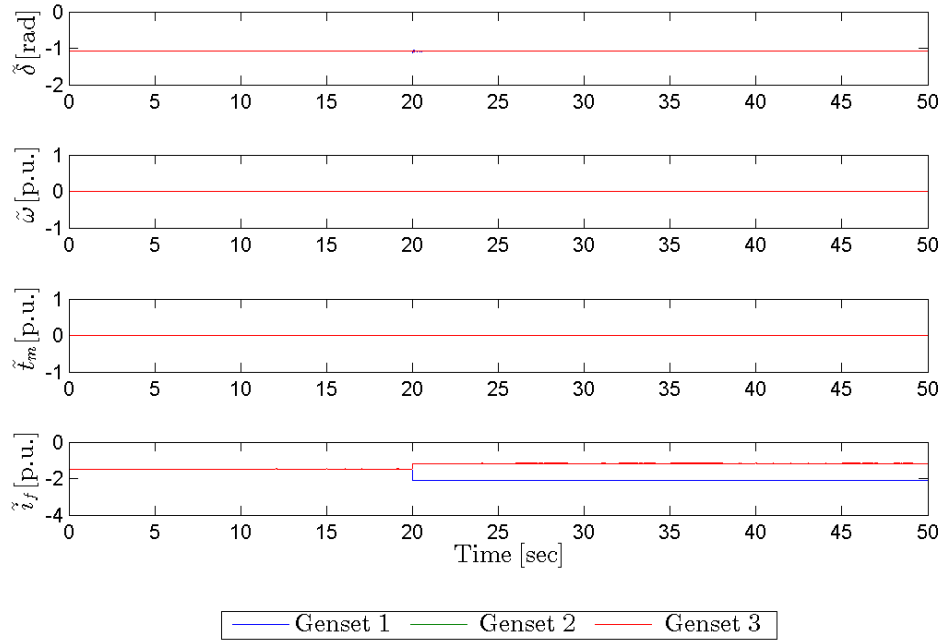


(b) State estimation error

Figure D.15: Nonlinear redundancy relations and state estimation error, run against control plant model, with failure AVR to maximum occurring after 20 seconds.



(a) Redundancy relations



(b) State estimation error

Figure D.16: Nonlinear redundancy relations and state estimation error, run against control plant model, with failure AVR frozen occurring after 20 seconds.